Carboxylated Cellulose Pulp Fibers: from Fundamentals to Applications

By

Goeun Sim

A thesis submitted to McGill University in partial fulfillment of the requirements for the degree of Doctor of Philosophy

Department of Chemistry, McGill University

Montreal, Quebec, Canada

2015

I dedicate this thesis to my family for their endless love and support

Acknowledgements

I would like to express my deepest gratitude to everyone who have helped me throughout my studies.

First and foremost, to my research supervisor Professor Theo van de Ven for the opportunity to work under his guidance and for all the support he provided to me. Thank you for being my mentor, inspiration, and a role model.

I thank Md Nur Alam and Louis Godbout for valuable discussions and technical training; Yanqing Liu, my summer student, for helping me out with the experimental work; Zohreh Sabzalian and Alois Vanerek for providing an access to the instruments at FPInnovations; and all the van de Ven group members for being such great colleagues and friends. Special thanks to Paul for French translation.

I am also grateful to Colleen McNamee for her thoughtful guidance, kindness and support, as well as all the staff in CSACS, FIBRE network, GFN network and the department of Chemistry.

Special thanks to Professor Akira Isogai at The University of Tokyo and his research group members for the opportunity to work in their facility and for making me a second home.

Last but not least, I would like to thank my family – mom, dad, and my dearest sister Nari Sim. I have always been and forever will be most proud to be your little girl.

Author Contributions

Dr. Theo van de Ven provided supervision, intellectual advice and funding for all the projects described in this thesis. Dr. Md Nur Alam provided training on chemical reactions; Louis Godbout, intellectual advice and proofreading of Chapter 2; Yanqing Liu, water absorbency tests in Chapter 5. Otherwise, all the work presented in this thesis was performed by the author.

Table of Contents

List of Tables

List of Figures

Abstract

Wood fibers are heterogeneous composite materials that are produced and engineered by nature. The unique arrangement of cellulose microfibrils in wood cell walls provides superior mechanical properties; at the same time, such high structural complexity hinders the fiber breakup which is necessary in most cellulose fiber processing. Understanding the cause and effect of the changes in fiber morphologies is the key in developing energy efficient and cost effective ways to prepare novel cellulose based products. Cellulose pulp fibers exhibit a characteristic "ballooning" phenomenon during fiber dissolution, derivatization, and nanofibrillation. Even though the ballooning behavior was first observed more than a century ago, no systematic studies have been conducted thus far to link the cellulose fibril arrangements in each secondary sublayer to the rise of balloon-like structures. The general goal of the studies presented in this thesis is to elucidate the morphological changes of pulp fibers undergoing a series of chemical and mechanical treatments, and to correlate the effect of the chemically modified fiber structures to the properties of the finished products.

Carboxylation chemistry is widely used to modify cellulose fiber surfaces by converting the reactive hydroxyl groups into carboxylates. In the case of carboxymethylation, pulp fibers swell by forming balloon-like structures, which is mainly caused by electrostatic repulsion. During the swelling of carboxymethylated fibers (CMF), the S1 layers are mainly responsible for the formation of balloons and collars, the S2 layers for the transversal stretching, and the S3 layers for providing continuity. In order to avoid the formation of balloons, physical constraints generated from the cellulose fiber arrangements in secondary sublayers must be effectively released. Varying the types and degrees of post-treatment of the CMF can yield either spherical gel particles or fiber fragments with wide size distributions. The outer layers of CMF can also be

carefully peeled off to have the S3 layers isolated from the swollen fiber structures for further characterization. The balloon-like structures of the CMF function as intrinsic water pockets, hence exhibit significantly increased water absorptivity. Superabsorbent CMF can be made into films with tunable properties including transparency, dry and wet strength.

Abrégé

Les fibres de bois sont des matériaux composites hétérogènes qui sont produites et fabriquées par la nature. La disposition unique de microfibrilles de cellulose dans les parois cellulaires du bois fournit des propriétés mécaniques supérieures; en même temps, une telle complexité structurelle élevée empêche la rupture de la fibre qui est nécessaire pour un grand nombre de traitements des fibres de cellulose. Comprendre la cause et l'effet des changements de la morphologie des fibres est la clé dans le développement de moyens efficaces d'améliorer l'efficacité énergétique et des coûts pour préparer les produits à base de cellulose. Les fibres de pâte de cellulose présentent un phénomène caractéristique; plusieurs régions des fibres sont ballonnées lors de la dissolution de la fibre, la dérivatisation et nanofibrillation. Même si ce phénomène de ces fibres a été observé pour la première fois plus d'un siècle, aucune étude systématique n'a été menée jusqu'à présent pour relier la disposition des fibrilles de cellulose dans chaque sous-couche secondaire pour expliquer les structures ballonnées. L'objectif général des études présentées dans cette thèse est d'élucider les changements morphologiques des fibres de pâte subissant une série de traitements chimiques et mécaniques et de corréler l'effet des structures de fibres chimiquement modifiées aux propriétés des produits réalisés.

La chimie de carboxylation est largement utilisée pour modifier les surfaces de fibres de cellulose en convertissant les groupes hydroxyles aux groupes carboxyles. Dans le cas de la carboxyméthylation, les fibres de pâte de bois gonflent formant des structures ballonnées; ceci

est principalement causé par répulsion électrostatique. Pendant le gonflement des fibres carboxyméthylées (CMF), les couches S1 sont principalement responsables de la formation de ballons et de colliers, les couches S2 pour l'étirage transversal et les couches S3 pour assurer la continuité. Afin d'éviter la formation de ballons, les contraintes physiques générées par les arrangements de fibres de cellulose dans les sous-couches secondaires doivent être effectivement libérés. En variant les types et degrés de post-traitement, les CMF peuvent produire soit des particules sphériques de gel ou de fragments de fibres avec des distributions large à propos des tailles. Les couches externes de CMF peuvent être soigneusement décollée pour avoir les couches S3 isolées des structures de fibres gonflées pour pouvoir faire la caractérisation supplémentaire. Les structures ballonnées des CMF fonctionnent comme des poches d'eau intrinsèques, donc démontrent une augmentation significative d'absorption de l'eau. Les CMF super absorbent peuvent être fait en pellicule avec des propriétés accordables comprenant la transparence, la résistance à l'humidité et de la sècheresse.

Chapter 1. Introduction

1.1 Pulp fibers

1.1.1 Wood cells

Wood is a heterocellular material where its cell types and arrangements depend heavily on the species. Tracheid is one of the cell types that carries two major functions: (1) supporting tree mass, (2) transporting water and nutrients from the root to the crown. Gymnosperms (softwoods) and primitive angiosperms (few hardwoods) are mainly composed of tracheids and ray cells [1]. As can be seen in **Figure 1-1a**, the dominant cell type of softwoods is tracheid – more commonly known as a fiber. Compared to softwoods, hardwoods have more advanced and complex structures with more specialized cells (**Figure 1-1b**). Hardwood tracheids and fibers are distinguishable from one another, as fibers take more evolved form of tracheids with enhanced structural rigidity. Hardwood fibers and tracheids mainly differ in their pit shapes and sizes. Fibers have smaller and less number of pit holes that are dot-like, whereas tracheids have large and conspicuous bordered pits [2]. Hardwood tracheids maintain their original functions, although water conduction is mainly done by other specialized cells, vessel elements. In most pulp and paper making contexts, however, the term hardwood fiber usually refers to a mixture of tracheids and fibers since separating these two elements is extremely difficult.

Wood fibers are long slender hollow cylinders with a length in the range between 0.5 – 4 mm, width 20 – 50 μm, and wall thickness 2 – 10 μm [2]. Softwood fibers are generally longer than hardwood fibers, although the length, width and the wall thickness all vary largely even within a single tree. See **Table 1-1** for length and width distribution of common wood fibers. In a single tree, major distinctions in fiber properties are found between sapwood and heartwood, and between earlywood and latewood. Sapwood is the younger, softer, highly porous, outer part of a

tree; whereas heartwood is the older, harder, less hydrated, central part. Both sapwood and heartwood contain fibers that are produced in different seasons, which also exhibit different properties. Earlywood or springwood fibers have thinner walls, larger lumens (hollow interiors), and radial cross-sections; whereas latewood or summerwood fibers have thicker walls, smaller lumens, and rectangular cross-sections [3]. As described above, wood fibers encompass enormous heterogeneity. Consequently, wood processing and engineering play critical roles in controlling the quality of the final wood based products, as they can refine this highly heterogeneous starting material to serve a set purpose.

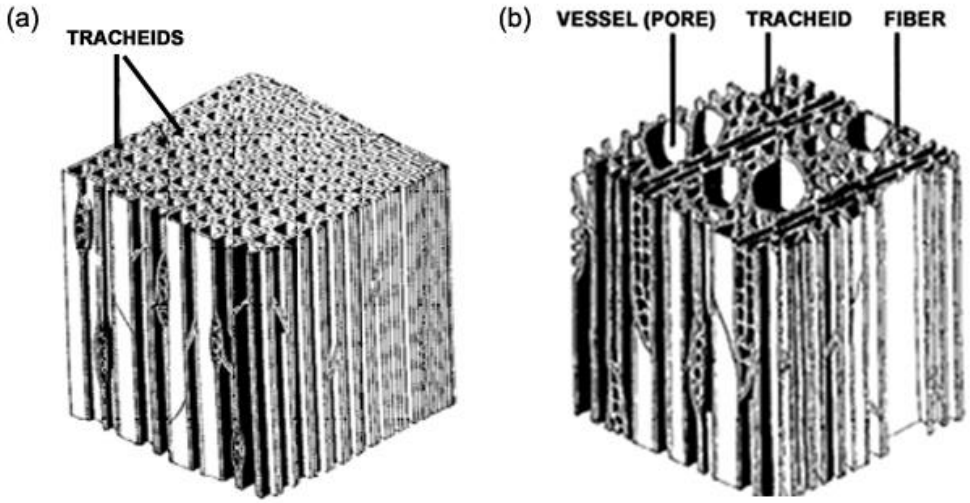

Figure 1-1. Schematic diagrams of (**a**) softwood and (**b**) hardwood cell wall cross-sections. Reprinted with permission from reference [4]. Copyright © Texas A&M University.

Table 1-1. Fiber length and width distribution of commonly used softwood and hardwood fibers

	Common name	Fiber length (mm)		Fiber width (μm)		Reference
		Average	Range	Average	Range	
Softwoods	Douglas fir	3.9	1.7-7.0	35-45		[5]
	Spruce	3.4	1.1-6.0	31	21-40	[6]
	Pine	3.2	0.5-4.9	39	16-60	[7]
Hardwoods	Eucalyptus	1.1	0.3-1.5	20	10-28	[8]
	Oak	1.1	0.5-1.6	23	14-30	[8]
	Birch	1.3		25		[9]

1.1.2 Chemical composition

The three major chemical components of the fibers are cellulose, hemicellulose, and lignin. Cellulose is providing the fiber backbone in a matrix of hemicellulose and lignin, while being mainly responsible for the mechanical strength of pulp fibers (see ***Table 1-2***). Although lignin has been traditionally considered as a waste from pulping and bleaching process, recent studies have shown that lignin can be utilized as precursors in chemical synthesis, organic electronics and such [10–12]. Hemicelluloses are carbohydrates that are usually branched. Commonly found hemicelluloses are galactoglucomannans, arabinoglucuronoxylans, methylated polygalacturonic acid, and glucuronoxylan. Hemicelluloses found in softwoods are galactoglucomannans, arabinoglucuronoxylans, and pectin such as methylated polygalacturonic acid. In hardwoods, it is mainly glucuronoxylan.

Cellulose is a linear polysaccharide consisting of glucose units connected by β-1, 4-linkages. Cellulose chains have a tendency to form intra and intermolecular hydrogen bonding. Such tightly bound cellulose chains form partly ordered crystalline regions and partly disordered amorphous regions. Repeating units of crystalline and amorphous cellulose form nanofibers, microfibers, and then wood cell walls. Hierarchical cellulose structure is illustrated in **Figure 1-2**. Native celluloses have crystalline structures called cellulose I_α and I_β, corresponding to a chain triclinic and a two-chain monoclinic unit cell, respectively. Cellulose I_α and I_β usually coexist in higher plants, although it is dominantly I_β in woods [13]. Cellulose I is a thermodynamically metastable form with a parallel structure and this allomorph has been considered to be produced only by living organisms, although this is still controversial. Out of other cellulose crystalline allomorphs (cellulose I, II, III_I, III_{II}, IV_I and IV_{II}), cellulose II is

another most common form as its antiparallel structure makes the crystal thermodynamically stable. Once interfibrillar hydrogen bonding is disrupted, for example by alkaline treatment, cellulose chains are recrystallized to form cellulose II. Amorphous cellulose regions are thought to be imperfections created during cellulose crystallization, and are more prone to the chemical reactions. Cellulose chemistry will be discussed later in more detail (section 1.1.4).

Table 1-2. Strength of cellulose, hemicellulose, and lignin

	Longitudinal Young's modulus (GPa) [14]	Tensile strength (MPa) [15]
Cellulose	90 – 140	750 – 1080
Hemicellulose*	2.0 [16], 8 [17]	-
Lignin	3.1	25 – 75

*Values reported from two different literature sources: [16] Salmen (2004); [17] Cousins (1978)

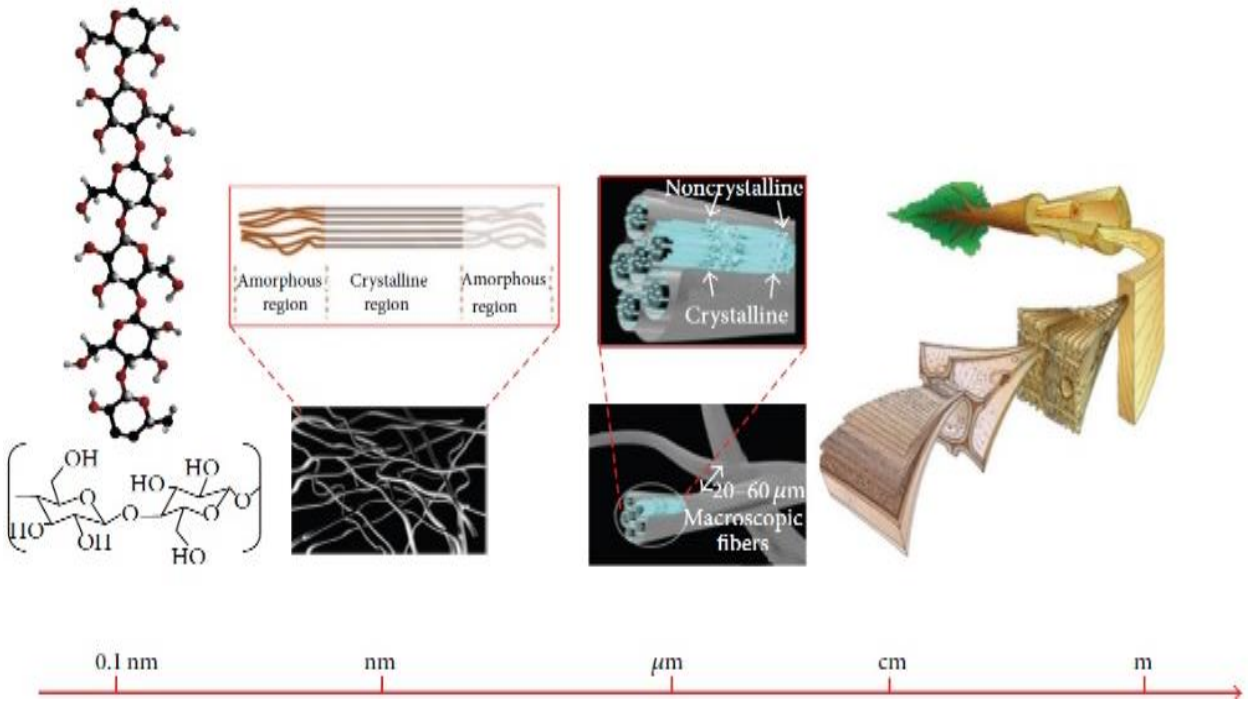

Figure 1-2. Hierarchical structure of cellulose (n = degree of polymerization, DP = typically around 10,000) from wood cell walls to microfibrils, nanofibrils, and cellulose chains (right to left). Reprinted with permission from reference [18]. Copyright © 2014 Yongfeng Luo et al.

Table 1-3. Chemical composition (weight %) of common softwood (top) and hardwood (bottom) fibers [19]

	Cellulose (%)	Hemicellulose (%)			Lignin (%)
		Glucomannan	Glucuronoxylan	Others	
Norway spruce	41.7	16.3	8.6	3.4	27.4
Scots pine	40.0	16.0	8.9	3.6	27.7
Eucalyptus (River red gum)	45.0	3.1	14.1	2.0	31.3
Silver birch	41.0	2.3	27.5	2.6	22.0

Kraft pulping is one of the most commonly used methods in producing cellulose pulp fibers. In this process, wood chips are treated with a mixture of sodium hydroxide and sodium sulfide under high pressure [19]. Pulping is intended to liberate, break down, and dissolve lignin without disrupting the cellulose backbone as much as possible. The kraft process is usually accompanied by a bleaching step, which removes the residual lignin to achieve high brightness. Although each fiber species contain different amounts of lignin (***Table 1-3***), fibers lose 20 – 30% of their total weight upon lignin removal. This results in more porous fiber structures, which enhances chemical accessibility.

1.1.3 Cellulose arrangement

Cellulose microfibrils are arranged in a tracheid by forming multiple concentric layers. A schematic diagram of a typical tracheid is shown in **Figure 1-3**. These layers are defined by cellulose arrangements in wood cell walls as they abruptly change from one layer to the other. From outside towards lumen (the hollow cavity inside the fiber) the layers are called middle lamella (ML), primary wall (P), and secondary wall (S). Secondary wood cell walls, or secondary layers, are subdivided into three layers: S1, S2, and S3 layers. ML is composed of almost all lignin, P contains mainly lignin, and S contains mostly cellulose and hemicellulose.

See ***Table 1-4*** for typical chemical distribution in P and S layers in volume (v) and weight (w) fractions. Kraft pulping completely removes the ML and a substantial amount of P. Cellulose rich S-layers survive the pulping process, therefore, it is mainly the S layers that are discussed in the literature when kraft fibers are used as a starting material.

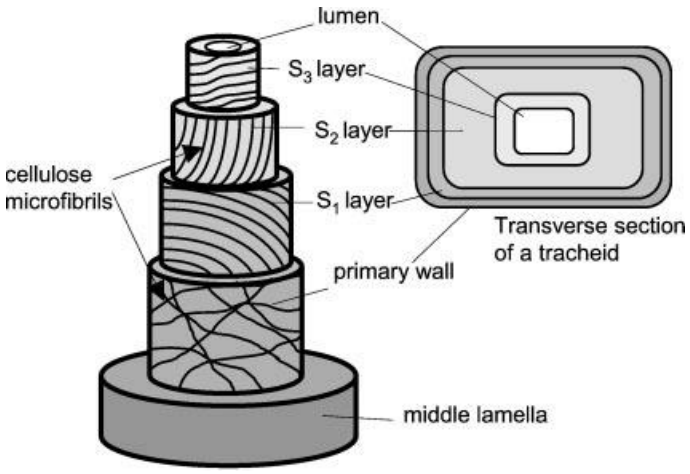

Figure 1-3. Ultrastructure of a typical tracheid. Reprinted with permission from reference [20]. Copyright © 2001 American Society of Plant Biologists

Table 1-4. Chemical distribution in wood cell layers by volume (v) and weight (w) fractions [14]

	Cellulose		Hemicellulose		Lignin	
	v	w	v	w	v	w
P	0.12	0.15	0.26	0.32	0.62	0.52
S1	0.35	0.28	0.30	0.31	0.35	0.41
S2	0.50	0.50	0.27	0.31	0.23	0.19
S3	0.45	0.48	0.35	0.36	0.20	0.16

The secondary cell wall is structured in such a way that the thickest S2 layer is sandwiched between the two thin S1 and S3 layers. The S2 layer contributes more than 90% of the total fiber mass; hence it dictates the overall fiber properties. See ***Table 1-5*** for average S layer thicknesses and their microfibril orientations for Norway spruce (softwood). It is the

microfibril arrangements that differentiate S1, S2, and S3 layers, which in turn, profoundly affect the fiber stiffness. The term microfibril angle (MFA) is used to express the deviation of the microfibril orientation from the long axis of the fiber. As can be seen in ***Table 1-5***, S1 and S3 microfibrils have much larger angles than those of S2 microfibrils. It is believed that the superior mechanical properties of cellulose wood fibers arise from the alternating microfibrils in the three S layers.

Table 1-5. Secondary layer thickness and microfibril angles. Average (left) and Norway spruce (right). EW = earlywood, LW = latewood.

	Average thickness (μm) [19]	Average MFA (°) [19]	Norway spruce		
			EW (μm) [21]	LW (μm) [21]	MFA (°) [14]
S1	0.2 – 0.3	50 – 70	0.26	0.38	70 – 90
S2	1 – 5	20 -30 (EW); 5 – 10 (LW)	1.66	3.69	30 (EW); 2 – 10 (LW)
S3	0.1	50 – 90	0.09	0.14	40 – 90

Early- and latewood fibers exhibit differences in MFA, wall thickness, and density. These differences result changes in longitudinal modulus of elasticity, where MFA alone accounts for more than 86% of the variation [1]. High MFA that are seen in juvenile, or earlywood fibers result in low Young's modulus and affect largely the longitudinal shrinkage upon drying. Mature, or latewood fibers show lower MFA, hence they exhibit increased Young's modulus while experiencing transverse shrinkage upon drying. Since MFA is a direct indicator of the pulp fiber quality, an extensive amount of studies has been done to accurately measure MFA and their variations between species, earlywood and latewood, tension wood and compression wood, etc. [1,22,23].

Numerous techniques have been applied to measure MFA such as x-ray diffraction (XRD), confocal laser scanning microscopy (CLSM), small and wide angle x-ray scattering

(SAXS, WAXS), polarization light microscopy (PLM), near infra-red (NIR), transmission electron microscopy (TEM), scanning electron microscopy (SEM) and so on. Each technique has its own limitations and the results obtained by them may or may not show significant discrepancy. For example, earlywood and latewood cells of Norway spruce were measured to be 9.0 (EW) and 8.1 (LW) by XRD [24] but 5 (EW) and 20 (LW) by SAXS [25]. It is difficult to point out the specific cause of this disagreement because of the intrinsic variance of MFA in pulp fibers. One of the most widely used methods in measuring MFA is XRD, in which the cellulose fibril orientations is determined by using the parameter derived from the (002) plane diffraction. XRD displays an advantage over other techniques such as giving MFA distribution in the cell wall and the shape of the cell wall cross sections [26].

1.1.4 Microscopy of cellulose fibrils

Commonly used microscopic techniques such as differential interference contrast (DIC) and phase contrast microscopy are not ideal in imaging birefringent materials such as cellulose fibers. As they operate by altering the phase of light, bundles of anisotropic cellulose crystals show a characteristic bright halo when white light is used as a light source. Hoffman modulation contrast (HMC), on the other hand, has a modulator disk which alters the amplitude of the scattered light instead. Changing the zeroth order maxima without disturbing the phase relationship of the light passing through the anisotropic material allows one to obtain the more likely representation of the specimen. HMC is able to produce a pseudo 3D representation of highly transparent materials unlike most bright field microscopy where the specimen appears to be invisible. Cross-polarization microscopy is also widely used in cellulose research as it is an excellent tool in determining the orientation of optically anisotropic elements [27].

1.2 Carboxylating pulp fibers

Cellulose has three hydroxyl groups in each anhydroglucose unit in C2, 3, and 6 positions (see **Figure 1-4**). The presence of these chemically reactive hydroxyl groups enables the functionality tailoring of cellulose chains. Cellulose derivatives such as cellulose acetate/triacetate and carboxymethyl cellulose (CMC) have been extensively studied and are currently used in medicine, food, and textile industries. The degree of hydroxyl group conversion is expressed in degree of substitution (DS), with the maximum DS being 3. The unit *mmol of substituted hydroxyl groups per gram of cellulose (mmol/g)* is also interchangeably used, where

$$\text{DS} = 3 = \frac{1}{0.162\ (\text{g/mmol cellulose})} \times 3\ \text{equiv. OH groups} \approx 18\ \text{mmol/g}.$$

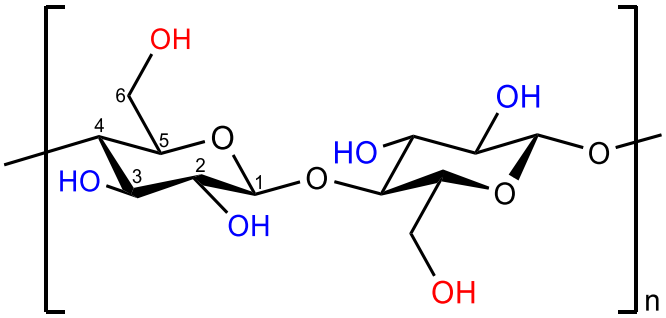

Figure 1-4. Cellulose structure. Reactive primary C6-OH groups (O6) are denoted in red, secondary C2, C3-OH (O2 and O3) are in blue.

Cellulose reactivity is considered to be one of the most critical factors in parameterizing optimum derivatization conditions. Different levels of cellulose reactivity between wood species and the extent of purification have been reported. For example, hardwood kraft pulp fibers show higher reactivity than sulfite pulp; sulfite pulp fibers from western hemlock show greater reactivity than those from southern pine [28]. As cellulose chains mainly exist as well ordered crystals, it is extremely difficult to completely solvate the cellulose fibers in most common solvents. Along with the complicated cellulose fibril arrangements, their insolubility causes

accessibility issues during the derivatization. Pretreatments such as mechanical refining and or prolonged fiber steeping are, therefore, often required to achieve higher yield.

Hydroxyl groups in cellulose chains can be replaced by carboxylates either selectively or non-selectively in aqueous media. Newly introduced carboxyl groups allow wide ranges of further chemical modifications, such as crosslinking, hydrophobizing, and grafting sensors or antibodies. Commonly used chemistries are (1) carboxymethylation, (2) periodate-chlorite oxidation, (3) TEMPO-mediated oxidation, and (4) enzymatic treatment.

1.2.1 Carboxymethylation

Carboxymethyl cellulose (CMC) is one of the most commonly used cellulose ethers because of its non-toxic and hypoallergenic nature. Due to its high viscosity and high surface charge group availability, it shows thickening properties, high water absorbency, good compatibility with mucous membranes, and film forming abilities. CMC is added into ice creams, eye drops, fat free products, toothpaste, detergents, textiles, etc., and is mass produced in North and South America as well as in Eastern Europe.

Carboxymethylation involves two spontaneously occurring competitive reactions [29].

$$\text{Cellulose–OH} + \text{ClCH}_2\text{COOH}^* + 2\ \text{NaOH} \rightarrow \text{Cellulose–OCH}_2\text{COONa} + \text{NaCl} + 2\ \text{H}_2\text{O} \quad (1)$$

$$\text{ClCH}_2\text{COOH} + \text{NaOH} \rightarrow \text{HOCH}_2\text{COONa} + \text{NaCl} \quad (2)$$

*where ClCH_2COOH (chloroacetic acid) is often referred to a CMA (carboxymethylating agent)

CMC can be prepared both heterogeneously and homogeneously by varying the solvent systems. Performing this reaction in water makes the side reaction (2) more dominant. As an alternative, solvent systems such as a 2-propanol-water mixture or a benzene-ethanol-water mixture are used where carboxymethylation proceeds completely heterogeneously [30]. A 2-propanol/water mixture is called a conventional medium in CMC production, and is currently the

most widely used solvent system for this chemistry. For softwood cellulose fibers, DS reported is as high as 1.24 (equivalent of [COO] = 7.44 mmol/g) [31] and the substitution is preferred in the order O6 ≥ O2 > O3. Carboxymethylated bacterial cellulose (BC), Avicel and cotton linters do not show any substantial differences in terms of substitution patterns. BC gives lower DS than wood fibers in comparable conditions and it requires higher DS (~1.5, equiv. of [COO] = 9.0 mmol/g) to be fully solubilized in water [32]. Considering that the slurry gives layer-by-layer heterogeneous reaction, this phenomenon is most likely due to the fact that BC has higher crystallinity with larger crystal sizes.

A complete cellulose dissolution is required in order to achieve homogeneous phase carboxymethylation. Cellulose can be dissolved in a few selected solvents (see section 1.4) in which carboxymethylation was attempted: LiOH/urea, $Ni(tren)(OH)_2$, $LiClO_4 \cdot 3H_2O$, N-methyl-morpholine-N-oxide (NMMNO), and 1-N-butyl-3-methylimidazolium ($Bmim^+$) [33–35]. Qi et al. prepared CMC in LiOH/urea without addition of NaOH, taking advantage of the inherent basicity of the solvent system [33]. They did not find any differences in regioselectivity between their homogeneous and the conventional heterogeneous reaction systems, which agrees with findings from Heinze and Liebert [34]. The fact that varying the solvent system does not affect the substitution patterns suggests that the cellulose etherification is not driven by diffusion, in which case the substitution should be random. Carboxymethylation in ionic liquids proceeds homogeneously as well, but causes severe cellulose chain degradation [35]. CMC prepared in NMMNO/DMSO mixtures yield DS of 1.8 (equiv. of [COO] = 10.8 mmol/g) [36] which is a lot higher than the maximum DS value achieved by heterogeneous reactions.

In preparation of CMC, an alkaline reaction condition is required to activate cellulose hydroxyl groups. Sodium hydroxide or any other comparable lye can be used for this purpose.

Above 12 to 15% lye concentration, cellulose crystal structures are disrupted by including NaOH and water molecules within the crystals [37]. This so-called "intercrystalline swelling" or mercerization occurs during alkaline treatments and is commonly used in textile industries to give cellulose fibers a lustrous appearance and high affinity for dyes. During carboxymethylation, the lye concentration governs the overall DS as temperature nor reaction time significantly affect DS when higher NaOH concentrations are used (typically above 30%). Unlike varying the solvent systems, varying NaOH concentrations can cause slightly different substitution patterns (O2 ≥ O6) [31]. The DS increases with an increased amount of NaOH to a certain extent. With an excess amount of NaOH, the formation of sodium glycolate ($HOCH_2COONa$, side product) becomes a predominant reaction; hence the DS decreases. Alkaline treatments and their contribution to fibers swelling will be discussed in section 1.4.1.

Increased amount of chloroacetic acid (carboxymethylating agent, CMA; $ClCH_2COOH$) results in higher DS at a set NaOH concentration and the maximum DS can be reached at a molar ratio of cellulose : CMA = 1 : 2.05 [29]. This is most likely due to the increased accessibility of CMA to the bulky cellulose hydroxyls, by bringing them into closer proximity. Performing carboxymethylation at 55℃ for 3 to 4 hours gives maximum DS at a given reagent concentration regardless of the cellulose fiber sources and solvent systems [29,31,36,38–40]. Authors state that below this temperature and reaction time, the reaction is not facilitated enough to give an optimum DS; above it, cellulose chains suffer from severe degradations. Cellulose degradation is undesirable as losing chain length directly results in the reduced mechanical strength.

1.2.2 Periodate-chlorite oxidation

Periodate oxidation is a regiospecific reaction which has been widely used to determine structures of complex carbohydrates as well as. See **Figure 1-5** for a reaction scheme. When

applied to cellulose, each C2 – C3 bond of the glucopyranose ring is cleaved and vicinal hydroxyl groups are converted into 2,3–dialdehyde per consumption of one equivalent of periodate. Periodate oxidation on cellulose present problems in low reactivity, chain scission, and low yield [41]. Studies have shown that this aqueous chemistry preferentially attacks more accessible amorphous regions prior to disrupting highly ordered crystalline regions. As a result, utilizing cellulose wood fibers with 60 – 70% crystallinity often requires prolonged reaction time, which is leading to a severe chain degradation. Periodate oxidation can be improved by pretreating the fibers using different types of salt, temperature and reaction time [42–45].

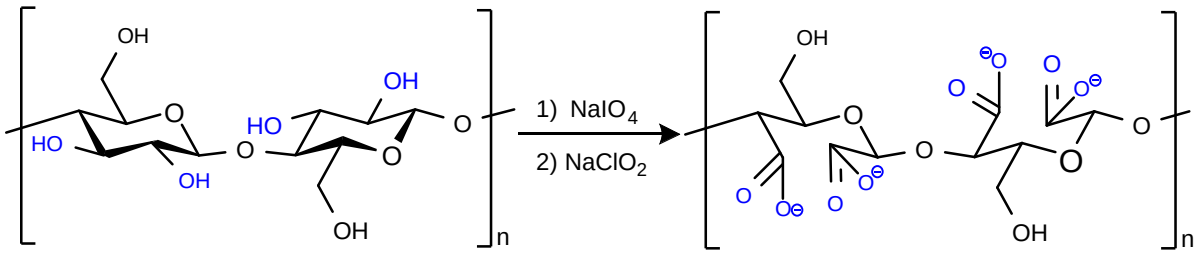

Figure 1-5. Reaction scheme of periodate, followed by chlorite oxidation of cellulose.

Metal chloride such as LiCl, $ZnCl_2$, and $CaCl_2$ actively participates in disrupting intermolecular hydrogen bonding which improves the low cellulose accessibility [46]. Due to the presence of nanopores in cellulose fibers, reaction kinetics can be improved by creating a concentration gradient with an addition of inert salt (NaCl), thereby shifting the Donnan equilibrium [42]. Despite the fact that sodium metaperiodate ($NaIO_4$) decomposes at 55℃, improved reaction yield and kinetics have been shown when the reaction was done at higher temperatures for shorter periods of time with higher $NaIO_4$/cellulose ratio [44].

Dialdehyde cellulose (DAC) prepared from periodate oxidation can then be converted into dicarboxyl cellulose (DCC) upon chlorite oxidation. This subsequent oxidation is done in

slightly acidic aqueous media in the presence of sodium chlorite. DAC already provides anchoring sites for further chemistry which is especially versatile with amino functionality. However, DAC solubilizes in water only after substantial amount of heating. Heating the DAC suspension is not always desired due to the chain degradation and increase in polydispersity [47]. By applying chlorite oxidation which converts non-charged dialdehyde groups into charged dicarboxylates, the modified cellulose chains can be readily solubilized without prolonged thermal treatments. Improved water compatibility allows further water based functionality modifications, which will be discussed further in section 1.3.

Recently, partial periodate-chlorite oxidation has been used to produce cellulose nanofibers (CNF) as well as highly charged nanocrystalline cellulose (electrosterically stabilized nanocrystalline cellulose, ENCC) [48]. This oxidation chemistry is applied prior to mechanical treatment to facilitate nanofibrillation. Converting vicinal alcohols into carboxylic acids not only disrupts the original interfibrillar hydrogen bonding but also introduces electrostatic repulsion with carboxyl contents starting from 0.38 mmol/g. Periodate-chlorite oxidized fibers significantly reduce the amount of mechanical energy required to produce CNF. Authors claim that the major properties of this dicarboxylated CNF are comparable to those prepared from TEMPO-mediated oxidation in terms of required oxidation level, viscosity, and transmittance of the films [49]. Dicarboxylated CNF, however, has an average width approximately 5 to 10 times thicker than TEMPO oxidized CNF. One advantage of applying this chemistry to cellulose fibers is that the native cellulose I structure is not disrupted. CNF and ENCC produced from periodate-chlorite oxidation maintain the cellulose I crystalline structure, most likely because the reaction preferentially occurs in amorphous regions without causing the intercrystalline swelling. Although it is still controversial, one of the most likely mechanisms is that the amorphous

regions are oxidized first, then the crystalline parts are modified from an outer layer towards the core and peel off the oxidized chains [50].

1.2.3 Other chemistries

TEMPO, 2,2,6,6-tetramethylpiperidine-1-oxyl radical, is a water soluble, stable radical which is used as a catalyst to convert primary alcohols to carboxylates. In this reaction, sodium bromide is used as a co-catalyst and sodium hypochlorite as a primary oxidant [51]. Similar to periodate-chlorite oxidation, TEMPO oxidation does not disrupt the crystalline structure either. Assuming that entire surface of the cellulose crystals can be converted, the theoretical maximum charge content one can obtain is approximately 1.7 mmol/g. Experimental findings have shown that wood fibers can easily reach this theoretical maximum, but bacteria cellulose stay below 1 mmol/g at comparable experimental conditions [52]. This chemistry is widely used to facilitate nanofibrillation. TEMPO-oxidized cellulose nanofibrils, TOCN, can be made into self-standing or composite films, transparent aerogels, etc. TOCN films show some fine qualities such as high transparency (< 90%), extremely low oxygen permeability (< 0.0008 $mL \cdot \mu m \cdot m^{-2} \cdot day^{-1} \cdot kPa^{-1}$ at 0% RH), as well as superior mechanical strength (200 – 300 MPa tensile, 6 – 7 GPa Young's modulus) arose from the exceptionally high aspect ratio of individual TOCN (typically above 200) [53–56].

Other commonly performed chemistries involve: acid hydrolysis for the production of NCC [57–60], enzymatic treatment for cellulose dissolution [61,62], and quaternization for preparing positively charged NCC [63]. Although each chemistry can be described by distinguishably different mechanisms, they often suffer from reduced accessibility, low yield, chain degradation and wide distribution of particle sizes and/or cellulose chain length. It is apparent that such high heterogeneity is originated from the native wood fiber structure itself,

which presumably gets worse as chemistry proceeds. We believe that the reduced accessibility of cellulose during the course of chemical reaction is induced by the structural changes that pulp fibers go through. In the following chapters, we will explore how chemically altered fiber structures affect the fiber properties.

1.3 Further chemical modifications

Carboxylated pulp fibers have readily available carbonyl groups which can be easily tailored further in aqueous media. Dying, fluorescent tagging, crosslinking, and hydrophobization can be done by simple bioconjugate chemistry, vapour deposition, polymer grafting and click chemistry. Bioconjugate chemistry often requires carbodiimide as an activator, for example, EDC (1-ethyl-3-(30dimethylaminopropyl) carbodiimide hydrochloride) in water based reactions, DCC (N,N'-Dicyclohexylcarbodiimide) in organic solvents. Note that neither EDC nor DCC are catalysts as they are both consumed completely and are not regenerated unless going through an extra regeneration treatment.

Figure 1-6 shows a reaction scheme of EDC coupling reaction. The chemistry occurs in support with NHS (N-hydroxysuccinimide) to form amide bonds from conjugating carboxylic acids with primary amine groups. The role of NHS is to stabilize the active intermediate to ensure the amide conversion in complete. Carboxylated cellulose undergoes this coupling reaction at slightly acidic pH 4.5 – 6. Diamines can substitute primary amines and be used as cross-linkers to enhance mechanical properties or to form hydrogels. Amine or diamine chain length has to be carefully chosen since longer chains introduce solubility problems. Tagging pulp fibers with fluorescent derivative, crosslinking fibers after embedding CMC into pores using water soluble dihydrazide crosslinkers, hydrophobizing the TOCN surface have been attempted and reported in literatures [64–68].

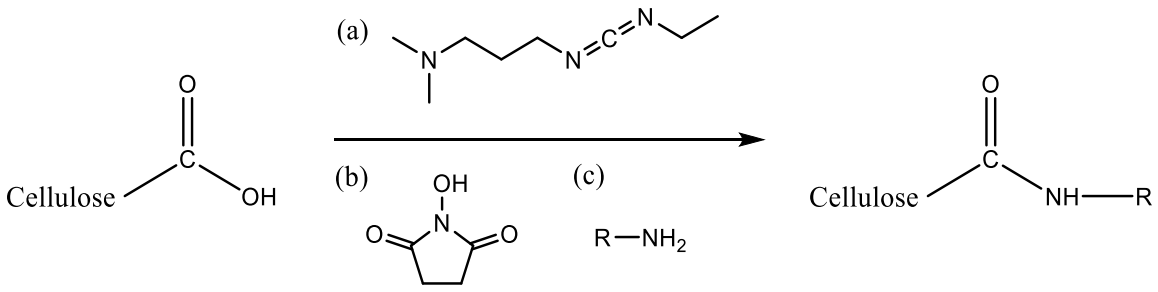

Figure 1-6. Aqueous bioconjugate chemistry applied on carboxylated cellulose. Reaction done at pH 4 -5. (**a**) EDC, (**b**) NHS, (**c**) primary amine where R = H, $(CH_2)_nCH3$.

The hydrophilic nature of carboxylated fibers is not always desirable for some applications, therefore, surface hydrophobization is often required to extend the field of applications. Vapour deposition of alkyl ketene dimers (AKD), alkenyl succinic acid anhydrides (ASA), methyltrichlorosilane (TCMS) can hydrophobize cellulose fibers or the films that are made from them [55,69,70]. Using cellulose or cellulose derivative as a substrate, living radical graft copolymerization, nitroxide-mediated polymerization, atom transfer radical polymerization can all be performed [71]. Recently, click chemistry is also employed to crosslink or to graft polymer chains onto the cellulose nanofibers with high yield [72–76].

1.4 Swelling of pulp fibers

Most cellulose fiber treatments partially or completely damage the native fiber structures. Such structural damages reduce compressive forces in the fibers, thereby inducing swelling. Swollen wood fibers typically form “balloons” and “collars” which refer to highly swollen and tightly wound regions respectively (see **Figure 1-7**). This “ballooning” effect has been shown during fiber dissolution in many conventional solvents, carboxymethylation, TEMPO-mediated oxidation followed by gentle mechanical treatment, and mechanical fibrillation. ***Table 1-6*** summarizes different systems which have reported ballooning phenomena. The ballooning is a

ubiquitous phenomenon where it can be seen in wide ranges of fiber sources and chemical environments.

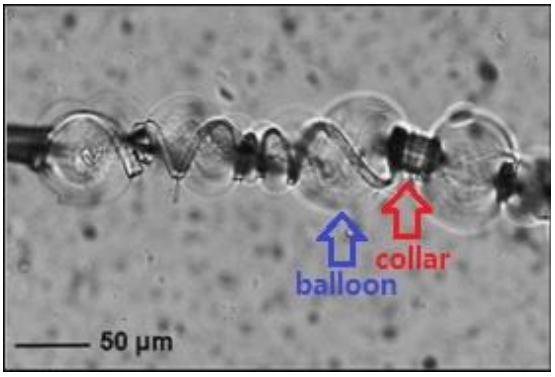

Figure 1-7. Swollen cotton fibers in NMMO/water (80/20) showing balloon-like structures. Reprinted with permission from reference [77]. Copyright © 2008 Wiley-VCH Verlag GmbH & Co.

Table 1-6. Systems and sources of cellulose fibers showing ballooning effect

System	Fiber source	Pulping	Ref
	Cotton	Bleached	
NaOH/25%water	Softwood (pine)	Vapour hydrolysis	[78]
	Softwood (fir)	Acid process	
79% NMMO/water	Cotton lint	Defatted/bleached	[79]
EtOH/HCl pretreatement	Softwood (spruce/pine:6/4)	Dissolving pulp	[80]
Carboxymethylation	Softwood	-	[81]
TEMPO-oxidation	Hardwood	Bleached, kraft	[82]
High-speed blender	Never-dried hardwood	Chlorite	[83]

The first appearance of balloons in fibrous cellulose is reported in 1864 by Nägeli [84], followed by several other papers reporting microscopic observations of structurally altered fibers undergoing chemical treatments [85–88]. The fiber deformation occurs mostly because of the disrupted intermolecular and interfibrillar hydrogen bonding networks. Depending on the DS and solvent effectiveness, fibers go through different stages and degrees of swelling. Mechanical

refining may also induce the same effect and promote the formation of balloon-like structures as well.

1.4.1 Solvent systems

Cellulose dissolution involves no functional derivatization. As cellulose chains associate with solvent molecules, fiber structures often loosen up and form balloons. Structural evolution of fibers may vary depending on the dissolution mechanism and the solvent quality is defined by it. Cuissinat and Navard categorized cellulose solvents into: (1) a good solvent that solvates cellulose fibers without ballooning, (2) a moderate solvent that induces swelling by ballooning which then eventually leads to a partial dissolution, and (3) a poor solvent that causes neither swelling nor dissolution [89]. Solvent systems such as sodium hydroxide at sub-zero temperatures (typically -5 to -8℃) or with urea, N-methylmorpholine oxide (NMMO), N,N-dimethylacetamide/lithium chloride (DMAc/LiCl), 1,3-dimethyl-2-imidazolidinone/LiCl (DMI/LiCl), dimethyl sulfoxide (DMSO)/tetrabutylammonium fluoride (TBAF) may fall into "good to moderate solvents" depending on the amount of water mixed with them [78,89–91]. More recently developed systems for cellulose dissolution are ionic liquids (ILs), which refer to salts that melt below 100℃ . ILs are considered to be "good solvents" and some examples are [C_4mim]OAc, [Amim]Cl, [Hemim]Cl, [C_2mim][(MeO)RPO_2], etc. Balloons formed during the dissolution process show balloon diameters ranging from 20 to 100 μm.

1.4.2 Chemical processes

Unlike fiber dissolution, cellulose derivatization permanently changes the chemical functionality and loosens the fiber structures. Upon replacing hydroxyl with more hydrophilic carboxyl groups, fibers become highly swollen by forming balloon-like structures that strikingly resemble those reported in the dissolution process. Derivatized balloons, however, show bigger

balloon sizes (50 to 200 μm) than the non-derivatized ones. This indicates that swelling can be enhanced by the electrostatic repulsion and the hydrophilic nature of the carboxyl groups. Depending on the chemistry applied, fibers may or may not require extra mechanical energy input to achieve balloon-like structures. For instance, TEMPO-oxidized wood fibers form balloons only after few days of magnetic stirring [82], whereas carboxymethylated fibers form balloons almost immediately [81]. When carboxymethylation is performed homogeneously, large amounts of CMC directly goes into solution without forming intermediate balloon-like structures [92].

1.4.3 Mechanical treatments

The two most common ways of refining pulp fibers are homogenization and microfluidization. Microgrinding and cryocrushing are also used for the same purpose but not as often. Homogenization is an energy intensive process where the fibers pass through rapid pressure drops, high shear, and impact forces typically around 10 – 20 times for nanofibrillation [93]. Microfluidizers are operated at higher pressures but at relatively constant shear rates and impact forces with less clogging problems compared to homogenizers [94]. Both homogenization and microfluidization are used to produce cellulose nanofibrils and studies have shown that fiber structures are severely damaged even at early stages of these mechanical treatments [58,95,96]. Uetani and Yano attempted nanofibrillation using a household high speed blender where they observed ballooning during the first 1 – 3 minutes of agitation [83]. As the treatment proceeds over time, balloons burst open and are fibrillated to liberate nanofibrils. This behaviour is not reported in most mechanical nanofibrillation processes, probably because more commonly used high pressure homogenizers or microfluidizers break the fibers into nanoscale

much more vigorously than household blenders. Findings in this thesis suggest that the degree of fiber refining may facilitate or suppress the ballooning effect.

1.5 Industrial applications

Superabsorbent polymers (SAP) are loosely cross-linked hydrophilic materials that can swell, absorb, and retain water. SAPs can swell up to 1000 times their own weight, which makes them extremely useful in areas where high water absorbency is required (i.e. personal hygiene products, tissue papers, wound dressing, etc.). Highly swollen SAPs form viscoelastic solid-like structures with internal percolating networks. The key in achieving high water absorbency is to create a system with a good ability to form 3D networks by tuning the degrees and types of the cross-linker [97]. The quality of hydrogel created by SAP is defined by its swelling capacity, reswellability, saline sensitivity, mechanical and thermal properties. SAP can be prepared from either natural or petroleum sources by applying conventional polymerization techniques. The final product can be in various forms such as nanoparticles, granules, fibers, membranes, etc. Although polysaccharide- or polypeptide-based biodegradable, natural polymers are available, most commonly used are acrylic acid based synthetic polymers that are prepared by inverse-suspension polymerization techniques mainly due to the low cost [98]. Synthetic polymers serve their role as a superabsorbent material but can cause skin dryness, rash, and irritation [99]. Partially carboxylated fibers are intrinsically hydrophilic where their water absorbency can be tailored by varying the DS. The main advantage of utilizing cellulose based superabsorbent materials in a fiber form is that their mobility is restricted once imbedded in a sheet. Granular SAPs, on the other hand, tend to migrate considerably and even flocculate upon wetting with saline water. The reduced surface areas of SAP granules cause undesirable deformation and restrict overall water absorbency [100]. The partially carboxylated fibers may not absorb water

as much as the synthetic polymer granules, but the fiber entanglement can enhance mechanical properties of the hydrogel. The strength of SAP composites are usually compromised to a certain extent by an increased water absorbency.

Aside from water absorbency, temporary wet strength is another important factor in preparing disposable products such as paper towels and sanitary tissues. Wet strength can be gained by enhancing the interfibriller bonding which resist breaking up against water [101,102]. One way to create this bonding is by adding cationic resins to the fiber networks that are naturally anionic. Since permanent wet strength is undesirable in most cases, resins with limited wet strength decay such as urea formaldehyde, melamine formaldehyde, and polyamide-epichlorohydrin are added as temporary strength enhancers [103]. Partially carboxylated cellulose fibers (CF) have both carboxylates and unreacted hydroxyl groups where the two groups in a close proximity can react to form esters when subjected to drying. The formation of the ester linkage is a reversible process, hence it increases the dry strength and temporary wet strength. CF can be, therefore, easily used in tissue making to serve multiple purposes – a dry strength enhancer, a temporary wet strengthener, and a superabsorbent. CF can also be used in "disappearing packages", a new market that is intended to reduce the paper waste. The main component of this packaging material is water soluble polymers which can dissolve away simply by wetting them.

1.6 Outline and scope of the thesis

Illustrated topics in the introduction to this thesis are the examples of commonly performed fiber treatments and the problems thereof. A long history of cellulose research provide us immense background knowledge. The technological platforms to utilize pulp fibers have been developed and improved over the centuries. However, high structural complexity of the fiber

structures leaves some of their key features still debatable and lots of obstacles in cellulose processing still exist. In order to transform the current treatment processes more green and cost efficient, it is critical to understand the structural dynamics of the cellulose fibers undergoing different chemistries and mechanical treatments. Newly obtained knowledge in this thesis may also help to bridge the well-known technology and the non-conventional cellulose markets. We present exemplary novel materials that are prepared from conventional chemical processing as well.

Chapter 2 elucidates structural changes in selectively damaged cellulose pulp fibers. Swollen fiber structures and their properties can be tuned by varying the chemistry or by applying pretreatment. Carboxymethylation and periodate-chlorite oxidation are performed as swelling aids; while non-refined and refined pulp fibers are used to study the effect of the mechanical pretreatment. Based on microscopic analysis of the swollen fiber structures, a close relationship between microfibril arrangements in the secondary layers and the ballooning effect is recognized. Swollen fiber models are proposed to illustrate how each S-layer promotes or hinders the overall structural deformation. Understanding structural evolution during pulp fiber treatment may affect largely in resolving some of the issues in cellulose derivatization, such as restricted accessibility. The results of this research have been published in the following paper: G. Sim, Md Alam, L. Godbout, T.G.M van de Ven. Structure of swollen carboxylated cellulose fibers. Cellulose (2014) 21 (6): 4595-4606. Md Alam provided training for chemical reactions and Louis Godbout contributed to the proofreading.

Chapter 3 and 4 describes how different post treatments can result greatly variable structural features.

Chapter 3 takes a closer look at the structures of highly swollen carboxymethylated fibers upon breaking up. Balloon-like swollen fiber structures have areas of different structural rigidity; hence intense agitation preferentially damages the weaker parts the swollen fibers and yield structures that are dominantly spherical. A prevailing feature of the spherical gel-like particles is the donut-shaped interior structure that consists of highly concentrated carboxymethylated cellulose chains. We propose a break-up mechanism of the balloon-like structure under intense mechanical treatment. The results of this research have been published: G. Sim and T.G.M. van de Ven. Spherical cellulose gel particles with donut-shaped interior structures. Cellulose (2015) 22:2, 1019-1026.

Chapter 4 describes features of isolated S3 layers from highly swollen carboxymethylated wood fibers. Due to the high complexity and extremely thin layer thickness, S3 layer has never been isolated for characterizations. Our current knowledge about the innermost S3 layer relies solely on cross-sectional microscopic studies and x-ray diffraction data. After carefully peeling off the outer S1 and S2 layers, partially carboxymethylated S3 layers can be successfully isolated and their chemical reactivity, microfibril angles, handedness, and dried layer thicknesses are examined and compared with the literature data. The results of this study have been published in the following paper: G. Sim and T.G.M. van de Ven, The S3 layer isolated from carboxymethylated cellulose wood fibers, Cellulose (2015) 22:1, 45-52.

Chapter 5 demonstrates exemplary products prepared from partially carboxymethylated pulp fibers. A wide range of optical and mechanical properties can be obtained depending on the charge contents, pH, and drying conditions. Preparation and characterization of air-dried transparent films with an emphasis on their water absorbing abilities are discussed with suggested potential applications. The results of this research is to be submitted for publication:

G. Sim, Y. Liu, and T.G.M. van de Ven, Transparent films prepared from chemically modified cellulose fibers. Yanqing Liu performed water absorbency test.

Lastly, chapter 6 gives a summary of the research outcomes and how some findings from this work may contribute to current and future cellulose markets.

1.7 References

[1] Barnett JR, Bonham V. Cellulose microfibril angle in the cell wall of wood fibres. Biol Rev Camb Philos Soc 2004;79:461–72.

[2] Ilvessalo-Pfäffli M-S. Fiber atlas - Identification of papermaking fibers. Springer; 1995.

[3] Hamilton DL. Methods for conserving archaeological material from underwater sites 1999:22–3. http://nautarch.tamu.edu/CRL/conservationmanual/ConservationManual.pdf (accessed February 26, 2015).

[4] Bergander A, Salmén L. Cell wall properties and their effects on the mechanical properties of fibers. J Mater Sci 2002;7:151–6.

[5] Isenberg I. Pulpwoods of the United States and Canada. Vol I - Conifers. 1980.

[6] Trendelenburg R, Mayer-Wegelin H. Das Holz als Rohstoff 2. München: 1955.

[7] Sierra A, Simon J. Atlas de fibras para pasta de celulosa. I parte - coniferas. 1969.

[8] Ezpeleta L, JLS S. Atlas de fibras para pasta de celulosa II parte, Voll. 1970.

[9] Aitken Y, F C, C V. Constituants tibreux des pätes papiers et cartons. Pratique de l'analyse. 1988.

[10] Dallmeyer I, Ko F, Kadla JF. Electrospinning of Technical Lignins for the Production of Fibrous Networks. J Wood Chem Technol 2010;30:315–29.

[11] Sonar S, Ambrose K, Hendsbee AD, Masuda JD, Singer RD. Synthesis and application of Co(salen) complexes containing proximal imidazolium ionic liquid cores. Can J Chem 2011;90:60–70.

[12] Wu A, Patrick BO, James BR. Inactive ruthenium(II)-xantphos complexes from attempted catalyzed lignin reactions. Inorg Chem Commun 2012;24:11–5.

[13] Sugiyama J, Vuong R, Chanzy H. Electron diffraction study on the two crystalline phases occurring in native cellulose from an algal cell wall. Macromolecules 1991;24:4168–75.

[14] Neagu RC, Gamstedt EK, Stig LB, Lindström M. Ultrastructural features affecting mechanical properties of wood fibres. Wood Mater Sci Eng 2006;1:146–70.

[15] Gibson LJ. The hierarchical structure and mechanics of plant materials. J R Soc Interface 2012;9:2749–66.

[16] Salmen L. Micromechanical understanding of the cell wall structures. C R Biol 2004;327:873–80.

[17] Cousins WJ. Young's modulus of hemicellulose as related to moisture content. Wood Sci Technol 1978;12:161–7.

[18] Luo Y, Zhang J, Li X, Liao C, Li X. The cellulose nanofibers for optoelectronic conversion and energy storage. J Nanomater 2014;2014:13.

[19] Sjostrom E. Wood chemistry: Fundamentals and applications. Second edi. San Diego: Academic press; 1993.

[20] Plomion C, Leprovost G, Stokes A. Wood formation in trees. Plant Physiol 2001;127:1513–23.

[21] Brändström J. Micro- and ultrastructural aspects of Norway spruce tracheids: a review. IAWA J 2001;22:333–53.

[22] Lichtenegger H, Reiterer a, Stanzl-Tschegg SE, Fratzl P. Variation of cellulose microfibril angles in softwoods and hardwoods-a possible strategy of mechanical optimization. J Struct Biol 1999;128:257–69.

[23] Sedighi-Gilani M, Sunderland H, Navi P. Microfibril angle non-uniformities within normal and compression wood tracheids. Wood Sci Technol 2005.

[24] Sahlberg U, Salmen L, Oscarsson A. The fibrillar orientation in the S2-layer of wood fibres as determined by X-ray diffraction analysis. Wood Sci Technol 1997;31:77–86.

[25] Lichtenegger HC, Reiterer A, Stanzl-Tschegg SE, Fratzl P. Determination of spiral angles of elementary fibrils in the wood cell wall : comparison of small-angle X-ray scattering and wideangle X-ray diffraction. Microfibril angle wood, 1998, p. 140–56.

[26] Tabet T, Aziz F. Cellulose microfibril angle in wood and its dynamic mechanical significance. Cellulose-Fundamal aspect, 2013, p. 113–42.

[27] Sawyer L, Grubb D, Meyers G. Polymer microscopy. New York: Springer; 2007.

[28] Lewin M, Pearce EM. Handbook of fiber chemistry. 2nd edition. New York: Marcel dekker Inc; 1998.
[29] Khullar R, Varshney VK, Naithani S, Heinze T, Soni PL. Carboxymethylation of cellulosic material (average degree of polymerization 2600) isolated from cotton (Gossypium) linters with respect to degree of substitution and rheological behavior. J Appl Polym Sci 2005;96:1477–82.
[30] Zhao H, Cheng F, Li G, Zhang J. Optimization of a process for carboxymethylcellulose (CMC) preparation in mixed solvents. Int J Polym Mater 2003;52:749–59.
[31] Heinze T, Pfeiffer K. Studies on the synthesis and characterization of carboxymethylcellulose. Die Angew Makromol 1999;266:37–45.
[32] Schlufter K, Heinze T. Carboxymethylation of bacterial cellulose. Macromol Symp 2010;294:117–24.
[33] Qi H, Liebert T, Meister F, Zhang L, Heinze T. Homogenous carboxymethylation of cellulose in the new alkaline solvent LiOH/urea aqueous solution. Macromol Symp 2010;294:125–32.
[34] Heinze T, Liebert TIM. Carboxymethylation of cellulose in unconventional media. Cellulose 1999:153–65.
[35] Mikkola J. Ionic liquid-aided carboxymethylation of kraft pulp. International Journal of Chemical Reactor Engineering. 2010;8; Article A102.
[36] Heinze T, Koschella A. Carboxymethyl ethers of cellulose and starch - A review. Macromol Symp 2005;223:13–40.
[37] Klemm D, Philipp B, Heinze T, Heinze U, Wagenknecht W. Comprehensive cellulose chemistry. Weinheim, New York, Cichester, Brisbane, Singapore, Toronto: Wiley-VCH; 1998.
[38] Kálmán F, Borsa J, Kemény S, Rusznák I. Effect of the reaction conditions on the degree of substitution of carboxymethyl cellulose. Colloid Polym Sci 1988;720:716–20.
[39] Adinugraha MP, Marseno DW. Synthesis and characterization of sodium carboxymethylcellulose from cavendish banana pseudo stem. Carbohydr Polym 2005;62:164–9.
[40] Pushpamalar V, Langford SJ, Ahmad M, Lim YY. Optimization of reaction conditions for preparing carboxymethyl cellulose from sago waste. Carbohydr Polym 2006;64:312–8.
[41] Abbott a. P, Bell TJ, Handa S, Stoddart B. Cationic functionalisation of cellulose using a choline based ionic liquid analogue 2009:784–6.
[42] Alam MN, Antal M, Tejado A, Ven TGM. Salt-induced acceleration of chemical reactions in cellulose nanopores. Cellulose 2012;19:517–22.
[43] Sirvio J, Hyvakko U, Liimatainen H, Niinimaki J, Hormi O. Periodate oxidation of cellulose at elevated temperatures using metal salts as cellulose activators. Carbohydr Polym 2011;83:1293–7.
[44] Varma a. ., Kulkarni M. Oxidation of cellulose under controlled conditions. Polym Degrad Stab 2002;77:25–7.
[45] Coseri S, Biliuta G, Simionescu BC, Stana-Kleinschek K, Ribitsch V, Harabagiu V. Oxidized cellulose—Survey of the most recent achievements. Carbohydr Polym 2012.
[46] Dumitriu S. Polysaccharides: Structural diversity and functional versatility. 2nd editio. New York: Marcel Dekker: Crc Press; 2005.
[47] Kim UJ, Wada M, Kuga S. Solubilization of dialdehyde cellulose by hot water. Carbohydr Polym 2004;56:7–10.
[48] Yang H, Tejado A, Alam N, Antal M, van de Ven TGM. Films prepared from electrosterically stabilized nanocrystalline cellulose. Langmuir 2012;28:7834–42.
[49] Liimatainen H, Visanko M. Enhancement of the nanofibrillation of wood cellulose through sequential periodate–chlorite oxidation. Biomacromolecules 2012;13:1592–7.
[50] Kim UJ, Kuga S, Wada M, Okano T, Kondo T. Periodate oxidation of crystalline cellulose. Biomacromolecules 2000;1:488–92.
[51] Isogai A, Saito T, Fukuzumi H. TEMPO-oxidized cellulose nanofibers. Nanoscale 2011;3:71–85.
[52] Okita Y, Saito T, Isogai A. Entire surface oxidation of various cellulose microfibrils by TEMPO-mediated oxidation. Biomacromolecules 2010;11:1696–700.

[53] Saito T, Hirota M, Tamura N, Kimura S, Fukuzumi H, Heux L, et al. Individualization of nano-sized plant cellulose fibrils by direct surface carboxylation using TEMPO catalyst under neutral conditions. Biomacromolecules 2009;10:1992–6.
[54] Fujisawa S, Okita Y, Fukuzumi H, Saito T, Isogai A. Preparation and characterization of TEMPO-oxidized cellulose nanofibril films with free carboxyl groups. Carbohydr Polym 2011;84:579–83.
[55] Fukuzumi H, Saito T, Iwata T, Kumamoto Y, Isogai A. Transparent and high gas barrier films of cellulose nanofibers prepared by TEMPO-mediated oxidation. Biomacromolecules 2009;10:162–5.
[56] Kobayashi Y, Saito T, Isogai A. Aerogels with 3D ordered nanofiber skeletons of liquid-crystalline nanocellulose derivatives as tough and transparent insulators. Angew Chemie 2014;126:10562–5.
[57] Bai W, Holbery J, Li K. A technique for production of nanocrystalline cellulose with a narrow size distribution. Cellulose 2009;16:455–65.
[58] Klemm D, Kramer F, Moritz S, Lindström T, Ankerfors M, Gray D, et al. Nanocelluloses: a new family of nature-based materials. Angew Chemie 2011;50:5438–66.
[59] Edgar C, Gray D. Smooth model cellulose I surfaces from nanocrystal suspensions. Cellulose 2003:299–306.
[60] Revol J-F, Godbout L, Dong X-M, Gray DG, Chanzy H, Maret G. Chiral nematic suspensions of cellulose crystallites; phase separation and magnetic field orientation. Liq Cryst 1994;16:127–34.
[61] Pääkkö M, Ankerfors M, Kosonen H, Nykänen a, Ahola S, Osterberg M, et al. Enzymatic hydrolysis combined with mechanical shearing and high-pressure homogenization for nanoscale cellulose fibrils and strong gels. Biomacromolecules 2007;8:1934–41.
[62] Hermanson GT. Enzyme modification and conjugation. In: Hermanson GT, editor. Bioconjugate Tech., Academic press; 1996, p. 630–8.
[63] Pei A, Butchosa N, Berglund L a., Zhou Q. Surface quaternized cellulose nanofibrils with high water absorbency and adsorption capacity for anionic dyes. Soft Matter 2013;9:2047.
[64] Hu TQ, Hayak A. Cellulose Materials with Novel Properties, US 2012/0041183 A1. 2012.
[65] Nakajima N, Ikada Y. Mechanism of amide formation by carbodiimide for bioconjugation in aqueous media. Bioconjug Chem 1995;6:123–30.
[66] Tejado A, Antal M, Liu X, van de Ven TGM. Wet cross-linking of cellulose fibers via a bioconjugation reaction. Ind Eng Chem Res 2011;50:5907–13.
[67] Johnson RK, Zink-Sharp A, Glasser WG. Preparation and characterization of hydrophobic derivatives of TEMPO-oxidized nanocelluloses. Cellulose 2011;18:1599–609.
[68] Sabzalian Z, Alam MN, van de Ven TGM. Hydrophobization and characterization of internally crosslink-reinforced cellulose fibers. Cellulose 2014:1381–93.
[69] Zhang H, Kannangara D, Hilder M, Ettl R, Shen W. The role of vapour deposition in the hydrophobization treatment of cellulose fibres using alkyl ketene dimers and alkenyl succinic acid anhydrides. Colloids Surfaces A Physicochem Eng Asp 2007;297:203–10.
[70] Tejado A, Chen WC, Alam MN, van de Ven TGM. Superhydrophobic foam-like cellulose made of hydrophobized cellulose fibres. Cellulose 2014:1735–43.
[71] Roy D, Semsarilar M, Guthrie JT, Perrier S. Cellulose modification by polymer grafting: a review. Chem Soc Rev 2009;38:2046–64.
[72] Liebert T, Hänsch C, Heinze T. Click chemistry with polysaccharides. Macromol Rapid Commun 2006;27:208–13.
[73] Krouit M, Bras J, Belgacem MN. Cellulose surface grafting with polycaprolactone by heterogeneous click-chemistry. Eur Polym J 2008;44:4074–81.
[74] Koschella A, Hartlieb M, Heinze T. A "click-chemistry" approach to cellulose-based hydrogels. Carbohydr Polym 2011;86:154–61.
[75] Filpponen I, Argyropoulos DS. Regular linking of cellulose nanocrystals via click chemistry: synthesis and formation of cellulose nanoplatelet gels. Biomacromolecules 2010;11:1060–6.

[76] Pahimanolis N, Hippi U, Johansson L-S, Saarinen T, Houbenov N, Ruokolainen J, et al. Surface functionalization of nanofibrillated cellulose using click-chemistry approach in aqueous media. Cellulose 2011;18:1201–12.
[77] Le Moigne N, Montes E, Pannetier C, Höfte H, Navard P. Gradient in Dissolution Capacity of Successively Deposited Cell Wall Layers in Cotton Fibres. Macromol Symp 2008;262:65–71.
[78] Cuissinat C, Navard P. Swelling and dissolution of cellulose Part 1: Free floating cotton and wood fibres in N-Methylmorpholine-N-oxide–water mixtures. Macromol Symp 2006;244:1–18.
[79] Jeihanipour A, Karimi K, Taherzadeh MJ. Enhancement of ethanol and biogas production from high-crystalline cellulose by different modes of NMO pretreatment. Biotechnol Bioeng 2010;105:469–76.
[80] Trygg J, Fardim P. Enhancement of cellulose dissolution in water-based solvent via ethanol–hydrochloric acid pretreatment. Cellulose 2011;18:987–94.
[81] Stawitz VJ, Kage MP. Ü ber die quellungsstadien der wasserlöslichen celluloseäther und die übermolekulare Struktur der Cellulose. Das Pap 1959;13:567–72.
[82] Saito T, Kimura S, Nishiyama Y, Isogai A. Cellulose nanofibers prepared by TEMPO-mediated oxidation of native cellulose. Biomacromolecules 2007;8:2485–91.
[83] Uetani K, Yano H. Nanofibrillation of wood pulp using a high-speed blender. Biomacromolecules 2011;12:348–53.
[84] Nägeli C. Über den inneren Bau der vegetabilischen Zellmembranen. Sitzber Bay Akad Wiss Munchen 1864:282–323.
[85] Pennetier G. Note micrographique sur les alterations du cotton. Bull Soc Ind Rouen; 1883.
[86] Hock CW. Degradation of cellulose as revealed microscopically. Text Res J 1950;20:141–51.
[87] Flemming N, Thaysen A. On the deterioration of cotton on wet storage. Biochem J 1919;14:25–8.
[88] Tripp VW, Rollins ML. Morphology and chemical composition of certain components of cotton fiber cell wall. Anal Chem 1952;24:1721–8.
[89] Cuissinat C, Navard P, Heinze T. Swelling and dissolution of cellulose. Part IV: Free floating cotton and wood fibres in ionic liquids. Carbohydr Polym 2008;72:590–6.
[90] Cuissinat C, Navard P. Swelling and dissolution of cellulose, Part III: plant fibres in aqueous systems. Cellulose 2007;15:67–74.
[91] Le Moigne N, Bikard J, Navard P. Rotation and contraction of native and regenerated cellulose fibers upon swelling and dissolution: the role of morphological and stress unbalances. Cellulose 2010;17:507–19.
[92] Jardeby K, Lennholm H, Germgård U. Characterisation of the undissolved residuals in CMC-solutions. Cellulose 2004:195–202.
[93] Nakagaito a. N, Yano H. The effect of morphological changes from pulp fiber towards nano-scale fibrillated cellulose on the mechanical properties of high-strength plant fiber based composites. Appl Phys A Mater Sci Process 2004;78:547–52.
[94] Spence KL, Venditti R a., Rojas OJ, Habibi Y, Pawlak JJ. A comparative study of energy consumption and physical properties of microfibrillated cellulose produced by different processing methods. Cellulose 2011;18:1097–111.
[95] Stelte W, Sanadi AR. Preparation and Characterization of cellulose nanofibers from two commercial hardwood and softwood pulps. Ind Eng Chem Res 2009;48:11211–9.
[96] Siró I, Plackett D. Microfibrillated cellulose and new nanocomposite materials: a review. Cellulose 2010;17:459–94.
[97] Laftah WA, Hashim S, Ibrahim AN. Polymer Hydrogels: A Review. Polym Plast Technol Eng 2011;50:1475–86.
[98] Zohuriaan-Mehr MJ, Kabiri K. Superabsorbent polymer materials: a review. Iran Polym J 2008;17:451.
[99] Odio M, Friedlander SF. Diaper dermatitis and advances in diaper technology. Curr Opin Pediatr 2000;12:4:342-346.

[100] Knack I, Beckert W. Superabsorbent fibre flocks, methods for their production and application. US Patent 5002814, 1991.
[101] Van Luu P, Worry G, Marinack RJ, Ostrowski HS, Bhat DM. Prewettable high softness paper product having temporary wet strength. US Patent 6059928, 2000.
[102] Dunlop-Jones N. Wet-strength chemistry. In: Roberts JC, editor. Pap. Chem. SE, Springer Netherlands; 1991, p. 76–96.
[103] Mohammadi KP, Seward LO, Rasch DM. Soft tissue having temporary wet strength. US Patent 6149769. 2000.

Chapter 2. Structure of Swollen Carboxylated Cellulose Fibers

The results of this research have been published in the following paper:

G. Sim, M. N. Alam, L. Godbout, and T.G.M. van de Ven. Structure of swollen carboxylated cellulose fibers. Cellulose (**2014**) 21 (6): 4595-4606

Abstract

Structural changes in cellulose fibers were elucidated for carboxymethylated fibers and fibers that are oxidized by periodate and chlorite. Non-fibrillated and partially fibrillated softwood, kraft fibers (SKF, m-SKF) were carboxymethylated to investigate the contribution of the S1 layer to the swollen fiber structures. Carboxymethylated non-fibrillated fibers (CMF) form balloon-like structures as they swell heterogeneously. When partially fibrillated SKF is carboxymethylated (m-CMF), the fibers do not exhibit this ballooning phenomenon due to the degradation of the S1 layer. Carboxymethylation disrupts the native cellulose crystalline structure without breaking the fibers apart. Periodate-chlorite oxidized fibers (PCF), on the other hand, swell homogeneously without disrupting the native cellulose I crystalline form. Periodate-chlorite oxidation damages all three secondary layers to the extent that any microfibril confinement caused by the swelling is removed. Each chemistry and mechanical treatment affects the cellulose fibers differently to yield various swollen structures.

2.1 Introduction

Cellulose wood fibers are highly complex, multilayer composites that serve the role of maintaining the structure of green plants [1, 2]. The wood cell wall can be divided into the

middle lamella (ML), the primary wall (P), and the secondary wall (S) [3, 4]. Secondary layers (S) of the wood cell wall are mainly composed of helically wound reinforcing cellulose fibrils [5]; hence, the S layers are resistant to chemical pulping processes which remove almost all lignin and some hemicelluloses. The ML and P, with high lignin content, on the other hand, are almost completely disintegrated after the pulping process [6].

The secondary layer can be further divided into three successive layers, namely, S1, S2, and S3 [7]. The outermost S1 and the innermost S3 layers have 100 – 200 nm thin walls with microfibril orientation almost perpendicular to the fiber axis (microfibril angles, MFA, 70 – 90°). S2 is the thickest layer (~5 μm) in the cell wall with MFA 7 – 40° and it is considered to be one of the dominant determinants of the wood fiber strength [8]. Structural studies of the wood cell walls have focused mainly on the S2 layer properties and only little is known about the S1 and S3 layers [9].

One of the emerging areas in the cellulose industry is the development of superabsorbent materials. The chemical process required to increase the water retention value of cellulose fibers usually involves carboxylation [10–12]. The swelling of these modified fibers inevitably alters the native fiber structure. Non-uniform swelling of cellulose fibers and how it leads to the formation of balloons was first reported more than a century ago [13]. Since then, an extensive amount of work has been done to understand the swelling and dissolution mechanism of cellulose fibers by chemical modification [14] or by varying the solvent systems. Ballooning has been reported during the dissolution of fibers in N-methylmorpholine-N-oxide (NMMO) – water mixtures [15, 16], in NaOH at -8 ℃ [17], in ionic liquids [18], and also during mechanical nanofibrillation [19]. Navard and his coworkers have reported different modes of fiber dissolution that could be tuned by varying the solvent quality, and they have also suggested a

fiber swelling mechanism. It is worth investigating whether or not the same mechanism holds for the chemically modified fibers, and how the overall swollen morphology is affected by the three S-layers. To our knowledge, differences in swollen fiber structures with respect to the different types of chemistry applied have not been closely examined.

The three most common ways to introduce carboxylate groups onto the cellulose fibers are: carboxymethylation, periodate-chlorite oxidation and 2,2,6,6-tetramethylpiperidine-1-oxyl (TEMPO) radical mediated oxidation. TEMPO-mediated oxidized fibers cannot exceed 1.7 mmol/g of carboxylate contents [20], which is not sufficient to induce severe fiber deformation without any post mechanical treatment [21]. Therefore, only the first two chemistries will be discussed in this work.

Carboxymethylation non-selectively attacks all three –OH groups that are available on cellulose. The reaction is usually carried out in isopropyl alcohol to minimize hydrolysis of sodium chloroacetate [22, 23]. Above 3 mmol/g of carboxylate content, fibers break apart and large amounts of carboxymethylcellulose (CMC) become soluble in water [24]. Commercially available CMC typically has an average DS of 0.7, corresponding to 4.2 mmol/g of carboxylate content. As carboxymethylation requires high concentrations of NaOH, portions of the non-derivatized native cellulose I crystals can be mercerized, and then transformed into the cellulose II crystalline allomorph. As carboxymethylation is often used in the industry to produce CMC, the emphasis of most studies is on the optimization of the CMC yield, without relating it to the swelling behaviour itself [25–27].

Periodate oxidation regioselectively converts vicinal –OH groups at C2 and C3 to yield 2,3-dialdehyde cellulose by opening the glucopyranose ring. The aldehyde groups are then further oxidized to form 2,3-dicarboxylic cellulose by chlorite oxidation [28]. According to

Tejado et al., this aqueous chemistry spontaneously breaks the fibers apart into both dissolved dicarboxylated cellulose (DCC) and nanofibrils at ~3 mmol/g of COO content. Unlike carboxymethylation, periodate-chlorite oxidation does not disrupt the cellulose I crystalline form. This reaction has been used in preparing nanofibrillated cellulose or highly charged cellulose nanocrystals [24, 29].

The objective of this study is to understand how the fiber structure evolves when different chemical and mechanical treatments are applied to wood fibers and to investigate the role of each secondary layer in fiber swelling. Understanding the swollen fiber structure will become particularly important in the preparation of cellulose-based superabsorbent materials.

2.2 Experimental

2.2.1 Materials

Non-fibrillated, bleached softwood kraft fiber sheets (SKF; Domtar, Canada) and partially fibrillated – mechanically treated – SKF (m-SKF, refined 4 times in a disc refiner with refining energy of 33 kWh/t; FPInnovations, Canada) from spruce were used as native cellulose material. Reagent grade sodium chloroacetate (CMA), sodium meta-periodate ($NaIO_4$), sodium chloride (NaCl), sodium hydroxide (NaOH), sodium chlorite ($NaClO_2$), hydrochloric acid (HCl), hydrogen peroxide (H_2O_2), N-(3-Dimethylaminopropyl)-N′-ethylcarbodiimide hydrochloride (EDC), and 5-aminofuorescein (A-fluo) were purchased from Sigma-Aldrich and were used as received.

2.2.2 Chemical modification

50 g of SKF sheets were torn into small pieces and soaked in distilled water overnight. The wet pulp was disintegrated by a household tilt-head stand mixer (Kitchenaid, Professional

550 plus), filtered to remove excess water, dried at 50℃. The dried pulp and sodium chloroacetate solution (100 g CMA in 130 mL water) were mixed together and placed in a 60℃ water bath for 4 hours for impregnation. Sodium hydroxide solution (62.5 g NaOH in 100 mL water) was then added and the pulp slurry was left overnight at room temperature. The pulp was then washed by 70-100% ethanol. The final product (carboxymethylated fibers, CMF, prepared from SKF) was dried at 50℃ and stored at room temperature. The same procedure was repeated for m-CMF, using m-SKF.

SKF was oxidized by the periodate-chlorite reaction to make periodate-chlorite oxidized fibers (PCF) following the method reported by Tejado et al. (2012).

2.2.3 Fluorescent tagging of the carboxyl groups of the fibers

Carboxyl groups of the chemically modified cellulose fibers can be fluorescently tagged via a carbodiimide-mediated coupling reaction as reported by Hu and Hayek [30]. Pulps of 0.1 % consistency (Cs) of (1) SKF, (2) CMF, (3) m-CMF and (4) PCF were mixed with A-fluo and EDC·HCl at pH 4 – 4.5 for 16 hours. A molar ratio of (COOH: A-fluo: EDC·HCl = 1: 0.5: 1) was used in all cases. Samples were dialyzed for 5 days for purification (Spectra/Por, MWCO 12,000).

2.2.4 Acid hydrolysis of CMF and PCF

As part of the structural studies, the chemically modified fibers were subjected to acid treatment to hydrolyze amorphous region to weaken the structure. 0.1 %w/w CMF and PCF suspensions were subjected to a mild acid hydrolysis using 1 N hydrochloric acid at 50℃ for 2 hours under magnetic stirring (250 rpm). Purification was done by dialyzing the sample for 3 days (Spectra/Por, MWCO 12,000)

2.2.5 Characterization

2.2.5.1 Charge determination

The carboxyl contents of CMF, m-CMF and PCF were measured by conductometric titration (Metrohm 836 Titrando). Titration was performed according to Yang et al. (2012)

2.2.5.2 Optical microscopy

Cellulose fiber dispersions were observed by Hoffman modulation contrast microscopy (HMC, Nikon Eclipse TE2000-U) and by fluorescence microscopy. In the first case, a few drops of 0.01 %w/v toluidine blue solution were added to the sample suspension at least 30 min prior to imaging. For fluorescence, A-fluo treated fibers were excited at λ = 494 nm with an exposure time of 6 – 800 ms. Images were later treated with analysis software ImageJ. The fibers were also observed by cross-polarized microscopy (Nikon Eclipse LV100 POL) in which a first order retardation plate (530 nm) was inserted. In confocal microscopy (Zeiss LSM510; 488 nm, Ar laser, 30 mW), each coverslip was sealed with a spacer (0.12 mm in thickness) to minimize the fiber deformation. All confocal imaging was done in water immersion.

2.2.5.3 Crystallinity determination

X-ray diffraction analysis was performed (Bruker Discover D8; VANTE C 2D detecto; CuKα radiation, λ = 1.54 Å) and the X-ray diffractograms were acquired with a 2θ (Bragg angle) range of 10-30° at a scan rate of 0.005°•s-1.

Solid state 13C NMR spectra were acquired (Varian, Agilent VNMRS-400) at 100.5 MHz for both functionality and crystalline structure determination. Samples were packed in 7.5 mm zirconia rotors and spun at 5500 Hz. Spinning side bands were suppressed using the TOSS

sequence. Spectra were acquired using a contact time of 2 ms and a recycle delay of 2 sec. Typically 6000 transients were acquired.

2.3 Results and Discussion

2.3.1 Microscopic observations of the native and swollen fibers

Native and swollen forms of cellulose wood fibers were observed by Hoffman modulation contrast microscopy, cross-polarizing microscopy, and confocal microscopy (**Figure 2-1**). After delignification, the wood fibers (SKF) become highly porous with a composition consisting of ~80% cellulose and ~20% hemicellulose [31]. Bordered and non-bordered pit-holes are clearly seen in **Figure 2-1; A1**, as well as in **Figure 2-1; A3**. Microfibril angles (MFA) or distinctive boundaries between each S-layers could not be identified. **Figure 2-1; A2** depicts retardation colors in SKF, which arises from birefringence of anisotropically oriented native cellulose. Fluorescent tagging of the COO groups on the pulp fibers were done by EDC-supported amidization reaction and conductometric titration results show that typically 20% of the total COO groups are converted into amides under current experimental conditions. See **Figure 2-1; A3** for stacked 2D images of the SKF. The naturally occurring COO groups on the native cellulose fibrils appear to be sufficiently well-distributed within the fiber wall to make the whole fiber fluorescent.

Carboxymethylated fibers (CMF) start to form “balloons” at [COO] ~ 1.2 mmol/g. The sizes of the balloons increase with an increasing amount of COO groups. CMF ballooning is a well-known phenomenon and terminal stages of the CMF swelling were first illustrated more than 50 years ago [15]. Jardeby et al. hypothesized that the ballooning occurs because wood cells have different reactivity due to their large dimensions and high density, thereby creating balloons and “collars” (2004). The maximum balloon size observed was ~200 μm in diameter, which occurred

at [COO] = 3.2 mmol/g. Above [COO] = 3.2 – 3.3 mmol/g, the CMF broke apart and CMC was released in solution. As illustrated in **Figure 2-1; B1**, the outer S1 and S2 layers swell and are stretched out in transverse directions. Most cellulosic materials after the chemical modification are contained inside the balloons as the yield is near 100%. Parallel streaks lying across the balloons are most likely stretched out fibrils from the S1 and S2 layers. Cellulosic materials within the balloons become transparent possibly because (1) their sizes are below the wavelength of the light, and/or (2) the differences in refractive indices between the inside and outside of the balloons become minimal due to the dramatic swelling. Axial compression of the CMF was expected as the fiber diameter can expend up to 6.7 times before the fiber breaks up. Le Moigne et al. reported that there is a maximum contraction ratio that wood fibers can withstand ([initial length of the fiber] / [length of the contracted fiber]). Above 1.7, the fiber disintegrates [32]. This suggests that the wood fibers can deform more in the transverse directions than the axial, which is probably due to the low microfibril angles (MFA) in the S2 layer. The S3 layer with MFA between 75 – 90° was also observed. Brandstrom et al. and Bergander et al. measured the MFA of Norway spruce and they have reported that the MFA of the S3 microfibrils is near 90° [33]. This indicates that the S3 layer did not suffer from significant changes in MFA – relative to the direction of the fiber – as much as the outer S1 and S2 layers.

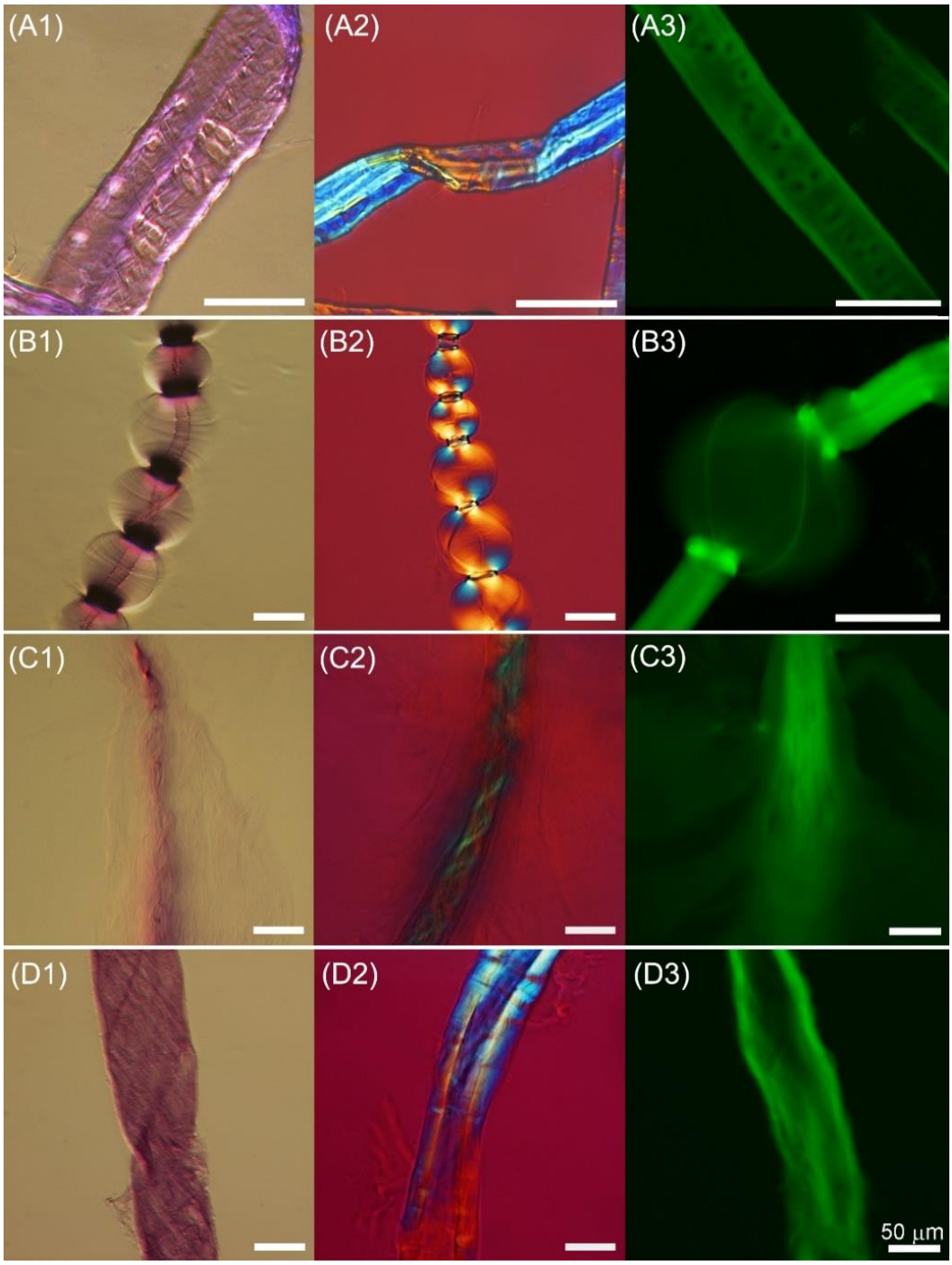

Figure 2-1. Hoffman modulation contrast light microscopy (HMC) of cellulose fibers dyed with toluidine blue (**A1, B1, C1, D1**); cross-polarized light microscopy, first order retardation plate inserted (**A2, B2, C2, D2**); confocal microscopy, samples dyed with A-fluo. Images are taken with an exposure time of 600 ms and are later z-stacked (**A3, B3, C3, D3**). Unmodified SKF (**A1, A2, A3**); CMF (**B1, B2, B3**, [COOH] = 2.6 mmol/g); m-CMF (**C1, C2, C3**, [COOH] = 2.5 mmol/g); and PCF (**D1, D2, D3**, [COOH] = 2.7 mmol/g). All scale bars are 50 µm.

Viewing CMF under the cross-polarizing microscope shows that the CMF stays birefringent and the cellulose chains are crossing perpendicularly at the collars (**Figure 2-1; B2**). This observation is comparable with that of wood fibers swollen in a NMMO-water mixture, which also showed cellulose chain orientations that resemble bipolar nematic droplets [16]. The authors claim that the birefringence is lost during the ballooning and the bright zones are localized only around the "non-swollen sections" or the collars. Considering that the fiber diameters increased by 3 – 4 times on average, the volume must have increased by at least 10 times. In other words, birefringence in the swollen region is not necessarily lost, but appears to be less pronounced than in the less- or non-swollen regions simply because of their low cellulose density.

Microfibrils that are surrounding the balloons helically can be seen in **Figure 2-1; B3**. The formation of helices of the wood fibers swollen in the NMMO-water mixture was examined by Le Moigne et al. who have claimed that this is due to the rolling up of the primary (P) layer which is caused by stress imbalances due to the chain extension and the changes in chain orientation that had occurred during the ballooning (2010). As kraft pulping almost completely removes the P layer, the helices that are seen in **Figure 2-1; B1** are most likely caused by the spiral extension of the S1 layer. The more pronounced staining of the collars is due to the fact that the highly charged cellulose chains are more densely packed in the collars than in the balloons. CMF remained highly swollen after fluorescent tagging.

The effect of the S1 layer in fiber swelling was examined by carboxymethylating the partially fibrillated (mechanically treated) SKF (m-SKF). The partial fibrillation was done by refining the high consistency SKF through a disc refiner 4 times, which damages the external fiber surface. The outermost S1 layer and some of the S2 layer are disintegrated by this mechanical treatment. When the m-SKF was subjected to carboxymethylation, the carboxymethylated fibers (m-CMF)

swell without forming balloons (**Figure 2-1; C1**). The formation of "threads" and "collars" [32] must have been prevented by the removal of the S1 layer. This observation agrees with the results reported by Gehmayr et al, who achieved homogeneous swelling by dissolving the wood fibers after altering the swelling capacity of the P and S1 layers by TEMPO-mediated oxidation [34]. **Figure 2-1; C2** shows that birefringent cellulose chains of the S3 layer are also helices with MFA between 40 – 45° when swollen. In the absence of the S1 layer, the surface fibrils of the m-CMF appear to be more dispersed than those of CMF; hence the birefringence appears to be less pronounced in C2. From the diffuse fluorescence in **Figure 2-1; C3**, it can be seen that the charges are more uniformly distributed in m-CMF than in CMF.

To understand how different chemistries affect the swollen structure, SKF was modified by a two-step oxidation chemistry: periodate, followed by chlorite oxidation. Periodate-chlorite oxidized fibers (PCF) showed homogeneous swelling without the formation of balloons. PCF begins to swell at [COO] ~ 1.6 mmol/g and the swollen fiber width increased with an increase of [COO] content. The maximum PCF width observed was ~200 μm, which occurred at [COO] = 3.0 mmol/g. Above [COO] = 3.1 mmol/g, the PCF breaks apart into microfibrils, CNF and dicarboxylated cellulose (DCC) [24]. As seen in **Figure 2-1; D1**, the three S-layers can no longer be distinguished from one another, suggesting that all three S-layers are damaged and swollen homogeneously. Notice that there are multiple microfibrils that are helically surrounding the uniformly swollen PCF, whereas there are only one or two "threads" surrounding the CMF balloons, the remaining ending up in the collars. Little realignment of cellulose microfibrils with respect to the fiber axis seems to have occurred (**Figure 2-1; D2**). Glucose ring opening and cellulose chain scission as a side reaction [35], must have effectively released any constrains that would have caused the formation of collars and balloons by damaging the amorphous regions of

the microfibrils. **Figure 2-1; D3** again represents the uniformly distributed COO groups inside the fiber wall. Upper part of the fiber appears to be hollow as the thin S3 layer seems to be completely broken up, whereas the lower part of it still shows the remaining S3 layer that has survived the chemical modification.

2.3.2 Changes in crystallinity

Carboxymethylation and periodate-chlorite oxidation are similar in a way that –OH groups are carboxylated and that the fibers become more hydrophilic. However, CMF goes through a crystalline structure rearrangement due to the high NaOH concentration used during the carboxymethylation [36]. Both x-ray diffraction and ^{13}C solid state NMR spectra [37] confirm that the native crystalline allomorph, cellulose I, is preserved in PCF but not in CMF (**Figure 2-2**). The cellulose chains that are not carboxymethylated recrystallize in a cellulose II allomorph; hence the CMF rather appears to be a mixture of cellulose II and amorphous cellulose.

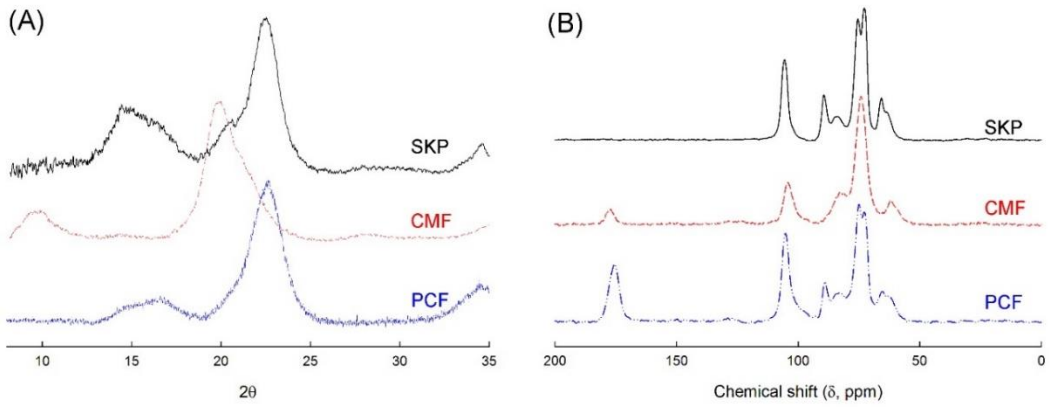

Figure 2-2. X-ray diffractograms of air-dried SKF, CMF, and PCF (**A**). Crystalline peak at 22.5° shown in SKF (native crystalline form) remains the same in PCF, but not in CMF. Solid state 13C NMR spectra of SKF, CMF and PCF (**B**). Cellulose I crystalline structure maintained in PCF, but not in CMF. C=O bend at chemical shift 180 ppm from carboxylate content appears in CMF and PCF.

2.3.3 Swollen fibers in 3D and their cross-sections

2D confocal microscopic images of wood fibers in native and swollen forms are reconstructed as 3D images (**Figure 2-3; A1, B1, C1, and D1**) and their cross-sections are shown in A2, B2, C2, and D2.

SKF is a thin, hollow tube (**Figure 2-3; A1**) showing numerous bordered and non-bordered pit holes on its surface. SKF suffers from the lumen collapse which took place at the initial drying process after pulping; hence its cross-section appears to be a wrinkled ellipsoid, not a circle (**Figure 2-3; A2**).

Once carboxymethylated, CMF absorbs large amount of water as individual microfibrils swell in all three S-layers (**Figure 2-3; B1**). Cellulose chains and hence the attached COO groups too, are densely packed at the collars and the microfibrils in the balloons appear to be oriented almost perpendicular to the fiber axis. This could be explained by the changes in MFA in the S2 layer due to the dramatic stretching in transverse directions. Assuming that the S3 layer can be at least partially separated from the S2 layer, the reduced fiber length due to the transversal stretching can cause the S3 layer to "crumple" inside the balloon. In this paper, we define "crumpling" as the longitudinal deformation of the S3 layer caused by the fiber swelling. It should also be pointed out that the microfibrils in the S3 layer have COO groups on their surface as well, which can be functionalized with A-fluo. From the cross-sectional image of the CMF (**Figure 2-3; B2**), it can be seen that the balloons are filled up with highly dispersed cellulose chains and the swollen S3 layer appears to be a circle with 11 μm in diameter.

Mechanically damaging the fiber surface prior to carboxylation prevents ballooning as can be seen in m-CMF. Partially fibrillated and charged surface fibrils are stretched outwards, thereby masking any detailed features inside the swollen fibers when reconstructed in 3D

(**Figure 2-3; C1**). The cross-section of the m-CMF reveals that the fiber refining has also damaged the outside of the S2 layer (**Figure 2-3; C2**). The cross-sectional diameter of m-CMF is about the same as that of CMF.

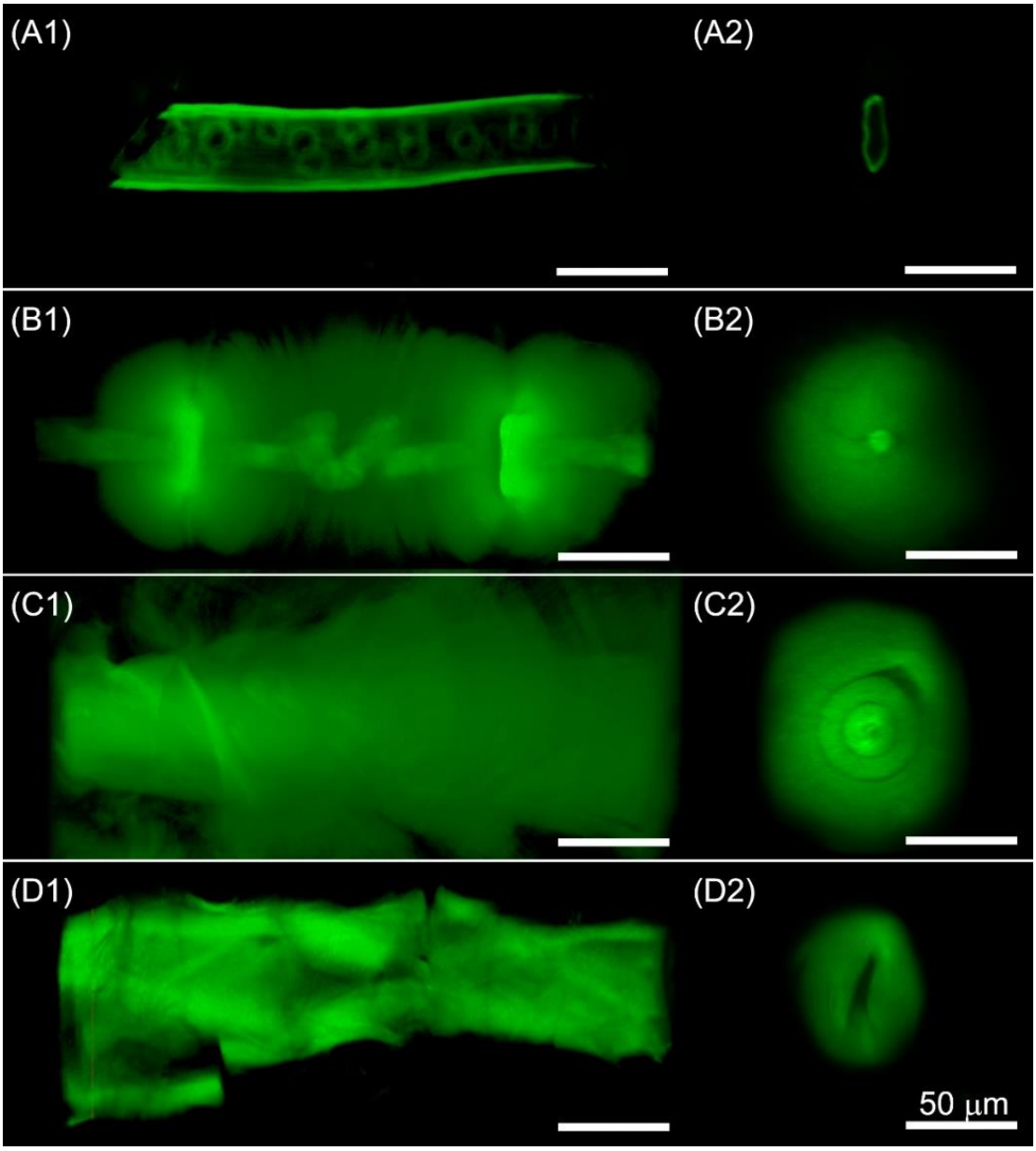

Figure 2-3. 3D reconstructed images of fibers from confocal microscopy in native form (**A1**, SKF) and swollen forms (**B1**,CMF; **C1**, m-CMF; **D1**, PCF). Cross-sections of each fiber on the right column (**A2**, SKF; **B2**,CMF; **C2**, m-CMF; **D2**, PCF). Images are taken with an exposure time of 800 ms. Scale bars are 50 μm.

Periodate-chlorite oxidation results in homogeneous swelling but causes cellulose chain scission. Therefore, the PCF appears to be a hollow tube with imperfections on the fiber surface (**Figure 2-3; D1**). The S3 layer must be broken in pieces since it is not visible from the 3D structure, nor from the cross-section (**Figure 2-3; D2**). The fiber wall, mostly S2 layer (~5 μm), is typically swollen 5 to 10 times in total.

One could argue that it is also possible for each secondary layer to have different chemical reactivity; hence the charge contents may vary accordingly. As fibers under tension exhibit reduced reactivity [32], the stress generated from the ballooning which has mainly originated from the S2 layer deformation may have suppressed the S3 layer to go through the same degree of chemical conversion as the S2 layer. Nevertheless, the S3 layer still swells as much as 10 times (**Figure 2-3; B2, C2**), which is about the same degree of the S2 layer swelling. While the charged S2 microfibrils are stretched out transversely to form balloons, the inner S3 layer is longitudinally compressed and crumpled. This changes cellulose distribution within the fiber, and hence the local charge density, which is directly proportional to the fluorescent intensity. The S3 layer contains charge groups and its microfibrils are densely packed together with high MFA to give a fluorescent intensity comparable to that of the S2 layer.

2.3.4 S2 and S3 layer separation

Acid hydrolysis results in cellulose chain scission as it breaks the glycosidic bond. The CMF and PCF were subjected to a very mild acid hydrolysis to observe how these swollen structures evolve further. After CMF was hydrolyzed for 2 hours, the collars and microfibril helices that surrounded the CMF were completely removed (**Figure 2-4; A**). A void space between the S2 and S3 layers became visible in the region where S3 is crumpled, which suggests that the fiber swelling, accompanied by a reduction in fiber length, induces the crumpling of the S3 layer and

the S2-S3 separation. Compared to CMF, PCF is more prone to fiber disintegration as more cellulose chains are damaged at the same degree of carboxylation. **Figure 2-4; B** shows that the hydrolyzed PCF surface is not as well-defined as that of hydrolyzed CMF. The inside of the PCF remains hollow as the S3 layer must have been damaged before crumpling occurs. Hydrolyzing PCF readily disintegrates the whole fiber structure, instead of leading to the S2-S3 separation.

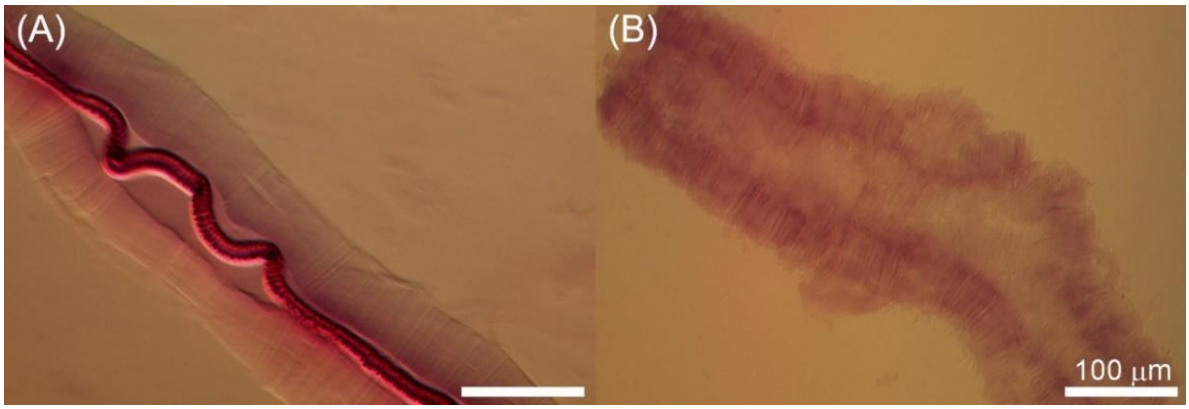

Figure 2-4. HMC of acid hydrolyzed CMF (**A**) and PCF (**B**) in 1N HCl at 50℃ for 2 hours. Toluidine blue dyed. Scale bars are 100 μm.

2.3.5 Model of fiber swelling

Figure 2-5 shows a model made with yarns oriented at angles similar to those in a typical fiber. Fibrils in the S1, S2, and S3 layers are color-coded as red, blue, and green. The swelling of SKF and m-SKF was mimicked by simultaneously pulling out the yarns at two different points in directions perpendicular to the fiber axis. Since the S2 layer contains approximately 50 times more microfibrils than the S1 and S3 layers, the driving force in morphological changes must arise from the S2 layer. Therefore, the blue yarns that represent the fibrils in the S2 layer were pulled out and a dramatic increase in their MFA was observed immediately (**Figure 2-5; A2**). The red S1 layer experienced both contraction and expansion at the same time, which respectively created collars and spiral coils that go around the balloons. Crumpling of the green S3 layer due to the S2-S3 separation as well as the reduced fiber length was also observed.

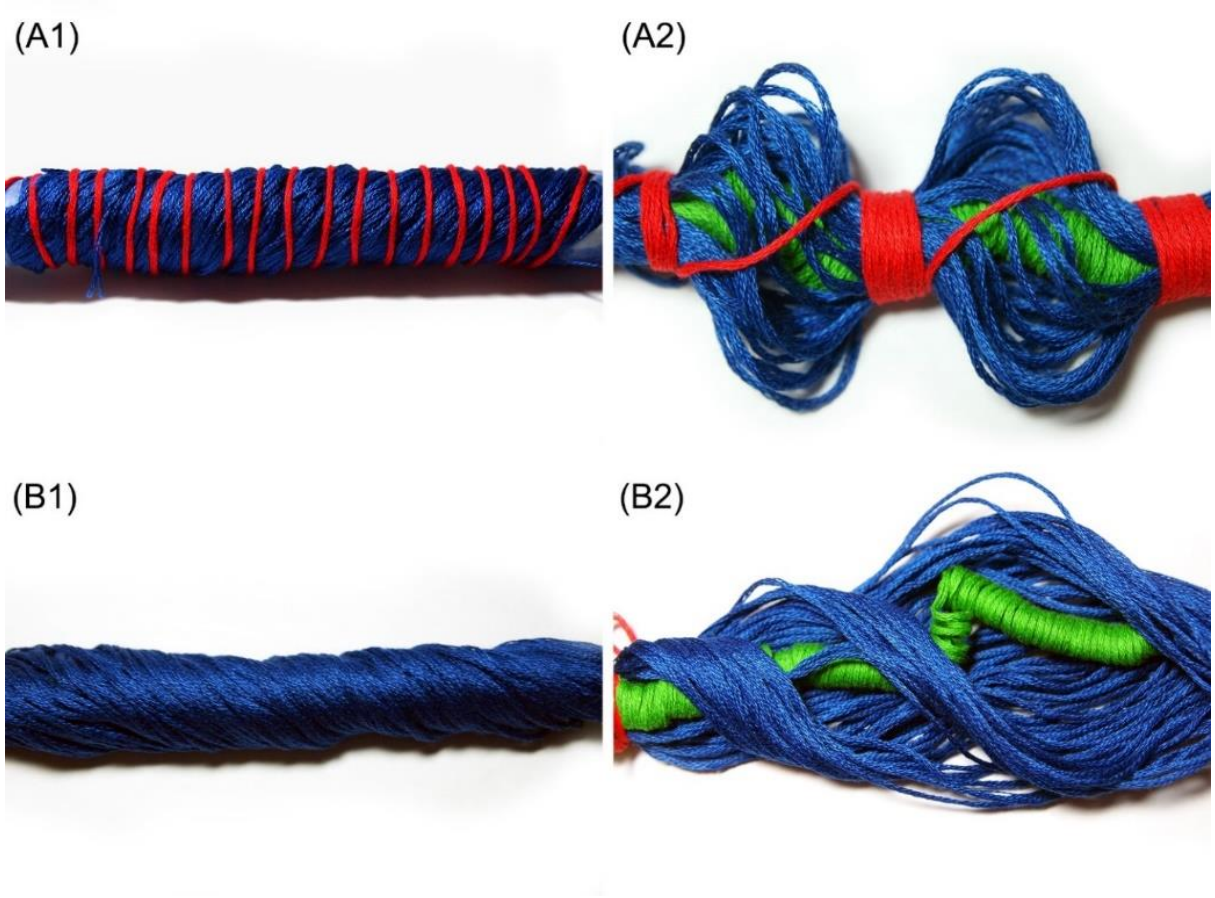

Figure 2-5. Fiber swelling was demonstrated using yarns to show how microfibrils behave. Changes mimicking the transition from SKF to CMF are shown in **A1** and **A2**; those from m-SKF to m-CMF are shown in **B1** and **B2**. Fibrils in each layer are represented in red (S1), blue (S2), and green (S3 layer).

To illustrate the effect of the S1 layer on swelling, the red yarn (S1) was removed and the blue yarns (S2) were pulled out in the same manner as before (**Figure 2-5; B2**). No ballooning was observed in this case and there was a lesser increase in the MFA of the S2 layer. The S3 layer crumpled inside the highly swollen S2 microfibrils. This indicates that the S1 layer plays a significant role in the formation of balloons, mainly due to their high MFA which constrains the homogeneous swelling of the inner layers.

2.3.6 Schematics of swollen fiber structures

Schematic diagrams of the native and swollen fiber sections are presented in Figure 2-6. As seen in **Figure 2-6; A1**, the longitudinal section of the unmodified SKF resembles that of the

hollow cylinder. Thickness of the S1 and S3 layers are typically 0.1 μm, whereas that of S2 is 5 μm. To make the diagram fit to scale, the S1 and S3 layers are represented as black lines, whereas the S2 layer is shown as a grey shade. **Figure 2-6; A2** illustrates the ellipsoidal SKF cross-section with well-defined S1, 2, 3 layers. Chemicals are accessible through the pores and the pit holes, which are represented as a cut.

Once carboxymethylated, all three S-layers swell up to 5 – 10 times. In **Figure 2-6; B1**, collars are represented as black rectangles and this is the area where microfibrils from all three S-layers are located: contracted S1, collared S2, and swollen S3 sitting inside the CMF. The helix created by the spiral extension of the S1 layer is represented as short lines which are diagonally aligned with each other. The highly swollen S2 layer is shown as a grey shade, where the S3 layer is represented as parallel lines in the longitudinal section (B1) and as a circle in the cross-section (**B2**). When the fiber crumpling induces the separation between the S2 and S3 layers, the S3 can be positioned anywhere in the empty space. In **Figure 2-6; B2**, the distance between the S2 and S3 layer is denoted as d_1, and the thickness of the S2 layer as d_2. The amount of [COO] groups and the crumpling of the S3 layer dictate the magnitude of d_1 and d_2, respectively. . In case of no S2 – S3 separation or no S3 crumpling, d1 can be as low as 0, which is the case in **Figure 2-3; B2**.

The S1 layer is damaged when passing through a refiner, and therefore it is not shown in either of the m-CMF sections. In **Figure 2-6; C1**, the longitudinal section of the homogeneously swollen m-CMF is illustrated. The overall geometry is comparable with that of SKF **(Figure 2-6; A1**), except that the S2 and S3 layers are thicker and that the S1 layer is absent in C1. Since the separation of the S3 from the S2 layer is also likely to happen, the cross-sectional image of the

m-CMF (**Figure 2-6; C2**) resembles that of CMF (**Figure 2-6; B2**). The distance range of d_1 and d_2 remains unchanged.

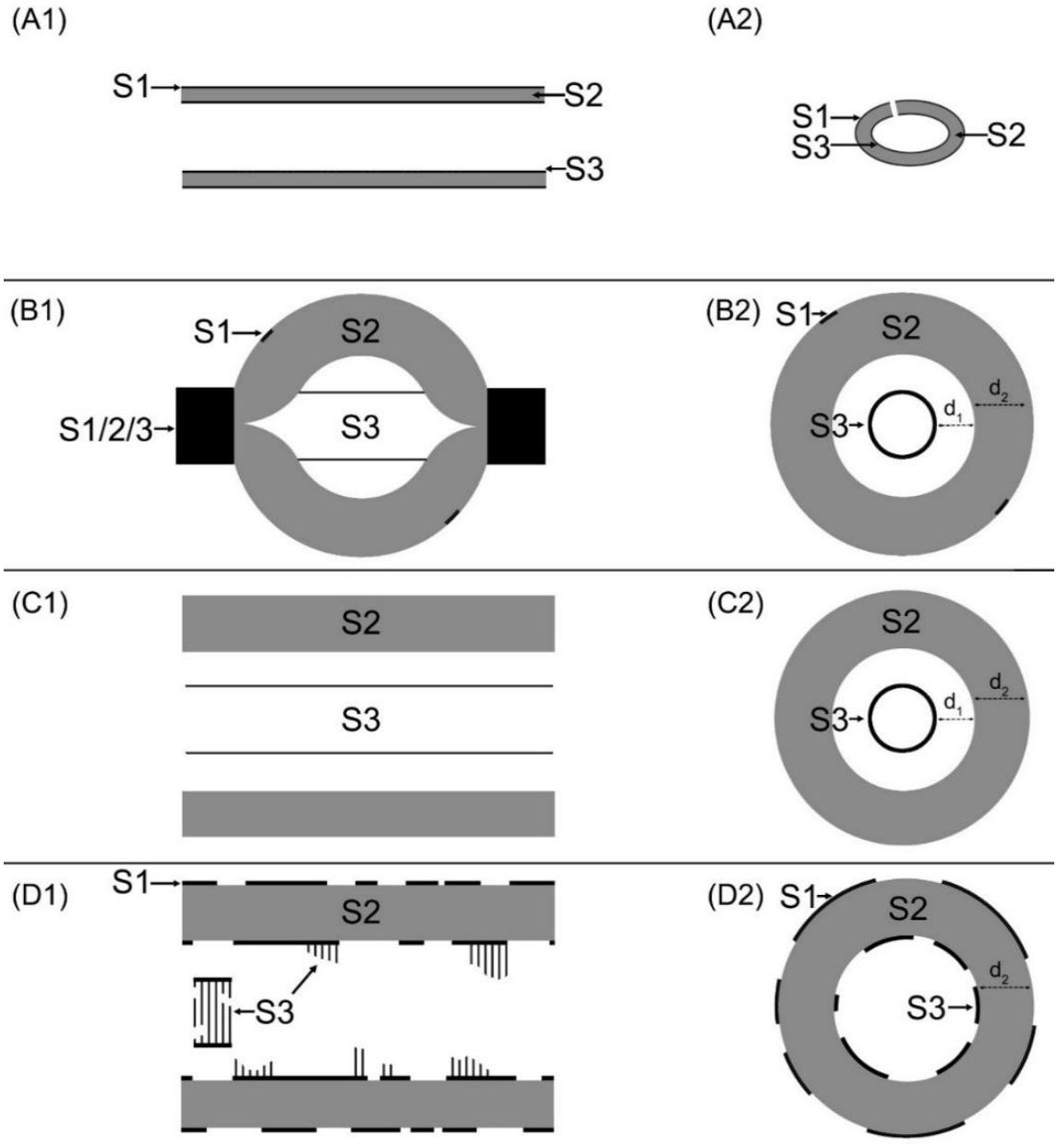

Figure 2-6. Schematic representation of (**A**) SKF; (**B**) CMF; (**C**) m-CMF and (**D**) PCF; longitudinal sections are on the left column (**A1-D1**) and cross-sections are on the right column (**A2-D2**). The distance between the S2 and S3 layer is denoted as d_1, and thickness of the S2 layer is denoted as d_2. Drawings are approximately to scale.

Partially damaged S1 and S3 layers are represented as non-continuous lines in **Figure 2-6; D1** to describe microfibril disintegration that had occurred during periodate-chlorite oxidation. The S2 layer swells to about the same degree as that in CMF; hence d_2 stays the same (**Figure 2-6; D2**). On the other hand, the partially broken S1 and S3 layers are still attached to the highly swollen S2 layers; hence $d_1 = 0$ in this case.

2.4 Concluding remarks

We have shown that the structure of the swollen wood fibers can be tailored by varying the mechanical and chemical fiber treatments. Carboxymethylated cellulose fibers swell by forming balloon-like structures. Exposure of the fibers to strong alkali during carboxymethylation transforms the native cellulose to cellulose II. Periodate-Chlorite oxidation, on the other hand, induces homogeneous swelling while keeping the cellulose crystals in their native form. Damaging the S1 layer by mechanical or chemical means gives rise to homogeneous swelling, which proves that the S1 layer is responsible for the ballooning effect. The thickest secondary layer, S2, experiences a large increase in microfibril angles which reduces the total fiber length. The transversal expansion, accompanied by longitudinal shrinkage of the fibers, causes the crumpling of the S3 layer, thereby leaving an empty space between the S2 and S3 layers.

The key factor in resolving the issue of low accessibility, hence the low reactivity of the cellulose fibers, is the reduction of stress buildup caused by the structural deformation of the fibers. In order to achieve a complete dissolution or a high yield derivatization instead of a heterogeneous mixture of fiber fragments and NCC (nanocrystalline cellulose), it is necessary to weaken the structural integrity of the fibers prior to applying any chemical treatments.

2.5 Acknowledgements

This work was supported by an NSERC Industrial Research Chair supported by FPInnovations, by the NSERC Green Fibre Network, and the Centre for Self Assembled Chemical Structures. Special thanks to Dr. Fred Morin at McGill NMR facility and Dr. Elke Küster-Schöck at McGill Cell Imaging and Analysis Network and Dr. Alois Vanerek for valuable suggestions.

2.6 References

[1] Ritter G. Composition and structure of the cell wall of wood. Ind Eng Chem 1928;20:941–5.
[2] O'Sullivan A. Cellulose: the structure slowly unravels. Cellulose 1997:173–207.
[3] Tabet T, Aziz F. Cellulose Microfibril Angle in Wood and Its Dynamic Mechanical Significance. Cellulose – Fundamal aspect., 2013, p. 113–42.
[4] Déjardin A, Laurans F, Arnaud D, Breton C, Pilate G, Leplé J-C. Wood formation in Angiosperms. C R Biol 2010;333:325–34.
[5] Booker RE, Sell J. The nanostructure of the cell wall of softwoods and its functions in a living tree. Holz Als Roh- Und Werkst 1998;56:1–8.
[6] Whiting P, Pulp DAIG. The topochemistry of delignification shown by pulping middle lamella and secondary wall tissue from Black spruce wood. J Wood Chem Technol 1981;1:111–22.
[7] Zhong R, Ye Z-H. Encyclopedia of Life Sciences. Chichester, UK: John Wiley & Sons, Ltd; 2001.
[8] Gustafsson J, Ciovica L, Peltonen J. The ultrastructure of spruce kraft pulps studied by atomic force microscopy (AFM) and X-ray photoelectron spectroscopy (XPS). Polymer (Guildf) 2003;44:661–70.
[9] Gibson LJ. The hierarchical structure and mechanics of plant materials. J R Soc Interface 2012;9:2749–66.
[10] Hubbe MA, Rojas OJO, Lucia LA LA, Sain M. Cellulosic nanocomposites: a review. BioResources 2008;3:929–80.
[11] Lin N, Bruzzese C, Dufresne A. TEMPO-oxidized nanocellulose participating as crosslinking aid for alginate-based sponges. ACS Appl Mater Interfaces 2012;4:4948–59.
[12] Aulin C, Ahola S, Josefsson P, Nishino T, Hirose Y, Osterberg M, et al. Nanoscale cellulose films with different crystallinities and mesostructures--their surface properties and interaction with water. Langmuir 2009;25:7675–85. doi:10.1021/la900323n.
[13] Nägeli C. Über den inneren Bau der vegetabilischen Zellmembranen. Sitzber Bay Akad Wiss Munchen 1864:282–323.
[14] Stawitz VJ, Kage MP. Ü ber die quellungsstadien der wasserlöslichen celluloseäther und die übermolekulare Struktur der Cellulose. Das Pap 1959;13:567–72.
[15] Jeihanipour A, Karimi K, Taherzadeh MJ. Enhancement of ethanol and biogas production from high-crystalline cellulose by different modes of NMO pretreatment. Biotechnol Bioeng 2010;105:469–76.
[16] Cuissinat C, Navard P. Swelling and Dissolution of Cellulose Part 1: Free Floating Cotton and Wood Fibres in N-Methylmorpholine-N-oxide–Water Mixtures. Macromol Symp 2006;244:1–18.
[17] Le Moigne N, Navard P. Dissolution mechanisms of wood cellulose fibres in NaOH–water. Cellulose 2009;17:31–45.

[18] Cuissinat C, Navard P, Heinze T. Swelling and dissolution of cellulose. Part IV: Free floating cotton and wood fibres in ionic liquids. Carbohydr Polym 2008;72:590–6.
[19] Uetani K, Yano H. Nanofibrillation of wood pulp using a high-speed blender. Biomacromolecules 2011;12:348–53.
[20] Okita Y, Saito T, Isogai A. Entire surface oxidation of various cellulose microfibrils by TEMPO-mediated oxidation. Biomacromolecules 2010;11:1696–700.
[21] Saito T, Kimura S, Nishiyama Y, Isogai A. Cellulose nanofibers prepared by TEMPO-mediated oxidation of native cellulose. Biomacromolecules 2007;8:2485–91.
[22] Khullar R, Varshney VK, Naithani S, Heinze T, Soni PL. Carboxymethylation of cellulosic material (average degree of polymerization 2600) isolated from cotton (Gossypium) linters with respect to degree of substitution and rheological behavior. J Appl Polym Sci 2005;96:1477–82.
[23] Heinze T, Pfeiffer K. Studies on the synthesis and characterization of carboxymethylcellulose. Die Angew Makromol 1999;266:37–45.
[24] Tejado A, Alam MN, Antal M, Yang H, Ven TGM. Energy requirements for the disintegration of cellulose fibers into cellulose nanofibers. Cellulose 2012;19:831–42.
[25] Jardeby K, Lennholm H, Germgård U. Characterisation of the undissolved residuals in CMC-solutions. Cellulose 2004:195–202.
[26] Jardeby K, Germgård U, Kreutz B, Heinze T, Heinze U, Lennholm H. Effect of pulp composition on the characteristics of residuals in CMC made from such pulps. Cellulose 2005;12:385–93.
[27] Jardeby K, Germgard U, Kreutz B, Heinze T, Heinze U, Lennholm H. The influence of fibre wall thickness on the undissolved residuals in CMC solutions. Cellulose 2005;12:167–75.
[28] Liimatainen H, Visanko M. Enhancement of the nanofibrillation of wood cellulose through sequential periodate–chlorite oxidation. Biomacromolecules 2012;13:1592–7.
[29] Yang H, Tejado A, Alam N, Antal M, van de Ven TGM. Films prepared from electrosterically stabilized nanocrystalline cellulose. Langmuir 2012;28:7834–42.
[30] Hu TQ, Hayak A. Cellulose Materials with Novel Properties, US Patent 2012/0041183. 2012.
[31] Duchesne I, Hult E, Molin U, Daniel G, Iversen T, Lennholm H. The influence of hemicellulose on fibril aggregation of kraft pulp fibres as revealed by FE-SEM and CP/MAS 13C-NMR. Cellulose 2001;8:103–11.
[32] Le Moigne N, Bikard J, Navard P. Rotation and contraction of native and regenerated cellulose fibers upon swelling and dissolution: the role of morphological and stress unbalances. Cellulose 2010;17:507–19.
[33] Neagu RC, Gamstedt EK, Stig LB, Lindström M. Ultrastructural features affecting mechanical properties of wood fibres. Wood Mater Sci Eng 2006;1:146–70.
[34] Gehmayr V, Potthast A, Sixta H. Reactivity of dissolving pulps modified by TEMPO-mediated oxidation. Cellulose 2012;19:1125–34.
[35] Whitmore PM, Bogaard J. Determination of the cellulose scission route in the hydrolytic and oxidative degradation of paper. Restaurator 1994;15:26–45.
[36] Yoon MJ, Doh SJ, Im JN. Preparation and characterization of carboxymethyl cellulose nonwovens by a wet-laid process. Fibers Polym 2011;12:247–51.
[37] Mittal A, Katahira R, Himmel ME, Johnson DK. Effects of alkaline or liquid-ammonia treatment on crystalline cellulose: changes in crystalline structure and effects on enzymatic digestibility. Biotechnol Biofuels 2011;4:41.

Bridging Section between Chapter 2 and 3

In the previous chapter, fiber deformation in relation to microfibril arrangements in the secondary layer was discussed. The swelling behavior of pulp fibers can be altered by mechanical pretreatment or by using chemistries involving reduction in chain length. In most common practice, ballooning is still unavoidable. To further break-down the swollen fiber structures, homogenization and or ultrasonication is often applied which can then liberate cellulose filaments in nanometer length scales. Observing the structural break down of carboxymethylated fibers undergoing intense mechanical shear can explain how some of the characteristic features of the balloon-like structures present different structural rigidity. In between the initial swollen stage to a complete fragmentation, fiber structures constantly evolve and go through numerous intermediate stages. Microscopic observations on such structural intermediates and related findings will be discussed in Chapter 3. The results of this research have been published in the following paper:

G. Sim and T.G.M. van de Ven, Spherical cellulose gel particles with donut-shaped interior structures. Cellulose (2015) 22:2, 1019-1026

Chapter 3. Spherical Cellulose Gel Particles with Donut-Shaped Interior Structures

Abstract

Partially carboxylated cellulose wood fibers (CMF) with highly swollen balloon-like structures were ultrasonicated to produce spherical cellulose gel particles with donut-shaped interior structure. The formation of these particles is most likely due to the characteristic microfibril arrangements in swollen CMF consisting of alternating regions of "balloons" and "collars", which have different structural rigidity. Upon applying an intense mechanical energy, the more physically strained parts break up prior to the flexible areas. Hence the helically extended S1 microfibrils and the axially compressed S3 layers are damaged first, while partially or fully carboxymethylated flexible cellulose chains in the S2 layers are rearranging themselves around the tightly wound collars. The interior donut structure likely originates from the collars, which do not collapse upon drying. The carboxymethylated spherical cellulose gel particles have a wide size distributions ranging from 15 to 200 μm in diameter with excellent rewettability and pH sensitivity in water.

3.1 Introduction

Utilizing cellulose based materials often requires substantial amounts of chemical and mechanical treatments. In preparation of cellulose nanomaterials, carboxylation is often used to facilitate the fibrillation process by introducing electrostatic repulsion and disrupting interfibrillar hydrogen bonding [1–5]. With increased amounts of carboxyl groups available on the fiber surface, the fiber becomes more and more swollen until the structures are completely disintegrated [6–8]. Microfibrils in the secondary wood cell wall undergo structural changes,

which vary depending on the type of pulp used and the chemistry applied. Understanding the deformed fiber structures is critical as they relate to some of the important issues in cellulose chemistry such as non-uniform fiber fragmentation and low reaction yield.

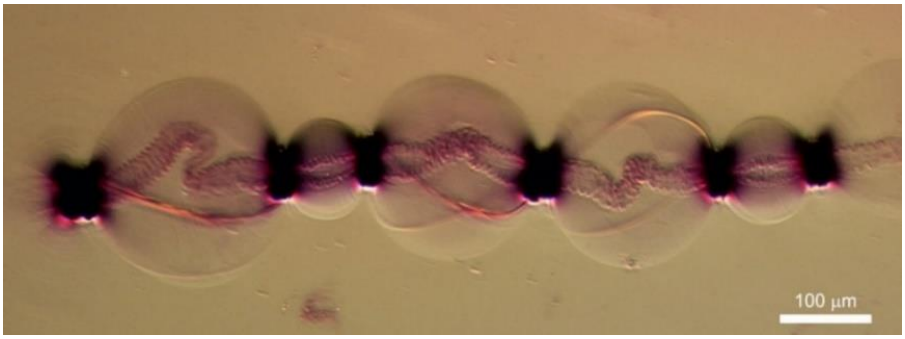

Figure 3-1. Hoffman modulation contrast microscopy of toluidine blue dyed carboxymethylated kraft, bleached softwood fiber (CMF) with 2.35 mmol/g of carboxylate contents. Image was taken prior to applying any mechanical treatments.

Balloon-like swollen fiber structures have been reported during carboxymethylation, quaternization, fiber dissolution in several solvents, and high pressure homogenization [9–14]. Carboxymethylation is widely used in many fields of applications as it forms pH responsive hydrocolloid microgel particles with increased water absorbency and viscosity [15, 16] while providing potential reaction cites which enables further tailoring [17–22]. **Figure 3-1** shows the characteristic features of carboxymethylated fibers (CMF) such as: (1) extended S1 microfibrils helically winding the exterior of the balloons, (2) tightly wound S1 microfibrils creating collars, (3) S2 microfibrils filling up the balloons, (4) innermost S3 layer with high microfibril angles (MFA).

In previous work, we found that CMF exceeding 1.5 mmol/g charge groups show balloon-like structures, which is caused by the microfibril arrangements in S1, S2, and S3 layers in wood cell walls [7]. While attempting to isolate the S3 layers from the balloons, we have learnt that the shapes of CMF fragments vary largely depending on the types and amount of energy applied to

the CMF suspensions [23]. Applying ultrasonication damages CMF and produces “spherical particles” that are distinguishably different from the highly swollen “flat rings” that were reported in other studies [10, 11, 13, 24, 25]. In this paper, we propose a break-up mechanism of CMF subjected to intense mechanical energy based on microscopic observations, which leads to the formation of spherical cellulose gel particles with donut-shaped interior structures. At the same time, studying the break-up of the balloons will provide additional information about their interior structure.

3.2 Experimental

3.2.1 Materials

Bleached softwood kraft fiber sheets (SKF; Domtar, Canada) were used as a starting material. Reagent grade sodium chloroacetate (MCA), sodium hydroxide (NaOH), hydrochloric acid (HCl), N-(3-Dimethylaminopropyl)-N′-ethylcarbodiimide hydrochloride (EDC), and 5-aminofuorescein (A-fluo) were purchased from Sigma-Aldrich and were used as received.

3.2.2 Preparation of CMF and CMF gel

Softwood kraft fibers were carboxymethylated and fluorescently tagged following the method reported by Sim et al [7]. The carboxyl contents of CMF were measured by conductometric titration (Metrohm 836 Titrando), according to Yang et al [26]. Both fluorescently tagged and untagged carboxymethylated fiber suspensions (CMF, 0.1 %w/w) were ultrasonicated (Hielscher, UP200H; 200 W, 24 kHz) for 1 minute to produce gel particles. To study intermediate structures, another CMF suspension was placed in the ultrasonic cleaning bath (Branson, B200; 19 W, 50/60 Hz) for 1 minute. Samples were drawn every 10 seconds for microscopic observations.

3.2.3 Microscopic observations

Ultrasonicated, untagged CMF gel suspensions were dyed with toluidine blue and observed by Hoffman modulation contrast microscopy (HMC, Nikon Eclipse TE2000-U). The sample slides were air dried overnight at room temperature and re-wetted by adding a drop of water between the slide and the coverslip.

For confocal laser scanning microscopy (CLSM), A-fluo treated CMF gel suspensions were excited at λ = 494 nm with an exposure time of 800 ms (Zeiss LSM510; 488 nm, Ar laser, 30 mW). Each coverslip was sealed with two spacers (0.24 mm in total thickness) to minimize gel deformation. All confocal imaging was done in water immersion to minimize refraction.

An aqueous suspension of gel particles was deposited on a mica surface, air-dried, and then sputter-coated with platinum with a thickness of 10 nm. Images were made with a high resolution field emission scanning electron microscope (FE-SEM; FEI Inspect, F-50) which was operated at an accelerating voltage of 5.0 kV to observe the surface morphology of the dried gel particles

3.3 Results and Discussions

Carboxymethylated fibers (CMF) with 2.35 mmol/g of COO groups are highly swollen and form balloon-like structures in water at neutral pH. The degree of "ballooning" mainly depends on the number of charged groups that are introduced by carboxymethylation. When carrying 2 – 2.5 mmol of charged groups, the ballooning effect is the most prominent whereas CMF with below 2.0 mmol of COO groups often have various ranges of non-swollen areas. Roughly above 3.0 mmol, the CMF disintegrates and dissolves in water as carboxymethylated cellulose (CMC) [27]. When an ultrasonication is applied to the CMF suspension for several tens of seconds, the

fibers break into small fragments that are predominantly spherical. Sizes of the spherical particles vary from 15 μm to 200 μm in diameter as can be seen in **Figure 3-2**. Toluidine blue is an ion exchange dye which can access the negatively charged groups in the pores of cellulose fibrils [28]. In Hoffman modulation light microscopy, all samples were dyed with toluidine blue at least 30 min prior to imaging for a better contrast.

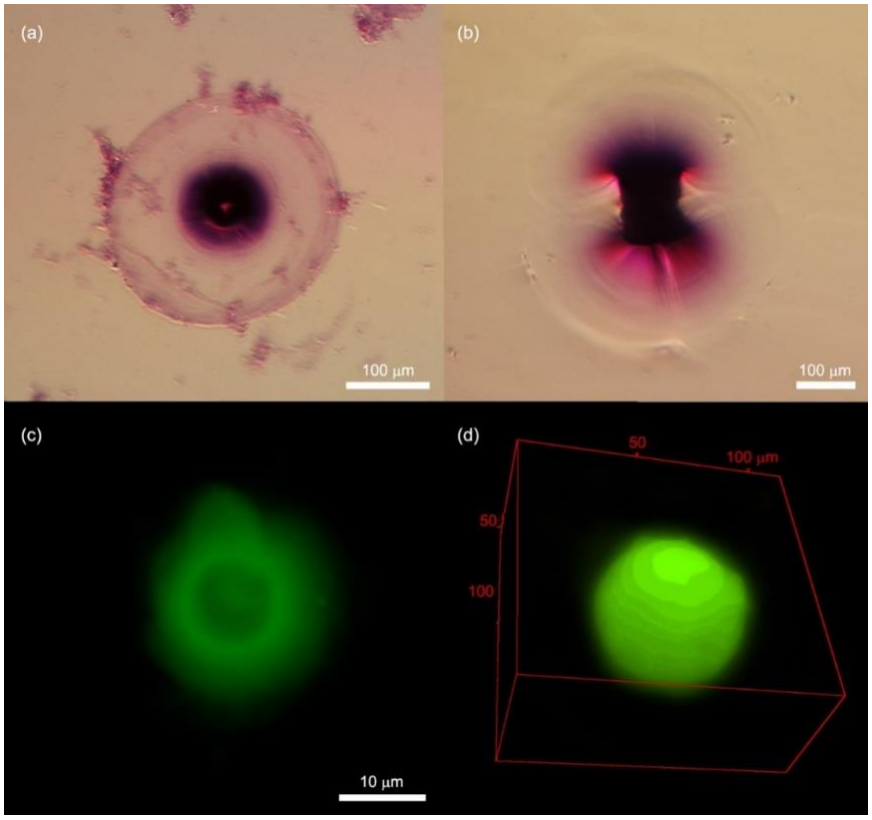

Figure 3-2. Spherical gel particles of various sizes. Toluidine blue dyed spherical gel particles observed by Hoffman modulation microscopy (**a, b**). A z-stacked confocal laser scanning microscopic (CLSM) image of a fluorescently tagged particle (**c**). A 3D image of the sphere from CLSM scans is shown in (**d**).

Within the spherical gel particles, the interior donut-shaped structures appear to be more heavily dyed than the balloon areas (**Figure 3-2a, b**), suggesting that the negatively charged cellulose chains are more densely packed in the donuts. The donuts are most probably originated from the "collars" in CMF, where microfibrils in all S1, S2, and S3 layers are deposited upon ballooning [7]. This is in agreement with the confocal laser scanning microscopic (CLSM)

observations, in which the COO groups in donut areas show stronger fluorescent intensity (**Figure 3-2c**). When CLSM scans were reconstructed in 3D, a sphere was observed as presented in Figure 2d. Studies have shown that during the fiber swelling and fragmentation in prolonged chemical treatments, the fiber breaks down into "flat rings" rather than spheres [25, 29, 30]. The break-up mechanism of the swollen fibers, CMF in this case, by applying ultrasonication is obviously different from that by increasing the chemical treatment time.

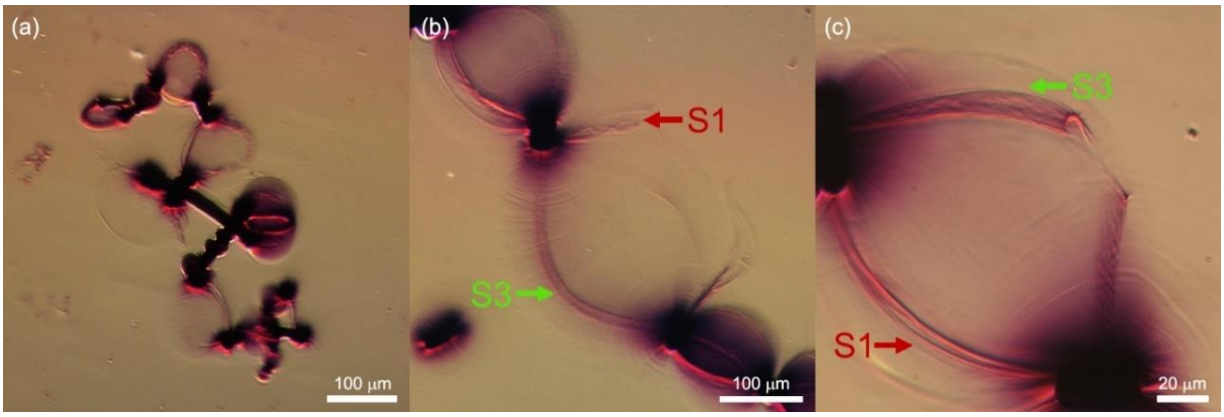

Figure 3-3. Fiber fragments in CMF suspension left inside the ultrasonic cleaning bath for 1 min. CMF experiences axial distortion (**a**), followed by S1 (**b**) and S3 layer break-up (**c**). S1 and S3 break-ups are not sequential.

In order to monitor intermediate structures of the CMF during mechanical break-up, a CMF suspension placed in an ultrasonic cleaning bath was microscopically observed. It appears that the helically wound S1 microfibrils are restricting the swollen fiber mobility during ultrasonication. This results a severe axial distortion and yields a structure shown in **Figure 3-3a**. As a consequence, an increased amount of tension is build up on the helices and it eventually reaches the point where they fracture (**3b**). Same principle applies to the S3 layers that are already under axial compression, hence they are cleaved before the balloons break open (**3c**).

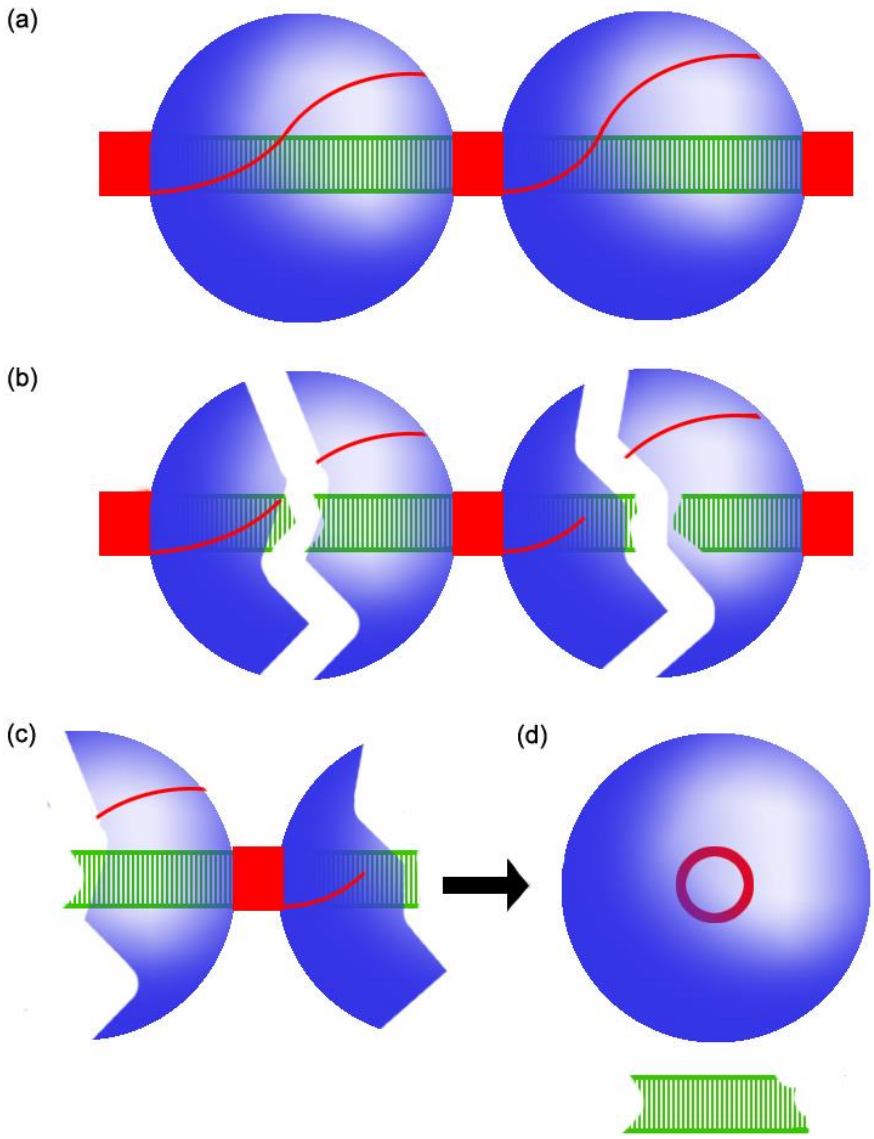

Figure 3-4. Proposed break-up mechanism of CMF by applying ultrasonication. Microfibrils in each secondary layer are color coded, S1 in red, S2 in blue, and S3 in green. A highly swollen, balloon-like structure before applying any mechanical treatments (**a**). Ultrasonication damages microfibrils in the balloon area and CMF starts to fragment (**b**). The fragment (**c**) rearranges into a sphere and the S3 layer is often separated from the sphere (**d**). All drawings are approximately to scale.

Based on microscopic observations made in **Figure 3-2** and **3-3**, we propose a break-up mechanism in **Figure 3-2**. When a highly swollen CMF suspension is ultrasonicated (**4a**), the balloons break apart (**4b**). The balloon break-up is associated with the damaged S1 microfibrils that are helically extended around the balloons, as well as the cleavage of the axially compressed S3 layers. Within the fiber fragments (**4c**), the S2 microfibrils rearrange to form spheres as

shown in **4d**. During this process, the S3 layers can be separated out and suspended in solution. The most remarkable transformation in our proposed mechanism is from **Figure 3–4c** to **4d**. This transition was not directly observed microscopically, conceivably because of the fast rearrangement of the S2 fibrils around the collars after the balloon break-up.

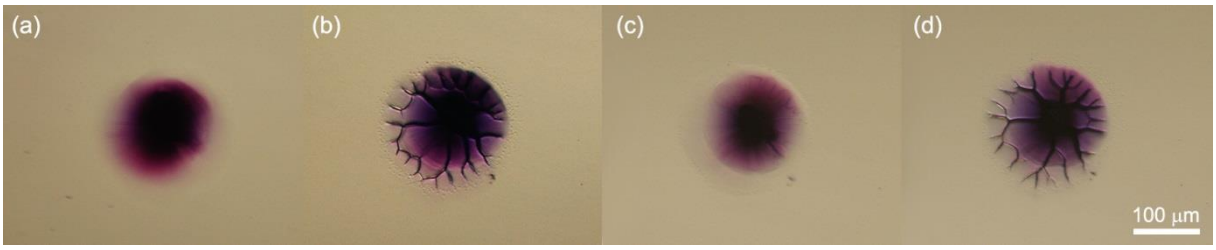

Figure 3-5. HMC of gel suspended in water (**a**), air-dried overnight at room temperature (**b**), rewetted by adding a drop of water (**c**), and then re-dried under the same condition as b (**d**).

The rewettability of the spherical gel particles was qualitatively analyzed by going through two drying cycles (**Figure 3-5**). After imaging 5a, the slide was left overnight in an ambient condition without removing the coverslip. Upon drying, thin branches that are rooted at the collars were formed to make globular structures as seen in **5b**. The formation of the branched structures is most probably a drying effect which occurs when the cellulosic materials held together inside the balloons – unmodified, partially and fully carboxymethylated cellulose chains – are dried together. As the dried samples were rewetted by adding a drop of water between the coverslip and the slide, the flattened sphere reformed to its swollen state back in a few seconds, **5c**. When the rewetted sample was dried again in the same manner as before, the thin branches were regenerated but they do not come together in same shape as before, **5d**. The fact that the sphere in **5c** is only slightly smaller diameter as in 5a suggests that these gel particles have a good rewettability.

The surface morphology of dried gel particles was observed by SEM. Thin branches seen in **Figure 5b** and **5d** were not observed in this case probably because of the differences in

surface energy of the two substrates, glass (**Figure 3-5**) and mica (**Figure 3-6**). Relatively rougher glass surface provides more anchoring sites than a smooth mica surface, thereby promoting cellulose chain aggregation that leads to the formation of branched structures. When the spherical particles were dried on a mica, the spheres are collapsed upon the collars, creating the interior donut-shaped structures. The dried donuts appear to be composed of approximately 1-2 μm thick spirals, where the literature reported thickness of the S1 layer in native softwood fibers is about 0.1 to 0.2 μm [31]. This may indicate that the collars are mainly composed of S1 microfibrils and that the flexible S2 cellulose fibrils held inside the balloons are collapsed on this interior skeleton. As a consequence, an apparent thickness of each spiral is increased by 5 to 10 times.

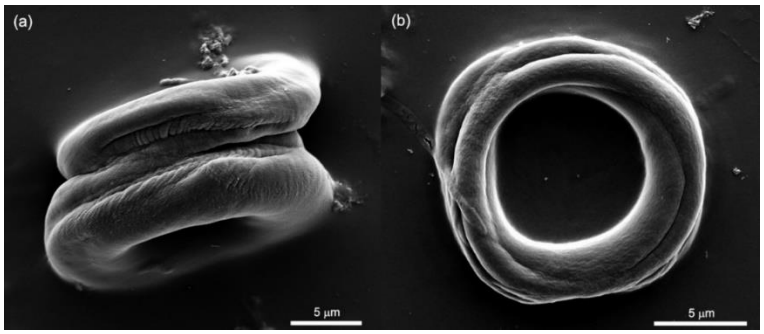

Figure 3-6. SEM of gel particles deposited on mica, air-dried overnight. All samples are Pt coated (10 nm). Thick donut-shaped structures that are composed of tight spirals are observed from the side (**a**); and from the top (**b**).

Due to the heterogeneous nature of the wood fiber structures, the chemically modified fibers often show various shapes and wide size distributions. Examples of non-spherical structures are shown in **Figure 3-7**. Chopped off CMF with more than two spheres are often seen, along with isolated S3 layers that are partially damaged or shortened (**7a**). Fluorescent tagged non-spherical particles show that the donut-shaped interior structure maintains the characteristic features of S1 collars, where the charged cellulose chains are highly concentrated while forming tightly wound spirals (**7b**). The surface tagged S3 layers sometimes remain inside

the spherical gel particles. **Figure 3-7c** shows a S1 microfibril protruding from the donut-shaped spirals, whereas **Figure 3-6** showed closed, thick donuts with an empty space in the middle.

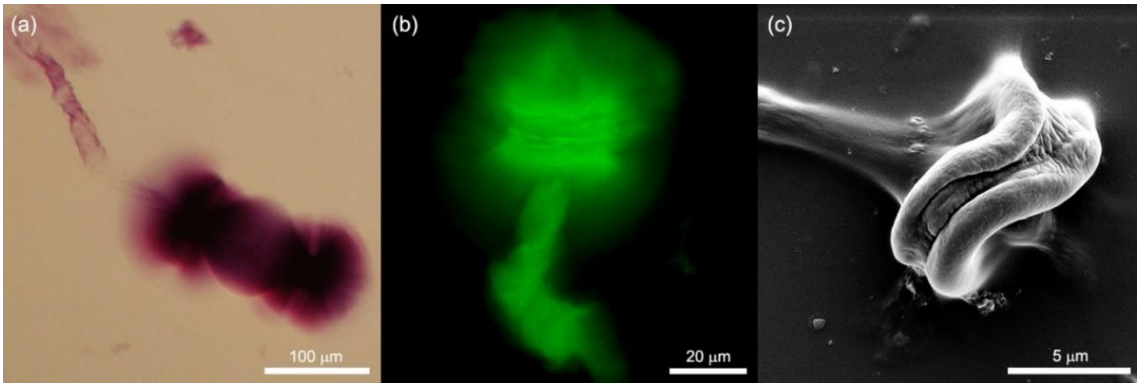

Figure 3-7. Non-spherical structures produced by ultrasonicating the CMF suspension. HMC of a series of spheres in a shortened CMF and an isolated S3 layer **(a)**; CLSM of a sphere with protruding S3 layers **(b)**; and SEM of dried non-spherical particle on a mica surface with a protruding S1 microfibrils **(c)**.

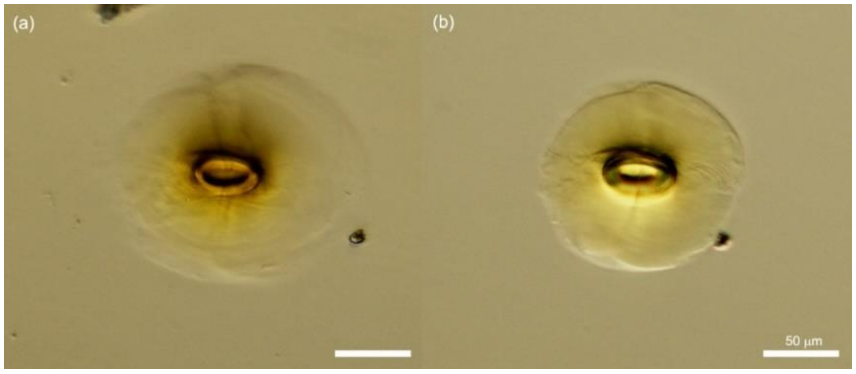

Figure 3-8. HMC of A-fluo tagged gel in water at neutral pH (**a**) and after adding a drop of 1M HCl (**b**).

Figure 3-8 shows a spherical gel particle before (**a**) and after (**b**) adding a drop of 1M HCl solution. As the free carboxyl groups are protonated, the gel boundary becomes more defined and the overall diameter decreases. Although there are no significant changes in the interior donut-shaped structure, they appear slightly thicker after the addition of acid.

3.4 Concluding Remarks

Efforts have been made to optimize cellulose processing by improving the cellulose fiber dissolution, which is unfavourable in many solvent systems including water. Heterogeneous swelling of the fibers, thereby creating balloon-like structures, is often seen while chemically processing the fibers. The fact that the ballooning occurs in both aqueous and non-aqueous solvent systems and during carboxylating chemistries indicates that this phenomenon is mainly related to the cellulose microfibril arrangements in fiber wall. The underlying findings of this work illustrate the structural evolution of partially carboxylated cellulose fibers while going through a subsequent mechanical treatment. Our proposed break-up mechanism based on microscopic observations suggest that the altered microfibril arrangements occurring at the swelling stage create areas of different structural rigidity, which prevents a complete fiber dissolution. The produced spherical gel particles with interior donut-shaped structure may have applications in drug delivery or sensing, where micrometer sized gel particles with rewettability and pH responsibility are required.

3.5 References

[1] Isogai A, Saito T, Fukuzumi H. TEMPO-oxidized cellulose nanofibers. Nanoscale 2011;3:71–85.

[2] Liimatainen H, Visanko M. Enhancement of the nanofibrillation of wood cellulose through sequential periodate–chlorite oxidation. Biomacromolecules 2012;13:1592–7.

[3] Klemm D, Kramer F, Moritz S, Lindström T, Ankerfors M, Gray D, et al. Nanocelluloses: a new family of nature-based materials. Angew Chem Int Ed Engl 2011;50:5438–66.

[4] Siró I, Plackett D. Microfibrillated cellulose and new nanocomposite materials: a review. Cellulose 2010;17:459–94.

[5] Eyholzer C, Bordeanu N, Lopez-Suevos F, Rentsch D, Zimmermann T, Oksman K. Preparation and characterization of water-redispersible nanofibrillated cellulose in powder form. Cellulose 2009;17:19–30.

[6] Saito T, Kimura S, Nishiyama Y, Isogai A. Cellulose nanofibers prepared by TEMPO-mediated oxidation of native cellulose. Biomacromolecules 2007;8:2485–91.

[7] Sim G, Alam M, Godbout L, van de Ven TGM. Structure of swollen carboxylated cellulose fibers. Cellulose 2014;21:4595–606.

[8] Rácz I, Borsa J. Swelling of carboxymethylated cellulose fibres. Cellulose 1997;4:293–303.

[9] Pei A, Butchosa N, Berglund L a., Zhou Q. Surface quaternized cellulose nanofibrils with high water absorbency and adsorption capacity for anionic dyes. Soft Matter 2013;9:2047.

[10] Jardeby K, Germgard U, Kreutz B, Heinze T, Heinze U, Lennholm H. The influence of fibre wall thickness on the undissolved residuals in CMC solutions. Cellulose 2005;12:167–75
[11] Cuissinat C, Navard P. Swelling and Dissolution of Cellulose Part 1: Free Floating Cotton and Wood Fibres in N-Methylmorpholine-N-oxide–Water Mixtures. Macromol Symp 2006;244:1–18.
[12] Le Moigne N, Montes E, Pannetier C, Höfte H, Navard P. Gradient in dissolution capacity of successively deposited cell wall layers in cotton fibres. Macromol Symp 2008;262:65–71.
[13] Le Moigne N, Bikard J, Navard P. Rotation and contraction of native and regenerated cellulose fibers upon swelling and dissolution: the role of morphological and stress unbalances. Cellulose 2010;17:507–19.
[14] Iwamoto S, Nakagaito a. N, Yano H. Nano-fibrillation of pulp fibers for the processing of transparent nanocomposites. Appl Phys A 2007;89:461–6.
[15] Rathna GVN, Mohan Rao D V., Chatterji PR. Hydrogels of gelatin-sodium carboxymethyl cellulose: synthesis and swelling kinetics. J Macromol Sci Part A 1996;33:1199–207.
[16] Chen H, Fan M. Novel Thermally Sensitive pH-dependent chitosan/ carboxymethyl cellulose hydrogels. J Bioact Compat Polym 2008;23:38–48.
[17] Pelton R, Hoare T. Microgels and their synthesis: an introduction. Microgel Suspens. Fundam. Appl., 2011, p. 3–31.
[18] Dhar N, Akhlaghi SP, Tam KC. Biodegradable and biocompatible polyampholyte microgels derived from chitosan, carboxymethyl cellulose and modified methyl cellulose. Carbohydr Polym 2012;87:101–9.
[19] Bochek a. M, Zabivalova NM, Yudin VE, Gofman I V., Lavrent'ev VK, Volchek BZ, et al. Properties of carboxymethyl cellulose aqueous solutions with nanoparticle additives and the related composite films. Polym Sci Ser A 2011;53:1167–74.
[20] Qi H, Liebert T, Meister F, Zhang L, Heinze T. Homogenous carboxymethylation of cellulose in the new alkaline solvent LiOH/urea aqueous solution. Macromol Symp 2010;294:125–32.
[21] Khullar R, Varshney VK, Naithani S, Heinze T, Soni PL. Carboxymethylation of cellulosic material (average degree of polymerization 2600) isolated from cotton (Gossypium) linters with respect to degree of substitution and rheological behavior. J Appl Polym Sci 2005;96:1477–82.
[22] Jiang L, Li Y, Zhang L, Wang X. Preparation and characterization of a novel composite containing carboxymethyl cellulose used for bone repair. Mater Sci Eng C 2009;29:193–8.
[23] Sim G, van de Ven TGM. The S3 layer isolated from carboxymethylated cellulose wood fibers. Cellulose 2015;22;1:45-52.
[24] Jardeby K, Germgård U, Kreutz B, Heinze T, Heinze U, Lennholm H. Effect of pulp composition on the characteristics of residuals in CMC made from such pulps. Cellulose 2005;12:385–93.
[25] Jardeby K, Lennholm H, Germgård U. Characterisation of the undissolved residuals in CMC-solutions. Cellulose 2004:195–202.
[26] Yang H, Tejado A, Alam N, Antal M, van de Ven TGM. Films prepared from electrosterically stabilized nanocrystalline cellulose. Langmuir 2012;28:7834–42.
[27] Tejado A, Alam MN, Antal M, Yang H, Ven TGM. Energy requirements for the disintegration of cellulose fibers into cellulose nanofibers. Cellulose 2012;19:831–42.
[28] Van de Ven TGM, Saint-Cyr K, Allix M. Adsorption of toluidine blue on pulp fibers. Colloids Surfaces A Physicochem Eng Asp 2007;294:1–7.
[29] Le Moigne N, Navard P. Dissolution mechanisms of wood cellulose fibres in NaOH–water. Cellulose 2009;17:31–45.
[30] Le Moigne N, Jardeby K, Navard P. Structural changes and alkaline solubility of wood cellulose fibers after enzymatic peeling treatment. Carbohydr Polym 2010;79:325–32.
[31] Booker RE, Sell J. The nanostructure of the cell wall of softwoods and its functions in a living tree. Holz Als Roh- Und Werkst 1998;56:1–8.

Bridging Section between Chapter 3 and Chapter 4

The formation and breakup mechanisms of carboxymethylated cellulose fibers were discussed in the preceding two chapters. One of the most striking observations made from the previous studies was that the innermost S3 layer remains intact within the fiber wall even after undergoing a series of chemical and mechanical treatments. A new experimental protocol was developed to isolate and characterize S3 layers from the swollen CMF. Prior to the work presented in the forthcoming chapter, all known features about the S3 layers were based on cross-sectional microscopic studies. In Chapter 4, microfibril arrangements, chemical reactivity, handedness, and the layer thickness of the isolated S3 layers will be discussed in detail. The results of this research have been published in the following paper:

G. Sim and T.G.M. van de Ven, The S3 layer isolated from carboxymethylated cellulose wood fibers, Cellulose (2015) 22:1, 45-52

Chapter 4. The S3 Layer Isolated from Carboxymethylated Cellulose Wood Fibers

Abstract

The innermost S3 layer is isolated from highly swollen, carboxymethylated cellulose wood fibers (CMF). The isolation is attempted by applying gentle magnetic stirring, ultrasonication, and acid hydrolysis, where each treatment has caused the formation of largely variable fiber morphologies. The S3 layer can be partially or completely isolated from the CMF by applying gentle shear or a mild acid hydrolysis. The S3 layer isolated from CMF is highly swollen with a volume 5 to 10 times its original value, and has microfibril angles (MFA) between 50 and 90°. Surface carboxylates on the S3 microfibrils are available for further chemical modifications. Dominant right handedness is observed from 3D reconstructed confocal microscopic images. When air-dried from water, the S3 layer collapses completely onto the substrate, giving an average layer thickness of 83 to 140 nm.

4.1 Introduction

Wood cell walls are carefully engineered structures that are capable of providing optimum stiffness, strength, and hardness to trees. The structures of the wood cell walls have been studied extensively on different levels – macroscopic, microscopic, nanoscale, and molecular – in order to thoroughly understand the properties of the wood based products [1–3]. The three major chemical components in wood fibers are cellulose, hemicellulose, and lignin. Since cellulose fibers have advantages in superior strength-to-weight ratio, corrosion and fatigue resistance, and abundance, utilizing cellulosic materials has been attracting much attention for the past few decades [4]. As cellulose chains are synthesized, accumulated and crystallized in nature, they

form bundles of nano-, and then microfibrils [5]. The microfibrils are arranged in specific angles (microfibril angles, MFA), which provide distinctiveness between the sublayers of the secondary (S) layer, namely, S1, S2, and S3 layers [6].

The S2 layer is typically 40 times thicker than the other two secondary layers, hence its properties and functions have been well studied [7–9]. A recent literature review reveals a controversy over the cellulose microfibril orientations in the S3 layer, as some report a cross-fibrillar structure while others report a single handedness [10]. It has been particularly difficult to characterize the S3 layer as it becomes even thinner with increasing age and height [11]. It is important to understand the properties of the S3 layer as this innermost layer is responsible for strengthening the cell against collapse while resisting transwall fracture in transverse directions [1]. Non-uniform swelling of the wood fibers generates balloon-like structures due to the alternating microfibril arrangements between the S-layers [12]. The S3 layer consisting of tightly wound microfibrils is often seen inside the balloons [13–16], but thus far, it has never been isolated to be examined. Most of the known properties of the S3 layers are from cross-sectional observations by electron microscopy [11,17].

In studying the swelling behavior of carboxylated wood fibers, we have observed that the homogeneously swollen fibers break apart on every level, including the S3 layer. However, the S3 layer remained intact when the fibers are swollen heterogeneously to form balloons [12]. In this study, we have attempted to isolate the S3 layer from the highly swollen carboxymethylated fibers (CMF) by applying mechanical or chemical treatments. Microfibril angles, degree of swelling, wall thickness, apparent handedness, and reactivity of the S3 layers will be discussed.

4.2 Experimental

4.2.1 Materials

Bleached softwood kraft pulp sheets (SKF; Domtar, Canada; <1% lignin, 10-20% hemicellulose, 80-90% cellulose) made from spruce were used as native cellulose material. Reagent grade sodium chloroacetate (MCA), sodium hydroxide (NaOH), hydrochloric acid (HCl), *N*-(3-Dimethylaminopropyl)-*N*′-ethylcarbodiimide hydrochloride (EDC), and 5-aminofuorescein (A-fluo). All chemicals were purchased from Sigma-Aldrich and were used as received.

4.2.1.1 Carboxymethylation

Small pieces of SKP sheets (50 g) were soaked in distilled water overnight, and then disintegrated by a household tilt-head stand mixer (Kitchenaid, Professional 550 plus). After filtering out the excess water, the pulp was dried at 50℃. Sodium chloroacetate (100 g MCA in 130 mL water) was mixed with the dried pulp and digested at 60℃ for 4 hours prior to mixing with sodium hydroxide solution (62.5 g NaOH in 100 mL water). The pulp slurry was left overnight at room temperature, followed by 5-6 successively washing with 70-100% ethanol. The carboxymethylated fibers (CMF) were dried at 50℃ and stored at room temperature until further use. They could be readily redispersed in water with gentle magnetic stirring.

4.2.1.2 Isolation of the S3 layer

Mechanical Treatment The CMF suspensions were mechanically treated by two different methods. (1) 250 mL of 0.1 %w/w CMF suspension was stirred at 350 rpm up to 5 days at room temperature. Samples (8 mL) were drawn every 24 hours to observe changes in fiber morphology. (2) Similarly, four 25 mL of 0.1 %w/w CMF suspensions were ultrasonicated (Hielscher, UP200H; 200 W, 24 kHz) for 15, 30, 45, 60 sec.

Chemical Treatment 0.1 %w/w CMF suspension was subjected to a mild acid hydrolysis using 1 N hydrochloric acid at 50℃ for 1 hour under magnetic stirring (250 rpm). Upon purification (5 day dialysis; Spectra/Por, MWCO 12,000), hydrolyzed CMF was re-dispersed in water and stirred for another 24 hours at 350 rpm.

4.2.1.3 Fluorescent tagging of the carboxyl groups of the fibers

Carboxyl groups of the CMF and the hydrolyzed CMF were tagged with fluorescein derivative by following the procedure reported by Hu and Hayek (2012). SKP and CMF suspensions (0.1 %w/w) were mixed with A-fluo and EDC·HCl (COOH: A-fluo: EDC·HCl = 2: 1: 2) at pH 4-4.5 for 16 hours. The samples were then dialyzed for 5-7 days (Spectra/Por, MWCO 12,000).

4.2.2 Characterization

4.2.2.1 Charge determination

The carboxyl contents of SKP and CMF were measured by conductometric titration (Metrohm 836 Titrando). Titration was performed according to Yang et al [19].

4.2.2.2 Microscopic imaging

Optical microscopy Cellulose fiber dispersions that are dyed with toluidine blue were observed by Hoffman modulation contrast microscopy (HMC, Nikon Eclipse TE2000-U). Fluorescently tagged fibers were examined by confocal microscopy (Zeiss LSM510; 488 nm, Ar laser, 30 mW). Confocal imaging was done in water immersion to minimize refraction.

Atomic Force Microscopy The S3 layers were deposited on a mica surface and air-dried overnight. The topography and the thickness of the S3 layers were examined under ambient conditions using an extended Multimode scanning probe microscope and Nanoscope IIIa

controller (Digital Instruments, Santa Barbara, CA). Images were acquired in contact mode with silicon nitride probes (Bruker, DNP-10) with a nominal spring constant of 0.12 N/m, tip length 205 μm, tip width 40 μm, and resonant frequencies 23 kHz.

Scanning Electron Microscopy The S3 layers were deposited on a mica, air-dried, and then sputter-coated with gold with a thickness of 8 nm. Images have made with a High resolution Field Emission Scanning Electron Microscope (FE-SEM; JEOL, JSM-7400F) which was operated at an accelerating voltage of 5.0 kV to observe the surface morphology of the dried S3 layer.

4.3 Results and Discussions

Bleached softwood kraft fibers (**Figure 4-1**) were carboxymethylated to produce balloon-like structures bearing 2.6 mmol/g of COO groups (**Figure 4-1b**). Inside these balloons, the S3 layers clearly remain intact while maintaining its native MFA. 0.1 %w/w carboxymethylated fiber (CMF) suspensions were treated both chemically and mechanically to isolate the S3 layer from the outer S1 and S2 layers.

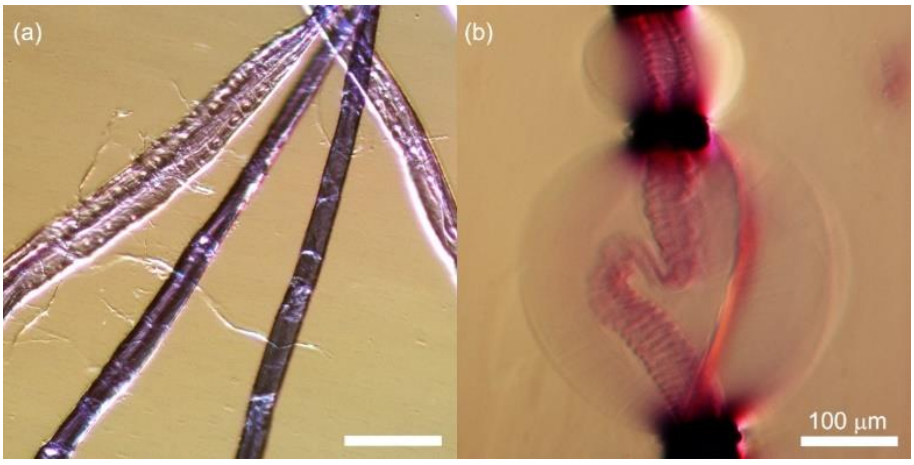

Figure 4-1. Hoffman modulation contrast light microscopy (HMC) of cellulose fibers dyed with toluidine blue. Bleached, kraft, softwood fibers (**a**); carboxymethylated fiber, CMF, (**b**) with [COO] = 2.6 mmol/g. Scale bars are 100 μm.

4.3.1 Mechanically treated carboxymethylated fibers

Carboxymethylation initially weakens the fiber structure by introducing charge groups and by disrupting the native crystalline form. CMF is, therefore, more prone to fiber breakup when treated mechanically. In order to isolate the S3 layer from CMF, it is necessary to understand how CMF behaves when subjected to various amounts of energy applied to the system. The CMF suspensions were subjected to a gentle magnetic stirring or ultrasonication while monitoring their structural changes over time.

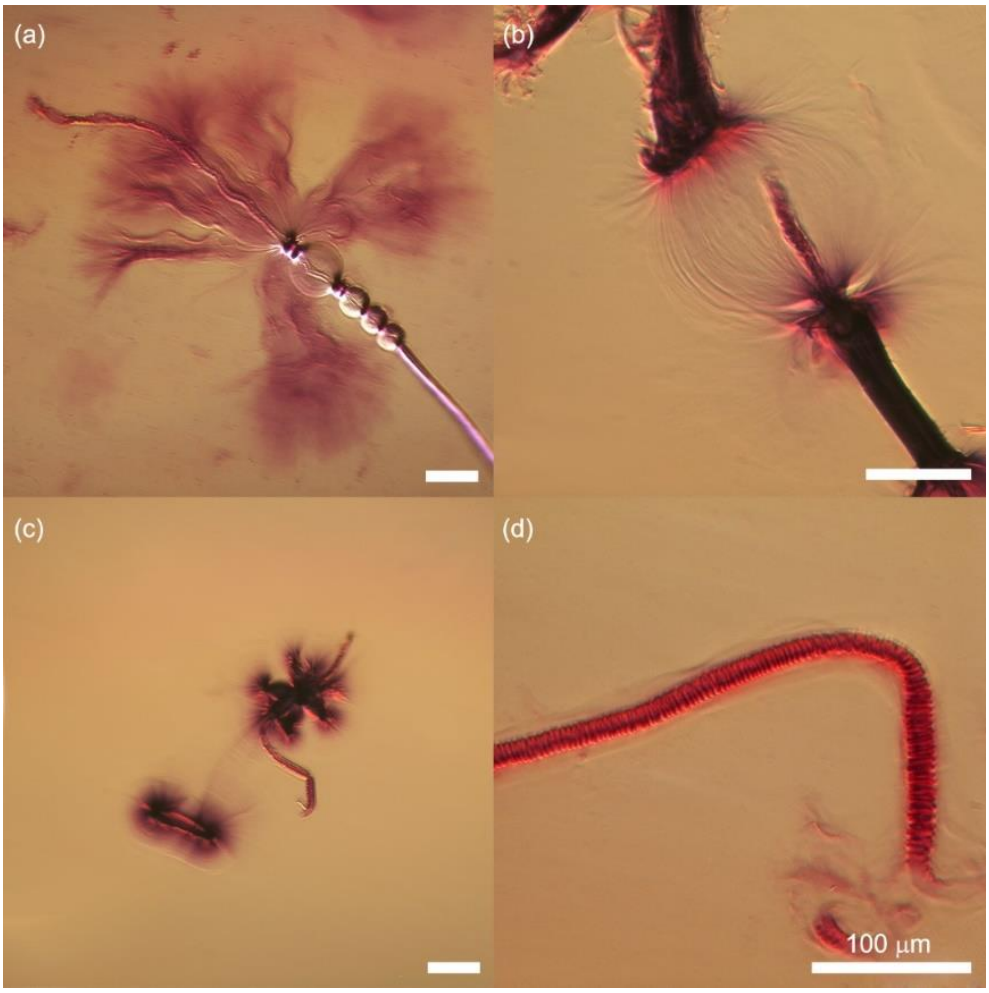

Figure 4-2. HMC of a 0.1% CMF suspension subjected to a gentle magnetic stirring at 350 rpm for 24 hrs (**a**), 48 hrs (**b**), 72 hrs (**c**) and 96 hrs (**d**). Scale bars are 100 μm.

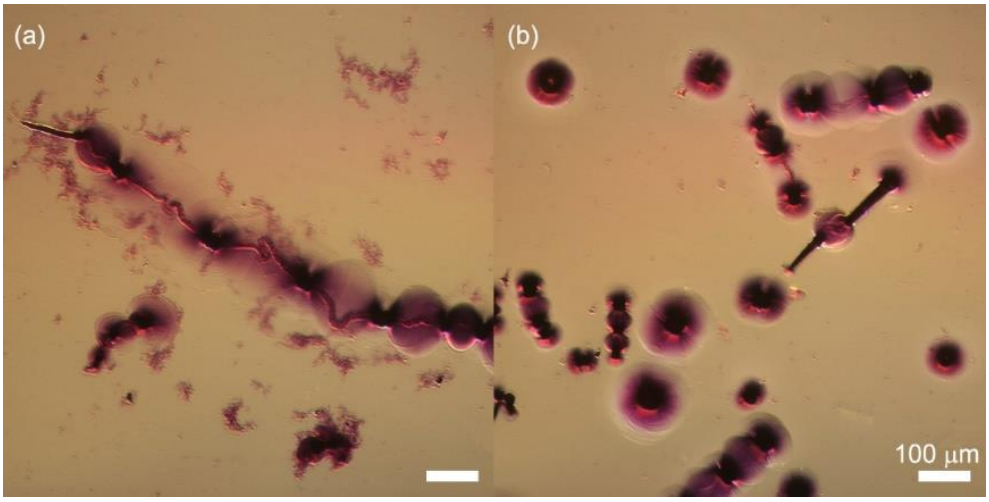

Figure 4-3. HMC of 0.1% CMF suspension is ultrasonicated for 15 sec (**a**); and 45 sec (**b**). Toluidine blue dyed. Scale bars are 100 μm.

In case of magnetic stirring at 350 rpm, the first stage of CMF break-up consisted of damaging the surface fibrils. The outermost S1 layer, which is responsible for keeping the balloons together, is damaged after 24 to 48 hours of stirring. As can be seen in **Figure 4-2a**, the protruding microfibrils that were enclosed inside the balloons are now released and stretched outwards due to the charge repulsion. Sometimes the S3 layer can also be damaged prior to the break-up of the balloons (**Figure 4-2b**). After 72 to 96 hours of stirring, most of the outer S1 and S2 layers are disintegrated and break into pieces of various sizes and shapes. Along with thin sheets of cellulosic materials and other irregular forms of CMF fragments, small balloons with broken S3 layers are observed as well (**Figure 4-2c**). At this point, some of the S3 layers appear to be completely isolated from the CMF as shown in Figure 2d. The isolated S3 layer has microfibril angles (MFA) as high as 85 – 90°, indicating that the S3 layer keeps its structural integrity after carboxymethylation, followed by this type of mechanical treatment. Other properties of the isolated S3 layers will be discussed in detail below.

When the CMF suspension is sonicated for 15 sec, some of the CMF are completely disintegrated, while some remain intact showing partial damage (**Figure 4-3a**). With an

increased amount of sonication time (45 sec), the CMF breaks down into spherical and disk-like structures (**Figure 4-3b**). The appearance of "flat rings" has also been reported during the dissolution of the fibers in NaOH-water solution at –6 ℃ [20]. The authors claim that the governing factor of the dismantlement and fragmentation of the fibers is the high swelling, not the shear stress applied during the dissolution process. In our case, the swelling has already been fully achieved prior to applying the mechanical energy.

Compared to the gentle magnetic stirring, ultrasonication provides much localized, intense mechanical energy. As the S3 layer provides the continuity in the CMF, the length of the CMF is defined by that of the S3 layer. The ultrasonication must be strong enough to simultaneously chop off all three S-layers, including the S3, thereby severely shortening the CMF within a minute. The intensity and the total amount of energy applied to the system can yield different forms of fiber break-up; hence the differences in **Figure 4-2** and **3**. For a better S3 layer isolation, an intense mechanical treatment should be avoided.

4.3.2 Hydrolyzed CMF

The CMF suspension was subjected to a mild acid hydrolysis to facilitate the isolation of the S3 layer by weakening the swollen fiber structure. See Figure 4 for the different forms of CMF observed during the hydrolysis. It appears that the S1 microfibrils are hydrolyzed away first, as there are only few balloons and collars are left while the S2 and S3 layers remain intact (**Figure 4-4a**). Some hydrolyzed CMF, on the other hand, show absolutely no collars at all (**Figure 4-4b**). The "series of balloons" has turned into a "double layered tube" with a partially crumpled S3 layers surrounded by a well-defined S2 layers. The boundary of the S2 layer can be disrupted and fragmented as seen in **Figure 4-4c**.

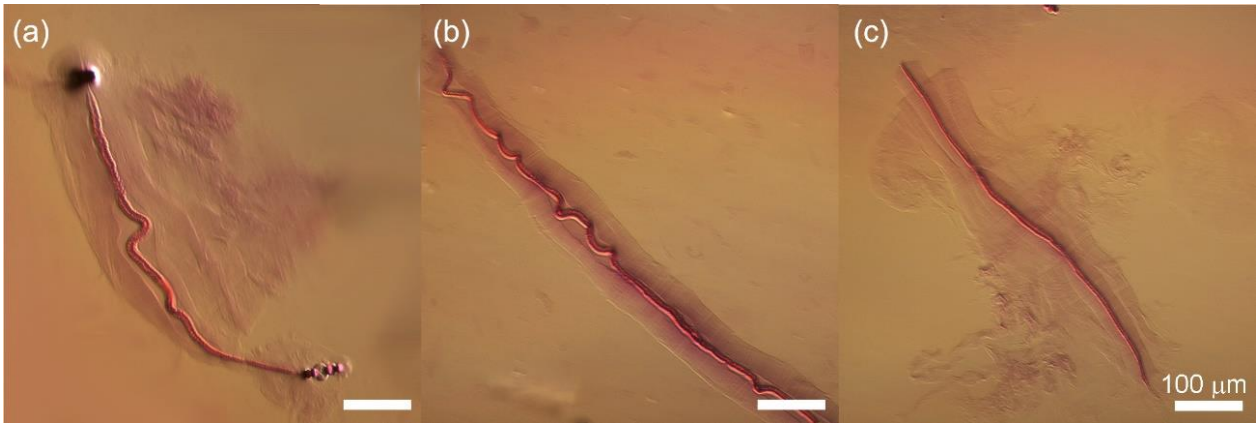

Figure 4-4. HMC of acid hydrolyzed CMF. The rates of CMF breakdown are not the same for all fibers, hence the structures vary. A single suspension contains all three different forms, (**a**) – (**c**). Toluidine blue dyed. Scale bars are 100 μm.

Unlike the other two secondary layers, microfibril arrangements in the S3 layer remain unchanged after a series of chemical treatments. This may imply that each S-layer has different chemical reactivity, or that the microfibril rearrangement within the S3 layer is somehow prevented. Considering that the chemical composition of the three S-layers became comparable to each other after kraft pulping, the reactivity differences must arise from the physical constrains that each layer experiences. Since the tightly wound S3 layers inside the CMF fluoresce with a similar intensity as the highly swollen S1 and S2 layers [12], it is difficult to identify how differently each layer is charged and how this is related to the reactivity of individual layers. As the chemicals have enough accessibility to the S3 layers from the lumen, there is no accessibility issue which may have suppressed the reactivity of the S3 microfibrils. It is more likely that the S2 layer, which is approximately 40 times thicker than the S1 and S3 layers [1], applies stresses on these two layers as it swells about 5 to 10 times. As a result of the S2 expansion, the external S1 forms collars while the S3 experiences axial compression. The compressed S3 layer can, therefore, maintain its MFA.

4.3.3 Isolated S3 layer

The partially hydrolyzed 0.1% CMF suspension was neutralized, purified, and then subjected to an overnight magnetic stirring to isolate the S3 layers from the "double layered tubes". The isolated S3 layers were then individually picked up and mounted on a slide to obtain images by Hoffman modulation contrast microscopy. **Figure 4-5a** shows an isolated S3 layer with some imperfections and cuts. These imperfections result in fiber shortening, which eventually leads to the wide length distribution of the partially or completely isolated S3 layers. The length of isolated S3 layers can vary anywhere between 100 μm to a few millimetres. As illustrated in **Figure 4-5b**, the MFA of the S3 layer is between 50 – 90° with variations from one specimen to the other. This variation is likely caused by the heterogeneous properties of the wood fibers themselves. In general, latewood cells often have lower MFA, smaller lumen and thicker walls than earlywood cells [21].

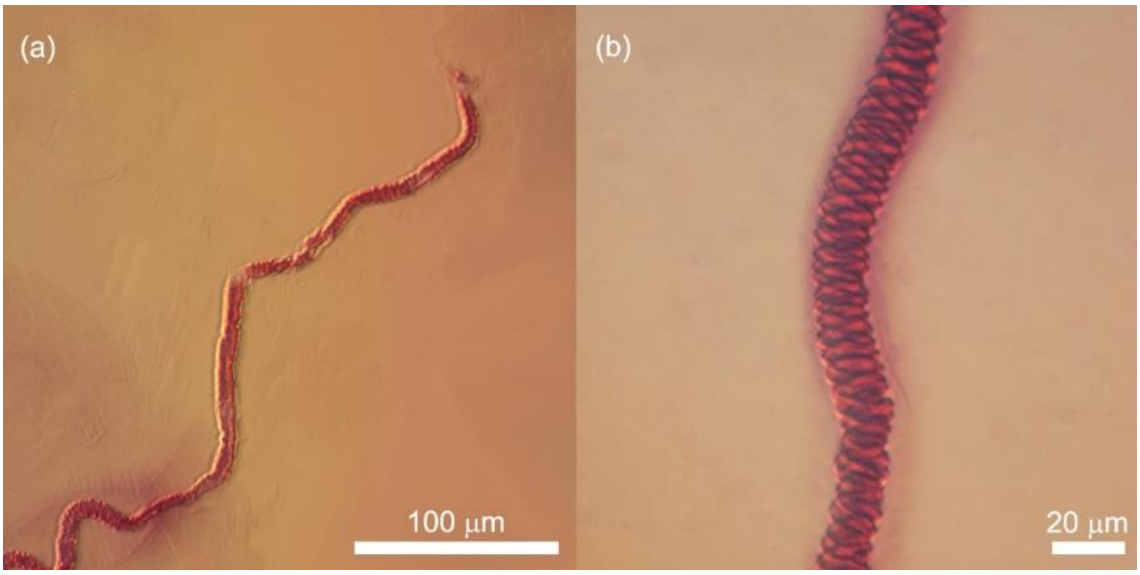

Figure 4-5. HMC of isolated S3 layer. Toluidine blue dyed. The isolated S3 layer shows partial damages and imperfections (**a**); and its MFA ranges from 50 – 90° (**b**).

The COO groups on the isolated S3 layer were fluorescently tagged by EDC assisted fluoresceinamine bioconjugation reaction. By confocal microscopy, the S3 layer in water was

reconstructed in 3D **Figure 4-6a**. The S3 microfibrils show a predominant right-handedness. A longitudinal section towards the left-hand side of (**a**) is shown in (**b**), right-hand side in (**c**). From (**b**) and (**c**), microfibrils are seen as parallelly stacked slanted lines, again suggesting that the fibrils are spiralling up in a single direction. Although it is difficult to identify whether or not all the microfibrils are right-handed in the S3 layer, we have observed dominant right-handedness when the S3 is viewed from outside. Our observation agrees with other studies which have reported more common right-handedness towards the S2 layer, with an occasional left-handedness towards the lumen [1,11]. The top and the bottom views of the S3 layer are shown in (**d**) and (**e**). These cross-sections are rather ellipsoidal than spherical, probably due to the lumen collapse which had occurred during the pulping process. The thickness of the ellipsoidal wall is approximately 1 μm, suggesting that the S3 wall is swollen 5 to 10 times [6]. This degree of swelling of the S3 layer is comparable to that of the S2 layer [12].

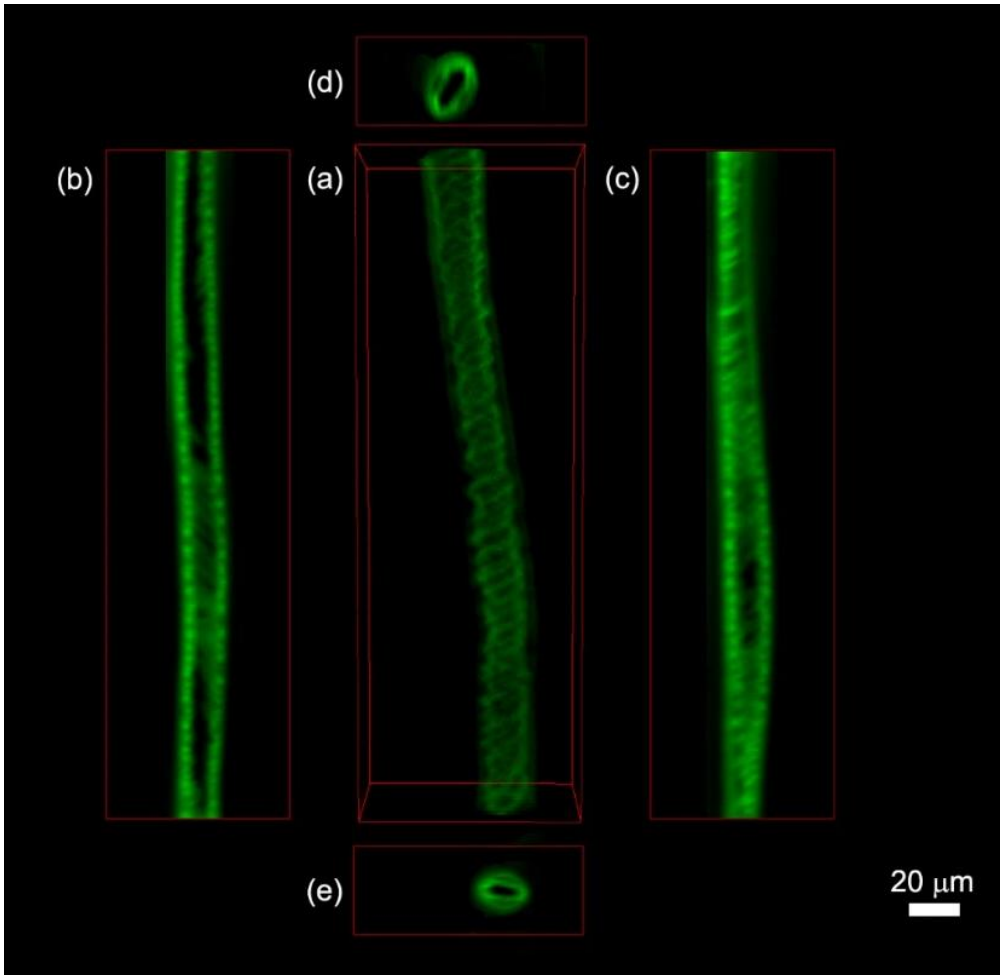

Figure 4-6. 3D reconstructed image of the isolated S3 layer from confocal microscopy (**a**); longitudinal side views (**b, c**); top (**d**); and the bottom view (**e**).

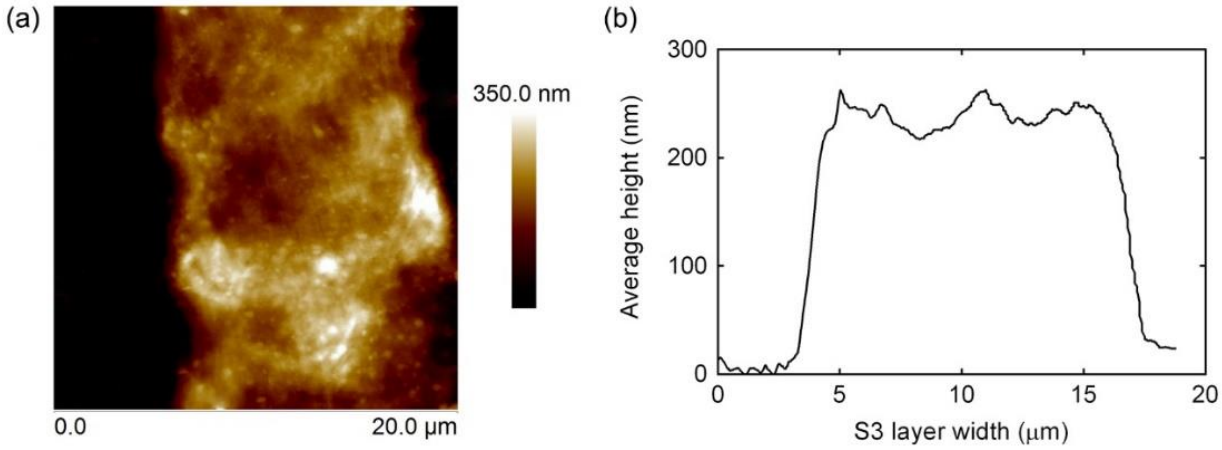

Figure 4-7. AFM of air-dried, isolated S3 layer deposited on mica. Surface height profile is obtained by AFM (**a**); and cross-sectional height profile is shown in (**b**).

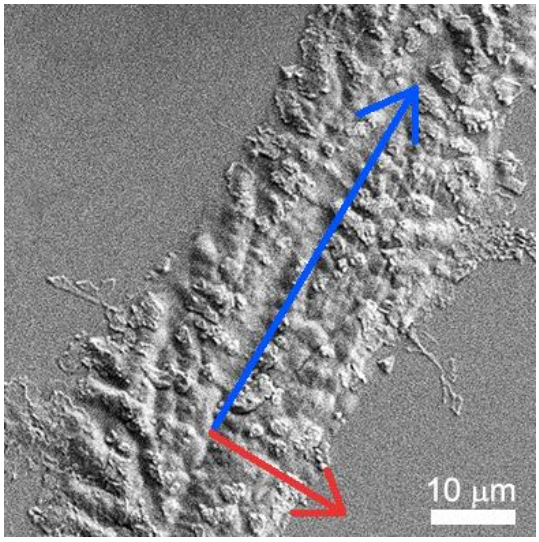

Figure 4-8. Surface morphology of air-dried, isolated S3 layer deposited on mica. Sputter coated with Au. Observation made by FE-SEM. Blue arrow annotes the fiber axis and red arrow is pointing in the direction of the microfibril. The angle between the two arrows is near 90°.

Air-dried S3 layers on mica were imaged by AFM (**Figure 4-7a**). An average cross-sectional height profile along the S3 layer shows that the dried S3 layer sample has an average height of 223 nm with the highest point of 350 nm (**Figure 4-7b**). This is equivalent to the double the thickness of the S3 layer, meaning that each carboxymethylated S3 layer is approximately 111.5 ± 28.5 nm thick. Literature reported S3 wall thicknesses are 90 nm and 140 nm for early- and latewood cells, respectively [10,22]. It is evident that the isolated and highly swollen carboxymethylated S3 microfibrils collapse completely onto the substrate when they are air-dried from water. In **Figure 4-8**, the surface morphology of the dried S3 layer is imaged by FE-SEM. Although it is difficult to resolve individual microfibrils due to the drying effect, the MFA still remains as high as 90° after drying.

4.4 Concluding remarks

The formation of the balloon-like structures via carboxymethylation facilitates the separation of the S3 layer from the S2 layer. The carboxymethylated S3 layers can be isolated from the balloon-like CMF by applying gentle magnetic stirring or a mild acid hydrolysis.

However, ultrasonication or prolonged magnetic stirring were not successful in isolating the S3 layer, as CMF was broken into spherical and disk-like structures instead. Unlike the S1 and S2 layers, the S3 layer maintains its original MFA after chemical treatments, probably due to the axial compression caused by the transverse expansion generated from the ballooning. The accessibility of the surface charge groups and the degree of swelling (5 to 10 times) are comparable in the S2 and S3 microfibrils, suggesting that the reactivity of the S3 layer is not particularly hindered. Predominant right-handedness in the S3 layer is observed.

4.5 References

[1] Booker RE, Sell J. The nanostructure of the cell wall of softwoods and its functions in a living tree. Holz Als Roh- Und Werkst 1998;56:1–8.

[2] Moon RJ, Martini A, Nairn J, Simonsen J, Youngblood J. Cellulose nanomaterials review: structure, properties and nanocomposites. vol. 40. 2011.

[3] Zhong R, Ye Z. Secondary cell walls. Encycl Life Sci 2009:1–9.

[4] Tabet T, Aziz F. Cellulose Microfibril Angle in Wood and Its Dynamic Mechanical Significance. Cellul. - Fundam. Asp., 2013, p. 113–42.

[5] Isogai A, Saito T, Fukuzumi H. TEMPO-oxidized cellulose nanofibers. Nanoscale 2011;3:71–85.

[6] Barnett JR, Bonham V. Cellulose microfibril angle in the cell wall of wood fibres. Biol Rev Camb Philos Soc 2004;79:461–72.

[7] Fahlén J, Salmén L. Cross-sectional structure of the secondary wall of wood fibers as affected by processing. J Mater Sci 2003;8:119–26.

[8] Sell J, Zimmermann T. Radial fibril agglomerations of the S2 on transverse-fracture surfaces of tracheids of tension-loaded spruce and white fir. Eur J Wood Wood Prod 1993;51:384.

[9] Déjardin A, Laurans F, Arnaud D, Breton C, Pilate G, Leplé J-C. Wood formation in Angiosperms. C R Biol 2010;333:325–34.

[10] Gibson LJ. The hierarchical structure and mechanics of plant materials. J R Soc Interface 2012;9:2749–66.

[11] Donaldson L, Xu P. Microfibril orientation across the secondary cell wall of Radiata pine tracheids. Trees 2005;19:644–53.

[12] Sim G, Alam M, Godbout L, van de Ven TGM. Structure of swollen carboxylated cellulose fibers. Cellulose 2014;21:4595–606.

[13] Jardeby K, Germgard U, Kreutz B, Heinze T, Heinze U, Lennholm H. The influence of fibre wall thickness on the undissolved residuals in CMC solutions. Cellulose 2005;12:167–75.

[14] Saito T, Kimura S, Nishiyama Y, Isogai A. Cellulose nanofibers prepared by TEMPO-mediated oxidation of native cellulose. Biomacromolecules 2007;8:2485–91.

[15] Le Moigne N, Bikard J, Navard P. Rotation and contraction of native and regenerated cellulose fibers upon swelling and dissolution: the role of morphological and stress unbalances. Cellulose 2010;17:507–19.

[16] Nakagaito AN, Yano H. The effect of fiber content on the mechanical and thermal expansion properties of biocomposites based on microfibrillated cellulose. Cellulose 2008;15:555–9.

[17] Neagu RC, Gamstedt EK, Stig LB, Lindström M. Ultrastructural features affecting mechanical properties of wood fibres. Wood Mater Sci Eng 2006;1:146–70.

[18] Hu TQ, Hayak A. Cellulose Materials with Novel Properties, US Patent 2012/0041183; 2012.
[19] Yang H, Tejado A, Alam N, Antal M, van de Ven TGM. Films prepared from electrosterically stabilized nanocrystalline cellulose. Langmuir 2012;28:7834–42.
[20] Le Moigne N, Navard P. Dissolution mechanisms of wood cellulose fibres in NaOH–water. Cellulose 2009;17:31–45.
[21] Brandt B, Zollfrank C, Franke O, Fromm J, Göken M, Durst K. Micromechanics and ultrastructure of pyrolysed softwood cell walls. Acta Biomater 2010;6:4345–51.
[22] Brändström J. Micro- and Ultrastructural Aspects of Norway Spruce Tracheids: a Review. IAWA J 2001;22:333–53.

Bridging Section between Previous Chapters and Chapter 5

Based on the structural analysis of carboxymethylated fibers presented in the previous chapters, we have found that CMF can be utilized in many fields of applications. Taking advantage of the presence of intrinsic water pockets – or balloons – from the swollen fiber structures, CMF can be used as a superabsorbing material which can potentially replace petroleum based superabsorbing polymers. Chapter 5 will discuss how evolved CMF structures contribute to the properties of final products, especially in the formation of films. CMF films show properties that are comparable to those prepared from partially carboxylated cellulose nanofibers without any energy intensive post-treatments. The results of this research will be submitted for publication.

Chapter 5. Transparent Composites Prepared from Chemically Modified Cellulose Fibers

Abstract

Naturally occurring mixtures of partially carboxymethylated softwood kraft pulp fibers (CMF) and carboxymethylcellulose (CMC) are made into CMF/CMC "composites" without mechanical fibrillation or high temperature pressing. Drying conditions largely influence the physical appearance of the pulp fibers upon carboxymethylation as an efficient and complete structural collapse of the swollen fibers is required to achieve transparency. Ethanol dried CMF/CMC mixtures produce white, fluffy fibers with increased water absorbency. Such improvement in water absorbency is most likely due to the presence of structurally deformed CMF which provide intrinsic water pockets along with the hydrophilic nature of CMC. On the other hand, thin films with different transparency can be prepared when CMF/CMC mixtures are dried at 50℃ from aqueous suspensions. Physical and optical properties of the CMF/CMC films are mainly dependent on the degree of substitution (DS), as well as pH. With an increase in the DS, tensile strength, Young's modulus, density, transparency, water absorbency, and gas barrier property are all increased. Tensile strength and Young's modulus of CMF/CMC films are as high as 165 MPa and 13 GPa, respectively. The oxygen transmission rate of CMF/CMC film at DS 0.45 is as low as 0.0161 $cm^3 \cdot \mu m \cdot m^{-2} \cdot day^{-1} \cdot kPa^{-1}$ at 0% relative humidity. In contrast to CMF/CMC in sodium form (Na-CMF/CMC), CMF/CMC in hydrogen form (H-CMF/CMC) make films with improved wet strength without sacrificing transparency. Transparent CMF/CMC films can be used in areas such as disappearing packaging, wound dressing, and moisture sensing.

5.1 Introduction

With increased environmental concerns, an enormous amount of efforts has been made to develop eco-friendly, energy efficient, cost-effective ways to develop new, novel, green materials to replace petroleum based products. One of the most highlighted research areas in related fields deals with cellulose nanomaterials including nanocrystalline cellulose (NCC) and cellulose nanofibrils (NFC) due to their abundancy and biodegradability [1,2]. Cellulose is a polysaccharide with a typical degree of polymerization of 13 000 where individual glucose rings are connected by β-[1,4]-linkages [3]. Widely accepted knowledge is that individual cellulose chains come together, crystalize, and the elongated crystals with periodic imperfections – amorphous region – make nanofibers, microfibrils, and eventually macrofibers. Cellulose nanomaterials, NFC in particular, make strong films with tensile strength of 200 – 300 MPa, near 90% transparency and oxygen permeability as low as 0.0004 $cm^3 \cdot \mu m \cdot m^{-2} \cdot day^{-1} \cdot kPa^{-1}$ at 0% RH [4-7]. It has been shown that applying chemical pretreatment (i.e. TEMPO-mediated oxidation, periodate-chlorite oxidation, enzymatic hydrolysis or carboxymethylation) can significantly reduce the energy requirement to prepare NFC. Nevertheless, some minimal mechanical post-treatment is still required in preparation of stable NFC dispersions.

In order to prepare transparent films, either the size of individual building blocks must be below the wavelength of visible light, or the interfaces between the material and the air should be minimized. Due to the dimensions of NFC (width 3 – 5 nm, length 200 – 1000 μm), they can be made into transparent films by simple solvent casting. NCC films can also be cast into transparent, iridescent films; but these are too brittle to be used in wide fields of applications. Other commercially available films such as cellophane are made from regenerated cellulose, which involves fiber dissolution in alkaline conditions or ionic liquids [8]. Translucent films can

also be made using microfibrils, but only after intense mechanical fibrillation or acid treatment followed by pressing [9]. Carboxymethylcellulose (CMC) based films are known as “edible films” and they have demonstrated potentials in pharmaceutics due to its pH sensitive solubility [10]. As illustrated above, the size of the cellulose building blocks plays an important role in film formation by governing both optical and mechanical properties. Despite the fact that cellulose based films are one of the most widely studied areas, highly transparent cellulose based “composite” films that are casted from a naturally occurring bulk mixture of dissolved cellulose chains and macrofibers have never been reported thus far.

Carboxymethylation is one of the most commonly performed cellulose chemistries. Due to its non-toxic and hydrophilic nature, carboxymethylcellulose (CMC) is often added to foods and medications mainly as a viscosity modifier. Carboxymethylation has also been used as an aid to prevent “hornification”, a technical term describing the irreversible structural collapse of the pulp fibers upon solvent removal [11]. During carboxymethylation, cellulose fibers are exposed to a highly alkaline condition which heavily disrupts the crystalline structure. As a consequence, solvent accessibility to the fibers improves significantly. Partially carboxymethylated fibers showing reduced degree of hornification can be, therefore, easily rewetted and redispersed in water without any notable aggregation.

Partially carboxymethylated cellulose pulp fibers (CMF) undergo moderate to severe morphological changes depending on the degree of substitution (DS). Upon carboxymethylation, the layer-by-layer structure of secondary wood cell walls create characteristic features such as ‘balloons” and “collars”. The formation mechanism of balloons and the contribution of each secondary layer to the swollen fiber structures have been discussed in a previous paper [12]. We have also found that the average balloon diameters increase with an increase in DS, but only up

to 0.45 – 0.5. At or above DS = 0.5, carboxymethylated fibers spontaneously break apart into smaller fragments including in the form of CMC [13]. During carboxymethylation, the balloons can be considered as intermediate structures, or the non-soluble fibrous fraction (CMF). With an increase of DS, the water soluble CMC fraction increases as more CMF loses its structural integrity to become soluble as CMC.

The DS of commercially available CMC ranges from 0.4 to 1.5 [14,15], whereas the DS of widely used CMC is typically around 0.70 with molecular weight (MW) of 90,000 [16]. When carboxymethylation is used to facilitate the nanofibrillation, the DS usually stays below 0.1 in order to preserve the cellulose crystalline structure while minimizing the soluble CMC fraction [7,17]. CMF with its DS between 0.1 and 0.4 should present improved water absorptivity while maintaining its fibrous form. This is advantageous in film formation as entangled fibers provide extra strength to the film. The conventional solvent system for CMC production is a mixture of isopropanol and water, where the side reaction is suppressed by using an increased amount of isopropanol [18].

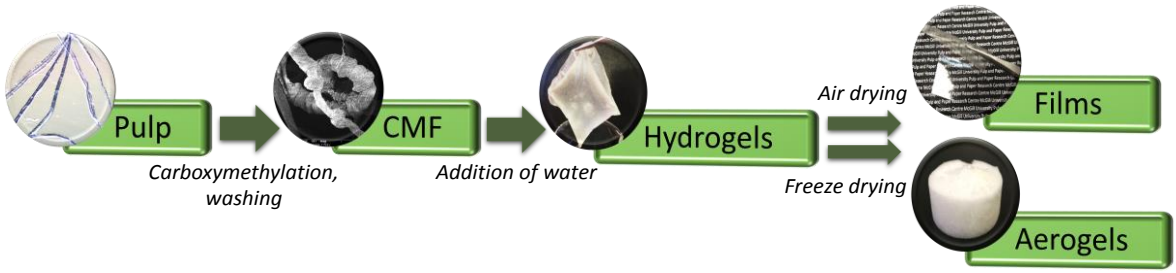

Figure 5-1. Processing steps of preparing carboxymethylated fiber based products

The formation of balloon-like structures during cellulose treatments has been considered to be undesirable as it causes random fragmentation, hence large polydispersibility [19-21]. In this study, we will discuss how such "undesirable" balloon-like structures contribute to the properties of CMF based final products. As illustrated in **Figure 5-1**, CMF displays high versatility even

with a simple variation in processing. We will mainly focus on the preparation and characterization of CMF/CMC composites, emphasizing their optical properties, pH effect, water compatibility, dry and wet strength.

5.2 Experimental

5.2.1 Materials

Non-refined, bleached softwood kraft pulp fibers (FPInnovations, Canada) are used as native cellulose material. Reagent grade sodium chloroacetate (MCA), sodium hydroxide (NaOH), hydrochloric acid (HCl), carboxymethylcellulose (CMC, DS 0.70, MW 90,000) and ethanol were purchased from Sigma-Aldrich and were used as received.

5.2.2 Carboxymethylation of cellulose pulp fibers

Air dried softwood bleached kraft pulp (FPInnovations) was mixed with a sodium monochloroacetate solution (g of MCA : g of pulp fiber : g of H_2O = 1x : 1 : 2.6; where x = 1, 1.5 or 2 to yield DS 0.20, 0.30, and 0.45, respectively) in a household mixer for 10-15 min and then placed into a 50 ℃ water bath for 4 hours for impregnation. A sodium hydroxide solution (g of NaOH : g of pulp fiber : g of H_2O = 1.25 : 1 : 2) was then added to the reaction vessel and mixed for 10-15 min. The treated pulp mixture was left overnight (24 hrs) at room temperature then successively washed with 70, 80, 90, and 100% ethanol.

5.2.3 Film preparation

The pH adjusted (pH 2 and 8) and purified 0.1% w/w CMF/CMC suspensions with different charge contents (DS 0.20, 0.30, and 0.45; see supporting information) and 0.1 %w/w CMC (DS 0.70) were subjected to magnetic stirring (150 rpm) under vacuum for 2 – 3 hours to remove air bubbles. Each suspension was poured into a polystyrene petri dish and placed in the

oven (50 ℃) until completely dried to make a thin film. Basis weight of 30 – 31 g/m^2 was used to cast all films.

5.2.4 Characterization

Optical imaging and charge determination of CMF/CMC

Ethanol purified and dried CMF/CMC were observed by high resolution field emission scanning electron microscopy (FE-SEM; FEI Inspect, F-50) at an accelerating voltage of 5.0 kV after sputter-coating the samples with gold with a thickness of 5 nm. Upon dispersing the ethanol dried CMF/CMC in deionized water at 0.1 %w/v, a drop of toluidine blue solution was added into the CMF/CMC suspension to obtain images with better contrast. Hoffman modulation contrast light microscopy (HMC; Nicon Eclipse TE2000-U) was used for optical imaging. Charge contents of carboxymethylated fibers was measured by conductometric titration (Metrohm 836 Titrando), following the method reported by Yang et al [22].

Water compatibility and solubility of CMF/CMC

Water absorptivity of CMF/CMC was measured by tea-bag tests. 0.08 – 0.10 g of ethanol dried CMF/CMC with DS 0.20, 0.30, and 0.45 were placed in teabags made from oxygen bleached paper (6.35 x 6.98 cm, 20 μm average pore size) and then placed in beakers containing 500 mL distilled water after sealed. The weights of each teabag containing swollen samples were constantly measured every 10 minutes for the first hour, then once every hour for the next 3 hrs. The final weights were obtained after 19 hrs. Upon measuring the final weights, each teabag was dried at 50 ℃ for 3 days before measuring the water absorptivity of the samples for the second wetting cycle. For each DS values, the test was done in triplicates. The same test was performed

after replacing distilled water with a 0.9 %w/v NaCl solution to determine water absorption in saline conditions. All reported values are corrected for the water absorption by the teabag itself.

Water retention values of CMF/CMC were measured by a standard centrifugation technique, in which a 0.2 %w/v CMF/CMC suspension was centrifuged at 1500 g for 15 min. In order to determine the weight % of (1) water soluble CMC fraction and (2) insoluble CMF fraction, the ethanol dried CMF with all three different DS values were made into highly dilute aqueous suspensions (0.05 %w/v) and centrifuged at 3000 g for 15 min. Supernatant containing the soluble fraction (CMC) was decanted and replaced by fresh deionized water repeatedly for 3 times. The collected residual, insoluble fraction (CMF) was then dried at 105 °C for 3 hours to obtain the dry weight.

CMF/CMC film characterization

Prepared film surfaces and cross-sections were imaged by HMC and FE-SEM. For FE-SEM, the samples were coated and imaged in the same manner as described before.

X-ray diffraction analysis was performed (Bruker Discover D8; VANTE C2D detecto; CuKα radiation, $\lambda = 1.54$ Å) and the X-ray diffractograms were acquired with a 2θ (Bragg angle) range of 10° – 30° at a scan rate of $0.005°S^{-1}$.

In order to distinguish the films prepared in at two different pH's – 2 (H-form) and 8 (Na-form) – FTIR spectra were recorded on a Perkin-Elmer spectrometer (single diamond ATR). Spectra were averaged over 32 scans in the range of 550 to 4000 cm^{-1} with a resolution of 4 cm^{-1}.

The % transmittance of CMF/CMC films in both Na and H forms were measured by a Varian UV-visible spectrophotometer with a xenon lamp. The spectra were acquired in the range

of 200-800 nm with an interval of 1 nm. Reported values for each sample are averaged over 5 replicates.

Tensile strength and Young's modulus of films were measured in a standard condition room (22 ℃ and 50% relative humidity, RH) using an Instron Mini 44 tensile tester with a 500 N load cell. Each sample was cut into 5 strips: 5 mm (w) x 50 mm (l). Strips were stretched at a cross-head speed of 10 mm/min with a specimen gauge length of 10 mm.

The wet strength of films made from CMF in hydrogen form (H-CMF) was measured tested after immersing 10 mm (w) x 50 mm (l) strips in DI water for 10 min using TMI LabMaster tensile machine at a crosshead rate of 25 mm/min.

Oxygen transmission rate (OTR) for films prepared from a CMF/CMC mixture at DS 0.45 in both H and Na forms were measured by MOCON Oxtran 2/21 Oxygen Permeability Instrument, following the standard ASTM D-3985 at 0% RH.

5.3 .Results and Discussions

It is widely known that carboxymethylation changes the hollow cylindrical cellulose pulp fiber structures into highly swollen balloons as shown in **Figure 5-2a** [12]. The ballooning phenomenon can be observed at or above DS ~ 0.15 and the average diameter of balloons increases with an increase in DS (see **Table 1, left column**). At DS 0.45, the insoluble, fibrous fraction of partially carboxymethylated pulp fibers (CMF) also show tube-like structures as presented in **Figure 5-2c**. Carboxymethylation most likely proceeds in a heterogeneous manner, generating different sized balloons caused by electrostatic repulsion in most common solvents including water. Heterogeneity of carboxymethylation in various solvent systems has been discussed in the past and the conventional solvent for carboxymethylcellulose (CMC) production

is a isopropanol/water slurry [23-25]. In the present study, water is the sole solvent used throughout the experiments and the [cellulose : CMA : NaOH : water] ratio was optimized to meet the targeted DS. Ethanol was used only in the purification step in order to reach near 100 % cellulose recovery by precipitating out the water soluble CMC fraction along with collapsed CMF balloons. In this case, the native cellulose crystalline structure (cellulose I) was not preserved due to the high concentration of NaOH [**Supporting information 1**].

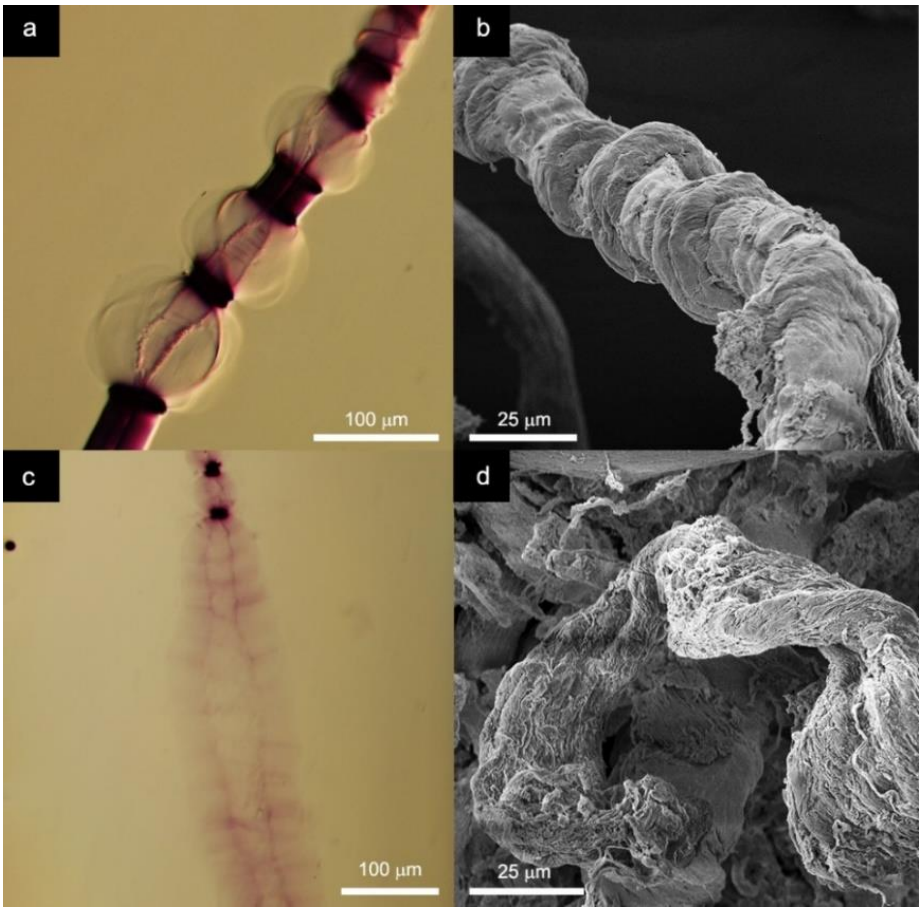

Figure 5-2. Hoffman modulation contrast (HMC) microscopy of toluidine blue dyed highly swollen carboxymethylated fiber with DS 0.45 in water at pH 8 show structures that are (**a**) balloon-like and (**c**) tube-like. FE-SEM of solvent exchange dried CMF using ethanol are shown in (**b**) and (**d**), which correspond to (**a**) and (**c**) respectively.

When the ethanol purified/dried carboxymethylated fibers are dispersed back in water below 0.1 %w/v consistency, the water soluble CMC fraction can be separated from the intact

fiber structures by centrifugation. After decanting the supernatant containing CMC, CMF residues were collected and their dry weight was measured. With an increase in DS, an increased amount of CMC was produced (see **Table 5-1, right column**). Films that are casted from ethanol dried carboxymethylated fibers which was re-suspended in water, therefore, include both CMF and CMC fractions, but in different proportions depending on the DS.

Table 5-1. Ethanol dried CMF at DS 0.20, 0.30, 0.45 were dispersed in water at 0.05 %w/v at pH 8. The insoluble, fibrous fraction (CMF) form balloon-like structures and their balloon diameters were measured (approx. 300 balloons) by HMC. Weight fractions (%) of the insoluble fraction (CMF) was separated from the soluble fraction (CMC) by centrifugation at 3000 rpm for 15 min, which was repeated 3 times. STDEV = standard deviation.

DS	Average balloon diameters (μm)	STDEV (μm)	Minimum balloon size (μm)	Maximum balloon size (μm)	Appearance of non-soluble fraction (CMF)	Average CMF weight %	STDEV CMF weight %
0.20	88.3	34.9	20.4	169.3	Balloons, unmodified fibers	95.8	2.9
0.30	148.4	56.7	23.7	351.3	Mostly balloons	70.3	11.0
0.45	176.0	65.4	26.2	332.3	Balloons, tubes	48.6	17.3
0.70	Negligible. All in CMC form						

5.3.1 Optical properties – Drying, DS, and pH effects

As briefly discussed in the previous section, drying methods greatly affect the optical properties of CMF/CMC mixtures. Unlike solvent exchange drying from ethanol which causes balloons to collapse onto the fiber skeleton in white, fluffy, fibrous form, drying the modified pulp fibers from water results in the formation of films that are semi- to highly transparent. The major contributor of this change in optical properties is arguably the dissolved CMC fraction. Ethanol, being a poor solvent, causes precipitation of both CMC and CMF in the initial solvent exchange purification/drying step. Therefore, the modified pulp fibers maintain their fibrous form even at DS 0.45. When ethanol dried CMF/CMC fibers are resuspended in water, near

50 % of CMC contents become solubilized at DS 0.45, thereby increasing the transparency of the films that are casted from CMF/CMC suspensions.

Table 5-2. Film transparency and density of CMF/CMC films in sodium (Na) and hydrogen (H) forms. Basis weight of all films are 30 – 31 g/m^2

	Na form		H form	
DS	$\%T_{600\ nm}$ (%)	Film density (g/cm^3)	$\%T_{600\ nm}$ (%)	Film density (g/cm^3)
0.20	4.1 ± 1.1	0.26 ± 0.08	3.8 ± 1.1	0.24 ± 0.09
0.30	13.9 ± 0.8	0.60 ± 0.04	12.4 ± 0.9	0.65 ± 0.06
0.45	86.2 ± 0.9	1.45 ± 0.10	84.5 ± 1.3	1.36 ± 0.12
0.70	92.8 ± 0.1	1.51 ± 0.02	90.1 ± 0.3	1.49 ± 0.04

Another contributor to this change in physical appearance is the structural collapse of the macroscale CMF. Varying the solvent means changes in the surface tension, which is directly related to the capillary force. CMF has regions of different structural rigidity that are under various types of physical constrains – tightly wound collars, extended helices, highly swollen balloons and crumpled innermost S3 layers. When capillary forces are exerted on this complicated structure, the collars may rupture, the extended helices may cleave, the balloons may burst open, and the S3 layers may completely and irreversibly collapse. None of these structural damages nor association between fibers seem to have occurred during the solvent exchange drying, most likely because of the low surface tension of ethanol which lowered the capillary force ($\gamma_{ethanol,\ 20\ ^\circ C}$ = 22.39 mM/m whereas $\gamma_{water,\ 20\ ^\circ C}$ = 72.86 mM/m). When dried from water, enhanced capillary forces induce more severe and effective collapse of the balloons. As a result, interfibrillar association becomes stronger and CMF are casted as films rather than individual fibers. At pH 8, the balloon collapse in water is a reversible process, as redispersing the CMF films in water give a suspension of balloon- and tube-like CMF. Along with the CMC that were originally presented upon carboxymethylation, the damaged portions of CMF are also

expected to liberate more CMC especially at higher DS. Rewettability of CMF at various pHs will be discussed below.

At pH 8, the counter cation for the carboxymethyl groups is sodium. When the films are prepared at pH 8, Na-CMF/CMC films show increased transparency with an increase in DS. At DS 0.20, 0.30, and 0.45, %T increased from 4%, 14%, 86%, respectively at 600 nm (**Figure 5-3a, b, c**; **Table 5-2**). Achieving high transparency using these macrofibers was possible likely because of the balloon collapse which reduced the fiber-air interfaces while having soluble CMC fraction working as a filler. Microscopic observations have confirmed that CMF in suspensions has circular cross-sections as spherical balloons stay highly swollen in water [12]. Removing water under ambient conditions – or at slightly elevated temperature (50 ℃) – causes CMF to collapse from circular cross-sections to ellipsoids. As can be seen in **Figure 5-3d** and **3e,** fiber collapse and flattening become more severe with an increase in DS. At DS 0.45, film cross-sections no longer show any defined structures (**3c**), which is expected for those of pure CMC films. The more the fibers are swollen, the more effective pore packing becomes; hence the film density increases accordingly (**Table 5-2**). The density of CMF films at DS 0.45 is close to that of cellulose crystals (1.51 – 1.67 g/cm^3) [26] and the pure CMC films at DS 0.70, indicating how densely the fibers are packed. The surface of DS 0.20 films did not display any distinguishable differences from the non-modified hand sheets (**Figure 5-3g**); whereas DS 0.30 ones showed slight gelation (**5-3h**). DS 0.45 CMF films almost all coalesced to form smoother surfaces (**5-3i**). The imperfections seen in **5-3i** that are bulging out of the surface are the collars maintaining their structural integrity. Note that CMC films (DS = 0.70) show highly smooth film surfaces, hence resulting near 93 %T. CMF/CMC films, on the other hand, probably cannot exceed ~85 %, unless the collars are completely removed.

Suspensions of carboxylated NFC or highly charged NCC can achieve stability mainly by electrostatic repulsion. Cation exchange from sodium to hydrogen reduces the surface charge and promotes the aggregation of cellulose nanoparticles. Yang et al. prepared films from highly charged NCC (ENCC, electrosterically stabilized NCC) in both H and Na forms and reported reduced transparency for the films prepared in H-form [22]. Fujisawa et al., however, reported only subtle differences in %T between the H and Na-forms of TEMPO-oxidized cellulose nanofiber (TOCN) films [5]. This discrepancy is probably due to the fact that ENCC was not mechanically treated after acidification, whereas a TOCN-H suspension was sonicated to completely redisperse the nanofibers in water prior to film casting. Fiber swelling, also driven by charge repulsion, can be suppressed by cation exchange. As the pH is brought down to 2, balloons shrink, and the semi-transparent CMF/CMC suspensions become cloudy. However, when CMF in H form are made into films after purification, only subtle differences in transparency were observed (**Table 5-2**). Differences in film densities between the two forms were also hardly distinguishable, suggesting that the reduction in fiber-air interface is effective in both Na and H-form and CMC aggregation at low pH is negligible in the film formation. Ballooning is an irreversible morphological change. Even if the size of balloons in suspension is reduced by the addition of acid, cellulose chains that are already pulled out from the original fiber structure can only stay within the balloons. Perhaps the balloon shrinkage at reduced pH is analogous to that occurring during drying; hence not greatly affecting the film transparency and density. (**See supporting information 2**)

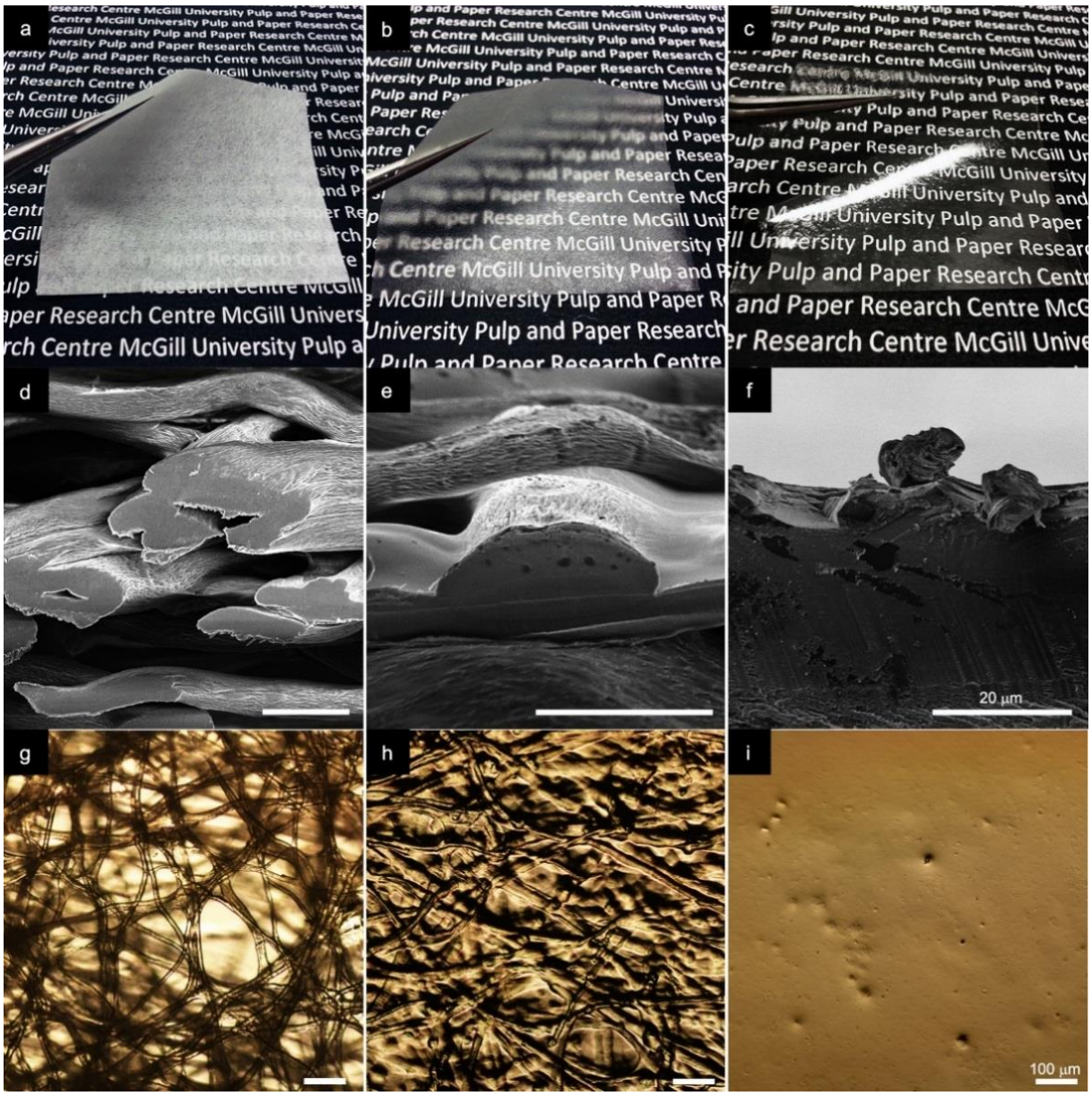

Figure 5-3. Films prepared from Na-CMF/CMC with different amounts of charge groups; **(a, d, g)** DS = 0.20; **(b, e, h)** DS = 0.30; **(c, f, i)** DS = 0.45, respectively. **(a, b, c)** Photographs of CMF/CMC films. **(d, e, f)** FE-SEM of Na-film cross-sections. Samples were sputter coated with Au with a thickness of 5 nm. Scale bars are 20 μm. **(g, f, i)** HMC of Na-CMF/CMC film surfaces. Scale bars are 100 µm.

The novelty of this product comes from the fact that transparent films are prepared in the presence of macrofibers without having to further treat them by mechanical means or to filter out the CMF fraction. Note that films that are prepared from mechanically fibrillated cellulose microfibrils make translucent sheets with %T of 42 [27], and carboxymethylation-assisted microfibrillated cellulose fibers of 82.5 % [17]. To achieve near 90 %T, pulp fibers must be

extensively beaten, which requires 700 to 1400 MJ/kg of energy input [4]. In this work, the energy requirement to produce films with ~ 85 %T was none. Another key point was collecting both CMF and CMC fractions by solvent exchange drying at the initial purification stage. When placing the ethanol dried fibers back in water, we have created naturally occurring CMF/CMC mixtures which can then be casted into CMF/CMC composite films. It is highly likely that the network forming structurally collapsed microfibers (CMF) and the flexible CMC chains functioning as fillers results in formation of highly transparent films at DS 0.45.

5.3.2 Water compatibility of CMF films

Hydrogels that are prepared from NCC, NFC, and other polymeric cellulose derivatives usually require an extra cross-linking step to create internal networks to function as water pockets. As individual building blocks of such hydrogels do not swell, their water absorbency is mainly governed by the cross-linking reaction conditions: chain length of the cross-linkers, concentrations, and functionality. Studies have shown that CMC can be cross-linked or conjugated with methacrylate, polyethylene glycol dimethacrylate, 1,2,3,4-butanetetracarboxylic dianhydride, and hyaluronic acid etc. to show water absorbency between 3 – 500 g/g [28-31]. For CMF/CMC hydrogels, the balloons function as water pockets to improve the water absorption of CMF, along with its intrinsic hydrophilicity. An intense alkaline treatment during carboxymethylation causes intra- and intercrystalline swelling, thereby permanently changing the cellulose crystalline structures. As a consequence, solvent penetration into the fiber walls becomes easier; hence the rewettability improves. The total water uptake of both ethanol dried fibrous CMF/CMC and water dried CMF/CMC films were measured by the “teabag test”. The results shown in **Figure 5-4** depict the high dependency of DS to the water absorbency of CMF/CMC.

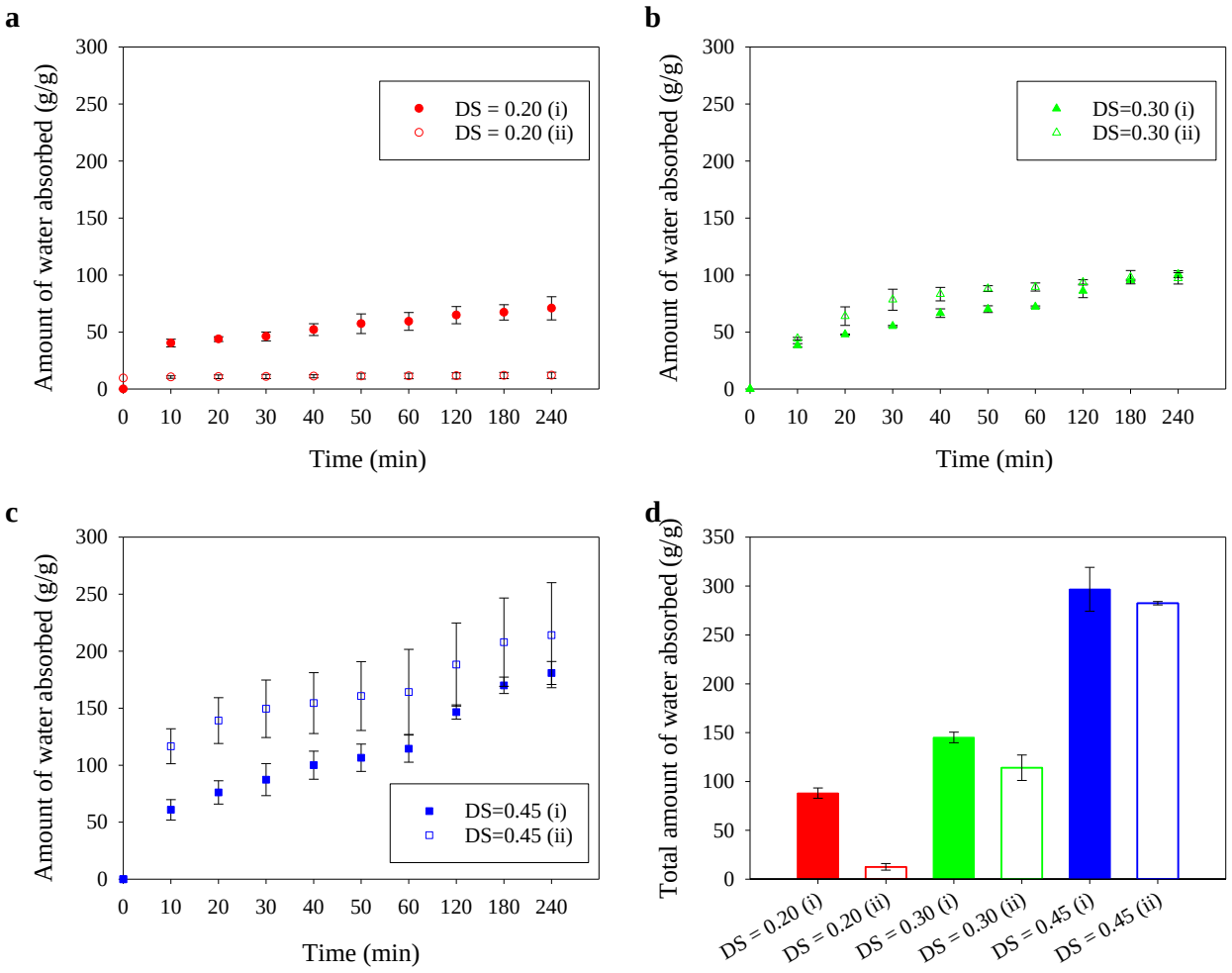

***Figure 5-4*. (a, b, c)** Water absorption rate of CMF at different DS for the first 4 hours. (i) Initial wetting cycle, (ii) second cycle. Solid markers represent ethanol dried CMF in the initial fibrous state (i), empty markers represent CMF films (ii). **(a)** DS = 0.20; **(b)** DS = 0.30; **(C)** DS = 0.45. **(d)** The total amount of water absorbed after 17 hours.

When ethanol dried CMF/CMC was immersed in water after being placed in a teabag, CMF with all three DS swelled but to a different extent (**Figure 5-4ai, bi, ci**). A higher DS results in more available hydrophilic carboxymethyl groups with larger balloon sizes. From DS 0.20 to 0.45, CMF/CMC water uptake was increased from 88 to 300 times their own weight. At fiber consistency inside the teabag, the water soluble CMC fraction is presumably trapped inside the highly swollen CMF gel. As opposed to CMF/CMC mixtures, pure CMC at DS 0.70 leaked out of the teabag completely. After drying the wetted CMF/CMC from their highly swollen state

inside the teabag, they were placed back in water for a rewettability test. The dried CMF/CMC after the wetting cycle are expected to make translucent films inside the teabag. Upon rewetting, DS 0.20 films failed to absorb as much water as before, but DS 0.30 and 0.45 ones showed water absorption comparable to those in fiber forms (**Figure 5-4aii, bii, cii**). For DS 0.30, the rate of water uptake in the first 60 min was higher than the first cycle; DS 0.45 films showed faster rate throughout the first 4 hours. Ethanol drying probably makes the hydrophilic groups including CMC embedded in the fiber structure upon drying, whereas water drying leaves them stretched out on the fiber surface. This explains the improved water uptake rate of the CMF in the second wetting cycle for DS 0.30 and 0.45. Reduced water absorbing performance for lower DS fibers suggest that more than 10 % of the hydroxyl groups must be converted to prevent hornification. DS higher than 0.30 start to show much improved rewettability. In a saline condition (0.9 %w/v NaCl), DS 0.20 and 0.30 CMF in fiber form no longer displayed superabsorbency. Compared to the results shown in ion-free conditions, the total amount of absorbed water went down from 88 to 22 g/g for DS 0.20, 145 to 20 g/g for DS 0.30, and 300 to 100 g/g for DS 0.45.

Table 5-3. Water retention value (WRV) measured by the standard centrifugation method (1500 g, 15 min)

DS	0.20	0.30	0.40
WRV (g/g)	61.9 ± 10.5	108.9 ± 15.6	192.1 ± 19.5

Table 5-3 shows water retention values (WRV) of CMF/CMC in fiber form. The results shown by the "teabag" test in **Figure 5-4b** encompasses not only the water contained within the swollen fiber walls but also the water held by fiber network. WRV, on the other hand, disregards any non-bound water by centrifugal forces and is a better indication of the amount of water absorbed within the fiber walls. Comparing the teabag test results to WRV, it can be concluded that a major proportion of the total amount of water picked up by CMF/CMC is contained within

entangled CMC and CMF walls, presumably inside the balloons. Since the water absorptivity of CMF/CMC is attributed to the combined effect of CMC gel and the balloon-like structure, rather than the fiber-fiber network formation, creating interfibrillar networks between CMF/CMC by cross-linking may enhance its water absorbing ability even further.

To understand the effect of pH on the water compatibility of the films, Na-CMF and H-CMF films were immersed in distilled water. Na-CMF/CMC films immediately swelled to form hydrogels, liberated individual CMF/CMC, and reformed CMF/CMC suspensions. On the other hand, H-CMF/CMC films stayed intact for a few days at room temperature with dramatically reduced water absorption (0.85 to 7.1 g/g for DS 0.20 to DS 0.45). This observation can be explained by the formation of different types of chemical bonding upon water removal which occurs between carboxymethyl and unreacted hydroxyl groups. Hydrogen bonding from recrystallization of mercerized cellulose occurs in both Na and H forms. However, the new hydrogen bonding between free carboxyl groups (COOH) and cellulose backbone, and the ester bonding between COOH and neighboring hydroxyls only occur during the formation of H-CMF films. Due to the formation of stronger fiber-fiber association described above, the water accessibility of the dried H-CMF films become more limited. Along with the less hydrophilic character of COOH than COONa, formation of extra hydrogen and ester bond is considered to be the major restraining force that prevents fiber swelling in many other cases too [5,21,32].

5.3.3 Mechanical properties of CMF films

Self-standing NFC films show tensile strength up to 200 MPa and Young's modulus of 8 GPa, while NCC films stay below 80 MPa (tensile strength) and 4 GPa (Young's modulus) [4,22]. Both NFC and NCC can be used in polymer composites as reinforcing agents as well [1,33,34]. Recent studies have reported that cellulose fibers dissolved in various solvent systems

make films with distinguishably different mechanical properties. Solvent systems such as simple alkaline solutions, alkali/urea solutions and ionic liquids all have different fiber disruption mechanism, thereby changing the film properties [8,35]. It is also known that fibers with higher water retention value (WRV) make stronger and tougher films as WRV is related to the exposed surface area [36,37].

Table 5-4. Dry tensile strength (σ), Young's modulus (E), elongation (EL); and tensile index (TI) of CMF/CMC films in Na and H forms. Wet strength is only measured for H-forms. CMC (DS = 0.70) used to prepare pure CMC films have an average molecular weight = 90,000.

	Na form			H form			
	Dry strength			Dry strength			Wet strength
DS	σ (MPa)	E (GPa)	EL (%)	σ (MPa)	E (GPa)	EL (%)	TI (Nm/g)
0.20	5.3 ± 0.7	3.77 ± 0.06	5.7 ± 1.3	4.7 ± 0.3	3.34 ± 0.28	5.1 ± 0.2	0.88 ± 0.26
0.30	100.9 ± 12.7	6.51 ± 1.43	7.1 ± 1.2	113.3 ± 8.8	5.94 ± 1.76	4.3 ± 1.1	4.80 ± 0.16
0.45	162.5 ± 5.6	9.17 ± 0.42	10.0 ± 1.0	162.9 ± 17.9	13.51 ± 8.62	7.1 ± 2.8	5.72 ± 0.36
0.70	83.9 ± 6.0	6.78 ± 0.68	6.5 ± 1.9	77.2 ± 4.4	6.17 ± 1.90	3.8 ± 1.2	-

CMF/CMC films in both Na and H forms were tested for their mechanical performance (see **Table 5-4**). A significant increase in tensile strength and elastic modulus was seen with increased DS. Commercial tracing papers made from mechanically fibrillated fibers with 15 % transparency showed tensile strength of 140.9 ± 5.6 MPa, Young's modulus 13.7 ± 0.4 GPa, and elongation 1.9 ± 0.1% (not shown in the table). Findings here suggest that chemically modifying pulp fibers can indeed achieve a much improved transparency compared to mechanically fibrillated fibers while maintaining comparable mechanical strength. Although no significant difference was seen between Na and H-CMF/CMC films in dry tensile strength, H-CMF films showed slightly improved Young's modulus at DS 0.45 while elongation was reduced for both DS 0.30 and 0.45 films. Both tensile strength and Young's modulus were significantly improved when DS 0.45 CMF/CMC films are compared to self-standing CMC films at DS 0.70. The

presented results are likely caused by the presence of both macrofibers (CMF) and CMC, where CMF provides extra fiber-fiber entanglement while CMC functions as a strength enhancer. Film strengthening ability of CMC has been widely illustrated in composites including CMC/starch, polyvinyl alcohol (PVOH), NCC, NFC etc. [38-40].

The most notable difference between Na and H-CMF/CMC films was the rewettability. Formation of hydrogen and ester bond must be a lot more effective in H-form, which significantly increase the wet strength of the films. In order to observe improvements in wet strength, DS > 0.20 is required. After 10 minutes of soaking the H-CMF/CMC films in water, DS 0.20, 0.30, and 0.45 film showed water absorption of 7.1, 1.1, 0.85 g/g, respectively. Upon rewetting, Na-CMF/CMC films readily dissociate to form hydrogels because of the negative charge repulsion and the partially diminished hydrogen bonding. The formation of new hydrogen and ester bonds in DS 0.20 H-CMF/CMC films was probably not enough to demonstrate any impressive improvement in wet strength, although they did not dissociate in water like Na-CMF/CMC films at the same DS. H-CMF/CMC films with DS 0.30 and 0.45 films, however, displayed much improved wet strength by showing tensile index (TI) around 5 – 6 Nm/g. Sheets of kraft pulp fibers show TI below 1 Nm/g, polymer conjugated cellulose fiber networks around 5 – 7 Nm/g [41-43], and cross-linked fibers up to 20 Nm/g [44]. Improving wet strength is particularly useful in applications such as tissue papers and other disposable paper based products. CMC can also be used as a wet strength enhancer upon conjugating with resins (i.e. glycidyltrimethylammonium chloride) or specific type of cations (i.e. Zr) [45,46]. However, H-CMC as a self-standing film does not display any wet strength, which is significantly different from CMF/CMC films.

5.3.4 Gas barrier properties

Oxygen transmission rate (OTR) of DS 0.45 films were measured to be 0.0161 and 0.0245 $mL \cdot \mu m \cdot m^{-2} \cdot day^{-1} \cdot kPa^{-1}$ for Na and H-form films, respectively at 0% RH. The measured values are significantly lower than those for the films prepared from mechanically fibrillated microfibers and even lower than cellophane (see **Table 5-5**). Carboxymethylation-assisted mechanically fibrillated fibers also make films with reduced OTR values that are comparable to the results reported here, indicating that the presence of carboxymethyl groups play a role in reducing the pore size and density of the films, hence the gas transport. TOCN films show OTR values two orders of magnitude lower than both Na and H-CMF films. This is most likely due to the highly efficient pore packing of the spaghetti-like nanofibrils with fine, uniform width distributions. Achieving low oxygen permeability is especially important for the packaging industry as well as in electronic device applications

Table 5-5. Oxygen permeability of cellulose base films at 0% RH unless otherwise specified.

Materials	OTR ($cm^3 \cdot \mu m \cdot m^{-2} \cdot day^{-1} \cdot kPa^{-1}$)	References
Na-CMF/CMC (DS = 0.45)	0.0161	Present study
H-CMF/CMC (DS = 0.45)	0.0245	Present study
CMC:PVOH (2:1) composite	0	[47]
MFC (mechanical)	3.52 – 5.03	[48]
MFC (Carboxymethylated, then homogenized, DS < 0.1)	(3 passes, homogenizer; 50 % RH) 0.04 – 0.05	[17]
	(10 passes, homogenizer; 0 % RH) 0.0006	[7]
TOCN (DS = 0.25)	0.0004 (Na form)	[6]
TOCN (DS = 0.29)	0.049 (H form) 0.0017 (Na form)	[5]
Cellophane	0.41	[7]

5.4 Concluding Remarks

Mixtures of partially carboxymethylated fibers (CMF) and precipitated CMC with improved water absorbing ability were made into transparent, composite films with improved strength and toughness than self-standing CMC films. Properties of the films prepared from this study are comparable to commercial tracing papers, as well as NFC films. The CMF/CMC composite films achieved high transparency and improved mechanical properties without applying any mechanical treatment during the film fabrication. Major contributing factors to this outcome are: (1) the water soluble CMC fraction functioning as a strength enhancer and a pore filler, (2) the structural deformation of the fibrous CMF fraction which increased the exposed surface area with permanently stretched out the pulp fibers in transverse directions. Due to the presence of constrained regions such as collars and non-swollen parts in CMF, it is difficult to obtain perfectly smooth film surfaces with high uniformity even at DS = 0.45. As a consequence, utilizing CMF/CMC films in high value applications such as display may not be ideal. Potential applications of the CMF/CMC films lean more towards a single use application; for example, disposable packaging and wound dressing. CMF/CMC can be further treated during or after the film casting to tune the water absorptivity, wet strength, hydrophobicity, and gas barrier properties. CMF/CMC films can also be used for heavy metal removal simply by immersing the films in hard water.

5.5 Acknowledgements

This work was supported by an NSERC Industrial Research Chair supported by FPInnovations, by the NSERC Green Fibre Network, and the FQRNT Centre for Self-Assembled Chemical Structures. Special thanks to Md Nur Alam at McGill University for valuable discussions, and Zohreh Sabzalian, Alois Vanerek, and Julie Bates at FPInnovations for tensile

strength measurements. Oxygen transmission rate measurements were done by Carrie Skagerberg at Mocon.

5.6 Supporting information

Sample names, DS 0.20, 0.30, 0.45, were assigned based on the results determined by conductometric titration of redispersed ethanol dried carboxymethylated pulp fibers. Obtained values of [COO^-] contents are presented in **Table S1**.

Table S1. Actual charge contents of ethanol dried CMF/CMC mixtures for samples DS = 0.20, 0.30, and 0.45

Sample name	$[COO^-]_{determined}$	DS conversion
DS 0.20	1.13 ± 0.07mmol/g	0.188
DS 0.30	1.71±0.12 mmol/g	0.285
DS 0.45	2.56±0.21 mmol/g	1.427

FT-IR spectra of CMF/CMC composites in Na and H form were obtained to confirm the cation exchange. See **Figure S1**.

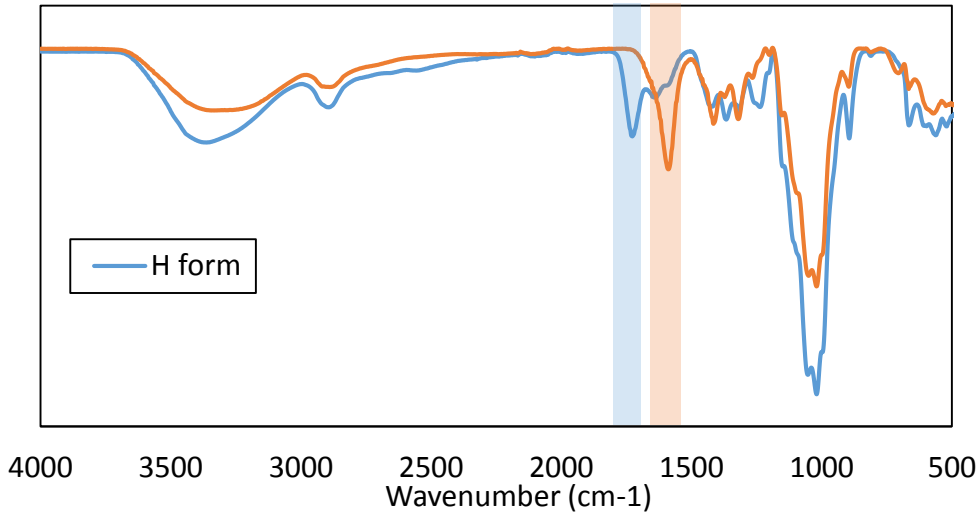

Figure S1. FTIR spectra of CMF/CMC composites at DS 0.45 in Na-form (orange) and in H-form (blue). Notice the clear peak shift from 1589 cm^{-1} (C=O stretching, COO-Na) to 1727 cm^{-1} (C=O stretching, COO-H). Literatures report 1600 cm^{-1} and 1720-1740 cm^{-1} for COO-Na and COO-H, respectively [5]

1.8 References

[1] Hubbe MA, Rojas OJO, Lucia LA LA, Sain M. Cellulosic nanocomposites: a review. BioResources 2008;3:929–80.

[2] Eichhorn SJ, Dufresne A, Aranguren M, Marcovich NE, Capadona JR, Rowan SJ, et al. Review: current international research into cellulose nanofibres and nanocomposites. J Mater Sci 2009;45:1–33.

[3] Fleming K, Gray DG, Matthews S. Cellulose crystallites. Chemistry 2001;7:1831–5.

[4] Isogai A, Saito T, Fukuzumi H. TEMPO-oxidized cellulose nanofibers. Nanoscale 2011;3:71–85.

[5] Fujisawa S, Okita Y, Fukuzumi H, Saito T, Isogai A. Preparation and characterization of TEMPO-oxidized cellulose nanofibril films with free carboxyl groups. Carbohydr Polym 2011;84:579–83.

[6] Fukuzumi H, Saito T, Iwata T, Kumamoto Y, Isogai A. Transparent and high gas barrier films of cellulose nanofibers prepared by TEMPO-mediated oxidation. Biomacromolecules 2009;10:162–5.

[7] Aulin C, Gällstedt M, Lindström T. Oxygen and oil barrier properties of microfibrillated cellulose films and coatings. Cellulose 2010;17:559–74.

[8] Yang Q, Fukuzumi H, Saito T, Isogai A, Zhang L. Transparent cellulose films with high gas barrier properties fabricated from aqueous alkali/urea solutions. Biomacromolecules 2011;12:2766–71.

[9] Van der Reyden D, Hofmann C, Baker M. Effects of aging and solvent treatments on some properties of contemporary tracing papers. J Am Inst Conserv 1993;32:177–206.

[10] Dieckman SF, Jarrell JG, Voris RS. Carboxymethylcellulose in the free acid form. Ind Eng Chem 1953;45:2287–90.

[11] Fernandes Diniz JMB, Gil MH, Castro JAAM. Hornification—its origin and interpretation in wood pulps. Wood Sci Technol 2004;37:489–94.

[12] Sim G, Alam M, Godbout L, van de Ven TGM. Structure of swollen carboxylated cellulose fibers. Cellulose 2014;21:4595–606.

[13] Tejado A, Alam MN, Antal M, Yang H, Ven TGM. Energy requirements for the disintegration of cellulose fibers into cellulose nanofibers. Cellulose 2012;19:831–42.

[14] Silva DA, de Paula RCM, Feitosa JPA, de Brito ACF, Maciel JS, Paula HCB. Carboxymethylation of cashew tree exudate polysaccharide. Carbohydr Polym 2004;58:163–71.

[15] Heinze T, Koschella A. Carboxymethyl ethers of cellulose and starch - A review. Macromol Symp 2005;223:13–40.

[16] Tharanathan RN. Biodegradable films and composite coatings: Past, present and future. Trends Food Sci Technol 2003;14:71–8.

[17] Siró I, Plackett D, Hedenqvist M, Ankerfors M, Lindström T. Highly transparent films from carboxymethylated microfibrillated cellulose: The effect of multiple homogenization steps on key properties. J Appl Polym Sci 2011;119:2652–60.

[18] Khullar R, Varshney VK, Naithani S, Heinze T, Soni PL. Carboxymethylation of cellulosic material (average degree of polymerization 2600) isolated from cotton (Gossypium) linters with respect to degree of substitution and rheological behavior. J Appl Polym Sci 2005;96:1477–82.

[19] Jardeby K, Germgard U, Kreutz B, Heinze T, Heinze U, Lennholm H. The influence of fibre wall thickness on the undissolved residuals in CMC solutions. Cellulose 2005;12:167–75.
[20] Jardeby K, Lennholm H, Germgård U. Characterisation of the undissolved residuals ID CMC-solutions. Cellulose 2004:195–202.
[21] Saito T, Kimura S, Nishiyama Y, Isogai A. Cellulose nanofibers prepared by TEMPO-mediated oxidation of native cellulose. Biomacromolecules 2007;8:2485–91.
[22] Yang H, Tejado A, Alam N, Antal M, van de Ven TGM. Films prepared from electrosterically stabilized nanocrystalline cellulose. Langmuir 2012;28:7834–42.
[23] Heydarzadeh H. Catalyst-free conversion of alkali cellulose to fine carboxymethyl cellulose at mild conditions. World Appl Sci. 2009;6:564–9.
[24] Heinze T, Liebert TIM. Carboxymethylation of cellulose in unconventional media. Cellulose 1999:153–65.
[25] Heinze T, Koschella A. Solvents applied in the field of cellulose chemistry: a mini review. Polímeros 2005;15:84–90.
[26] Sun C. True density of microcrystalline cellulose. J Pharm Sci 2005;94:2132–4.
[27] Sehaqui H, Liu A, Zhou Q, Berglund L a. Fast preparation procedure for large, flat cellulose and cellulose/inorganic nanopaper structures. Biomacromolecules 2010;11:2195–8.
[28] Adinugraha MP, Marseno DW. Synthesis and characterization of sodium carboxymethylcellulose from cavendish banana pseudo stem (Musa cavendishii LAMBERT). Carbohydr Polym 2005;62:164–9. doi:10.1016/j.carbpol.2005.07.019.
[29] Chang C, Duan B, Cai J, Zhang L. Superabsorbent hydrogels based on cellulose for smart swelling and controllable delivery. Eur Polym J 2010;46:92–100.
[30] Kono H, Fujita S. Biodegradable superabsorbent hydrogels derived from cellulose by esterification crosslinking with 1,2,3,4-butanetetracarboxylic dianhydride. Carbohydr Polym 2012;87:2582–8.
[31] Barbucci R, Magnani A, Consumi M. Swelling Behavior of Carboxymethylcellulose Hydrogels in Relation to Cross-Linking, pH, and Charge Density. Macromolecules 2000;33:7475–80.
[32] Ek M, Gellerstedt G, Henriksson G. Paper chemistry and technology. Walter De Gruyter Inc; 2009.
[33] Koga H, Saito T, Kitaoka T, Nogi M, Suganuma K, Isogai A. Transparent, conductive, and printable composites consisting of TEMPO-oxidized nanocellulose and carbon nanotube. Biomacromolecules 2013;14:1160–5.
[34] Siqueira G, Bras J, Dufresne A. Cellulosic bionanocomposites: A review of preparation, properties and applications. Polymers (Basel) 2010;2:728–65.
[35] Tovar-carrillo KL, Tagaya M, Kobayashi T. Bamboo fibers elaborating cellulose hydrogel films for medical applications. J Mater Sci Chem Eng 2013;1:7–12.
[36] Klemm D, Kramer F, Moritz S, Lindström T, Ankerfors M, Gray D, et al. Nanocelluloses: a new family of nature-based materials. Angew Chemie 2011;50:5438–66.
[37] Nakagaito a. N, Yano H. The effect of morphological changes from pulp fiber towards nano-scale fibrillated cellulose on the mechanical properties of high-strength plant fiber based composites. Appl Phys A Mater Sci Process 2004;78:547–52.

[38] Tongdeesoontorn W, Mauer LJ, Wongruong S, Sriburi P, Rachtanapun P. Effect of carboxymethyl cellulose concentration on physical properties of biodegradable cassava starch-based films. Chem Cent J 2011;5:6.
[39] Oun AA, Rhim J-W. Preparation and characterization of sodium carboxymethyl cellulose/cotton linter cellulose nanofibril composite films. Carbohydr Polym 2015;127:101–9.
[40] Zheng Q, Cai Z, Gong S. Green synthesis of polyvinyl alcohol (PVA)-cellulose nanofibril (CNF) hybrid aerogels and their use as superabsorbents. J Mater Chem A 2014;2:3110–8.
[41] Chen N, Hu S, Pelton R. Mechanisms of aldehyde-containing paper wet-strength resins. Ind Eng Chem Res 2002;41:5366–71.
[42] Saito T, Isogai A. Introduction of aldehyde groups on surfaces of native cellulose fibers by TEMPO-mediated oxidation. Colloids Surfaces A Physicochem Eng Asp 2006;289:219–25.
[43] Ishino Y. Absorbent fibrous structures and producing method thereof. US Patent 5173521, 1992.
[44] Tejado A, Antal M, Liu X, van de Ven TGM. Wet cross-linking of cellulose fibers via a bioconjugation reaction. Ind Eng Chem Res 2011;50:5907–13.
[45] Pahimanolis N, Salminen A, Penttilä P a., Korhonen JT, Johansson LS, Ruokolainen J, et al. Nanofibrillated cellulose/carboxymethyl cellulose composite with improved wet strength. Cellulose 2013;20:1459–68.
[46] Louis B, Onslow H. Carboxyalkyl cellulose ether fibers and films of good wet strength. US2420949, 1947.
[47] Muppalla SR, Kanatt SR, Chawla SP, Sharma A. Carboxymethyl cellulose–polyvinyl alcohol films with clove oil for active packaging of ground chicken meat. Food Packag Shelf Life 2014.
[48] Syverud K, Stenius P. Strength and barrier properties of MFC films. Cellulose 2009;16:75–85.

Chapter 6. Conclusions and Future Research Suggestions

6.1 Conclusions

In this thesis, a series of studies is presented to describe the relationship between the structural evolvement of individual cellulose pulp fibers upon chemical modification and the properties of the end products that are prepared from them. Even though both CMC chemistry and pulp fiber structures are well developed research areas with centuries long history, surprisingly little is known about the link between the two. Understanding the dynamic structural changes by selectively damaging the secondary wood cell walls by chemical means not only provides an insight to the cellulose processing optimization but also an inspiration to the structural design of man-made fibers.

In Chapter 2, contributions from the outermost S1 layer in ballooning phenomenon are explained. Despite the thin wall thickness, the presence of the S1 layer is the dominant factor in creating balloon-like structures mainly due to its high microfibril angles. Alternating microfibril angles between S1, S2, and S3 layers create characteristic features when the fibers are highly swollen, which include extended helices, collars, balloons, and crumpled S3 layers. The S1 layers create helical chains that are extended around the balloons, as well as the tightly wound collars that are mechanically resistant. Dramatic expansion of the S2 microfibrils in transverse directions compresses the swollen fibers in axial directions. As a result, S3 layers are often crumpled. Mechanically grinding the exterior of pulp fibers or chemically removing the physical constrains by effective chain scission and glucose ring opening can help avoid ballooning.

Chapter 3 discusses the breakup mechanism of the highly swollen, balloon-like CMF. Mechanically treating TEMPO-oxidized fibers can effectively liberate nanofibrils. When highly

swollen CMF is exposed to a similar condition, however, the highly swollen fibers break apart to form spherical gel particles with donut-shaped interior structures prior to random fragmentation. Microscopic observations have revealed that areas under physical stress, i.e. helically extended S1 microfibrils and axially compressed S3 layers, are preferentially damaged. The interior donuts are most likely originated from the collars, while carboxymethylated S2 microfibrils are rearranged around this pre-defined structure to form pH sensitive, highly swollen spheres.

In Chapter 4, isolated S3 layers are characterized for their chemical and physical properties. S3 microfibril surfaces are clearly carboxymethylated; hence can be tagged with a fluorescent dye via carbodiimide bioconjugate chemistry. Although a direct relationship between cellulose twists at the molecular level and the handedness of macrofibers has not been fully identified yet, the S3 layers also show the same apparent right-handedness as NCC and NFC. Our observations in both swollen and dried states of the isolated S3 layers confirmed that the dried layer thickness and microfibril angles match up with the literature reported values.

Chapter 5 demonstrates types of products which can be made from CMF. The results show that drying CMF from different solvents affect the optical property and the fiber-fiber association; pH affects Young's modulus, moisture content, and wet strength of the films prepared from CMF; and the degree of substitution mainly dictates the mechanical and optical properties. CMF films at DS 0.45 demonstrate high transparency, superabsorbency, and dry strength comparable to NFC films. CMF films will be particularly suitable for disposable packaging due to the low preparation cost, non-toxic nature, and biodegradability. Varying the drying condition of CMF suspension can make products with significantly different physical appearance and mechanical properties.

6.2 Future Research Suggestions

It would be worthwhile investigating the properties of the balloon walls and the internal structures of the balloons. It is still not clear if the content inside the balloon is contained within a membrane wall, or the whole balloon is a viscose gel that is composed of highly entangled cellulose chains with different size scales. An indentation test using a micromanipulator may give information regarding the elasticity of the balloon walls, as well as the viscosity of the content inside the balloons. Variations in this micro-indentation test can be made by using poking the balloons with different sized beads on the tips of the needles. Embedding a colloidal particle inside the balloons and tracking the Brownian motion is one of the other possibilities to gather information about the viscosity inside the balloon.

Note that some tracheid cells do not have S3 layers at all, some have helical thickening, and some show helical thickening overlaid S3 layers. Since our investigation was restricted to pulp fibers from softwoods, it would be interesting to speculate fibers from plants or compression wood fibers to learn more about the innermost secondary layer.

Unlike air-drying from water which produces thin films, freeze-drying CMF suspensions make highly porous aerogels. It would be interesting to study their acoustic properties to test out the potential of CMF as a sound-proofing material.

Appendix. Swelling Behaviour of Various Pulp Fibers

As described in Chapter 1, softwood and hardwood fibers show different ranges of physical properties including fiber length, width, thickness, and microfibril angles. Other than the types of carboxylating chemistry and the degrees of refining, factors including fiber sources and pulping methods can possibly alter the swelling behaviour upon chemical modification. Studies presented in this thesis were done using bleached, kraft fibers from black spruce (*Picea mariana*), which is a type of widespread softwood species across Canada. To investigate further, one other type of softwood (red cedar, *Juniperus virginiana*) and a hardwood (gum trees, *Eucalyptus*) were selected to examine whether or not there is a dependency on fiber sources to the swelling behaviour. Also, chlorite pulp and dissolving pulp fibers were carboxymethylated to compare the results obtained from kraft pulp fibers.

Table A-0-1. Cell types in volume fractions (%), fiber dimensions, and microfibril angles (MFA) of three different sources of wood fibers [1]

Species	**% of Total Volume**					**Fiber Dimensions**		**MFA**
	Fibers	Tracheids	Vessels	Rays	Other	Length (mm) Avg, range	Width (μm) Avg, range	Early-latewood
Eucalyptus	49		21	14	16	1.1 (0.3 - 1.5)	20 (10 - 28)	21.45 - 4.96
Red cedar		93.1		6.9	Trace	3.5 (1.4 - 5.9)	(30 - 40)	12.2-16.5; 17.9
Black spruce		94.8		5	0.2	3.5 (1.5-5.7)	(28 - 40)	5 - 50

Softwood vs. Hardwood Kraft Fibers

The two selected softwood fibers, red cedar and black spruce, are mainly composed of tracheids and show similar fiber dimensions (see **Table A-1**). Unlike MFA of black spruce

which vary a lot from earlywoods to latewoods, those of red cedar stay between 12 to 18 degrees. Note that MFA reported in literatures refer to S2 microfibril angles only. Compared to softwood fibers, Eucalyptus fibers are shorter and narrower with a MFA range lower than that of Black spruce. Since hardwood fibers are evolved to specifically provide an optimum structural support, they are denser and less porous than softwood tracheids in which water transportation is required [2]. Such properties may or may not hinder the chemical reactivity but definitely have a substantial impact on physical properties of the end products such as strength and softness [3].

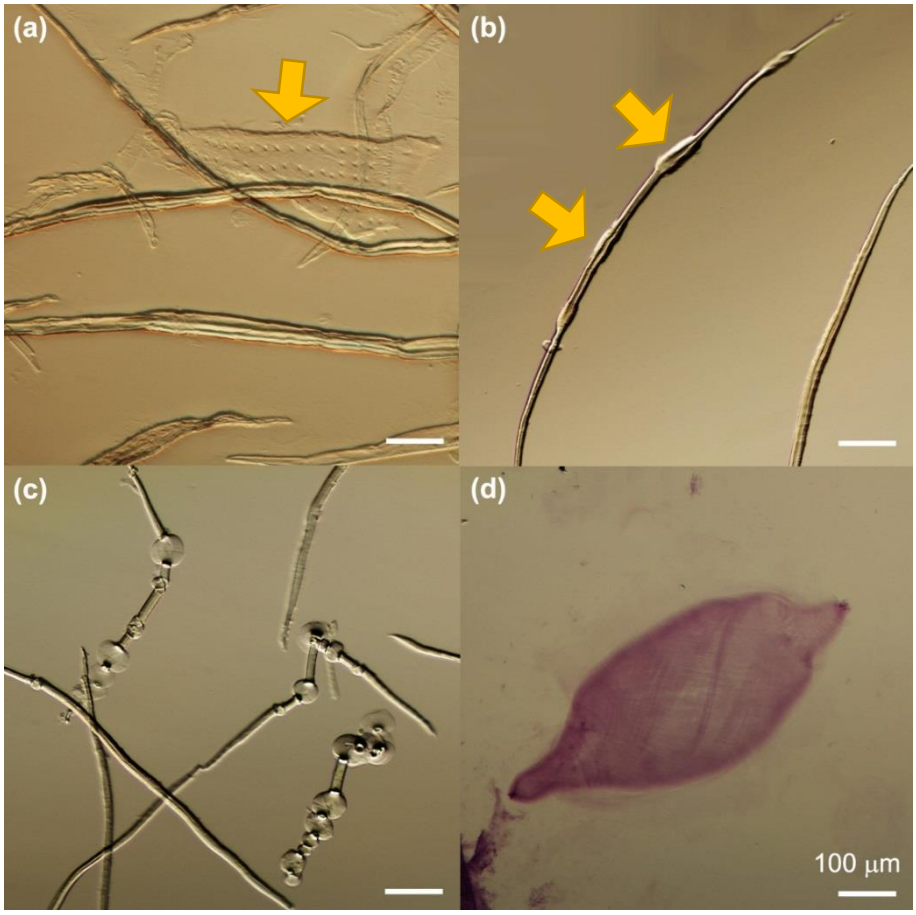

Figure A-1. HMC of hardwood kraft fibers (Eucalyptus) undergoing carboxymethylation. (**a**) Non-treated fiber suspension; (**b**) beginning of the fiber deformation at DS = 0.09; (**c**) swollen fibers via ballooning at DS = 0.25; (**d**) highly swollen hardwood fiber at DS = 0.40, toluidine blue dyed to achieve better contrast. All scale bars are 100 µm.

Figure A-1 contains images of kraft Eucalyptus pulp fibers undergoing carboxymethylation. Hardwoods are mainly composed of fibers as well as vessel elements that are thicker and more porous (**A-1a, arrow**). Upon carboxymethylation, fibers start to swell (**A-1b**) at different points at the same time (arrows). As carboxymethylation proceeds, hardwood fibers form balloon-like structures just as Black spruce fibers (**A-1c**). Regardless of the lower MFA in S2 layers of Eucalyptus, the presence of S1 layers must have constricted homogeneous swelling. **Figure A-1d** could be a reacted vessel element, or a highly swollen fiber with damaged S1 layers from extensive carboxymethylation.

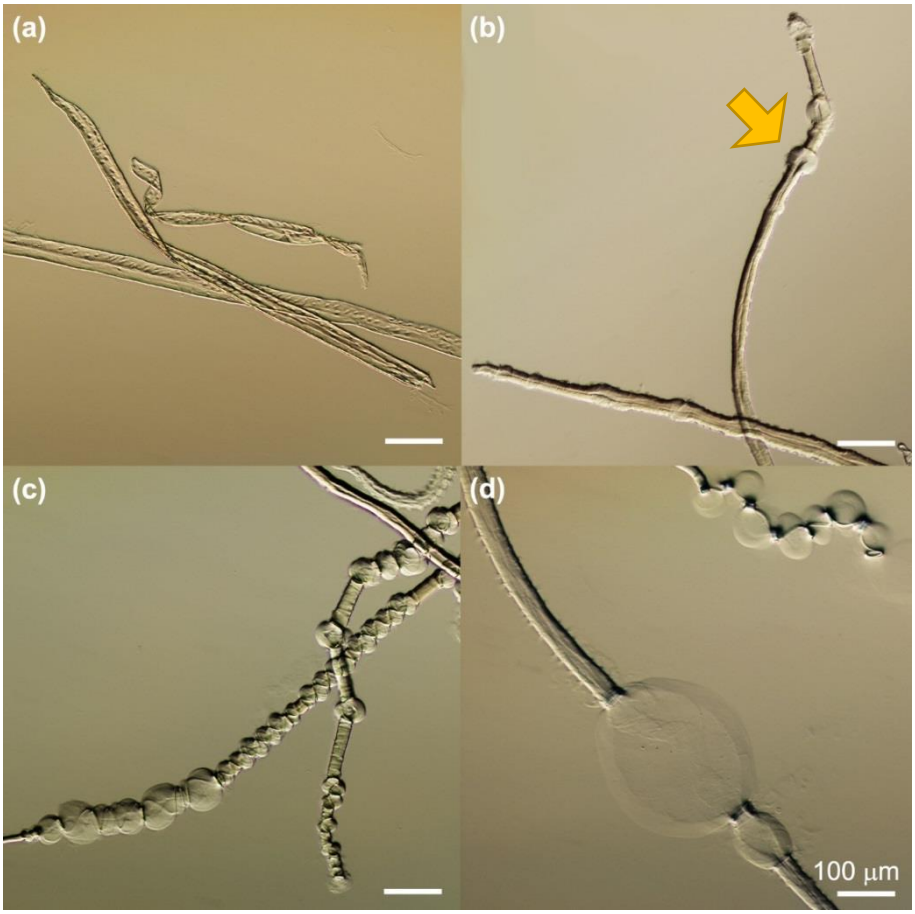

Figure A-2. HMC of softwood kraft fibers (Red cedar) undergoing carboxymethylation. (**a**) Non-treated fiber suspension; (**b**) beginning of the fiber deformation at DS = 0.10; (**c**) formation of "series of pearls" or "balloons" at DS = 0.22; (**d**) a highly swollen fiber with a large balloon diameter at DS = 0.40. All scale bars are 100 µm.

Kraft Red cedar fibers undergoing carboxymethylation are presented in a similar manner as before in **Figure A-2**. No strikingly different features were observed between Red cedar and the other pulp fibers. In general, the higher the DS, the larger the average balloon size becomes. When comparing **FibureA-1c** to **A-2c**, slightly more pronounced helical windings were noticed in carboxymethylated Red cedar fibers. One could argue that the presence of numerous pit holes in softwood fibers can better distribute the chemicals inside the fiber wall, thereby inducing reasonably more efficient expanding of the S2 layers. Negatively charged S2 microfibrils repel each other, stretch out in transverse directions to a certain degree until they experience a restriction applied by the tightly wound outer S1 microfibrils. Fibers make free rotations in suspensions to relieve the stress caused by the outer S1 coils to swell more and form larger balloons. Forming larger sized balloons may or may not necessarily go through the stage shown in **A-2c**. **A-2d** shows highly swollen fibers with a balloon diameter over 200 μm, which is comparable to the average size of carboxymethylated black spruce fibers.

Based on microscopic observations, carboxymethylation causes ballooning regardless of the wood fiber species. The characteristic ballooning behaviour is caused by the microfibril arrangement itself. The fiber sources merely has an effect on the formation of balloons – as long as their secondary cell walls have multilayer structures.

Chlorite vs. Dissolving Pulp Fibers

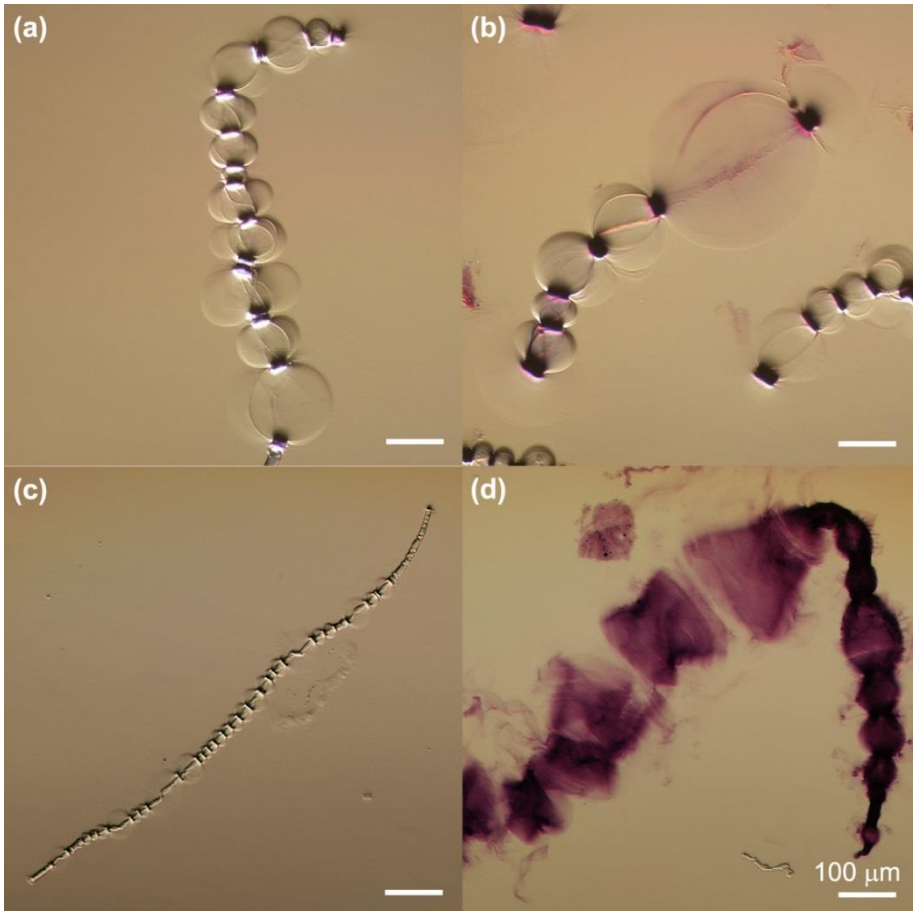

Figure A-3. HMC of carboxymethylated (**a, b**) chlorite pulp fibers and (**c, d**) dissolving pulp fibers at DS = 0.40. Toluidine blue dyed (**a, b, d**). All scale bars are 100 µm.

One of the most widely used pulping methods nowadays is kraft pulping, which is also known as sulfate pulping. During kraft pulping, wood chips are cooked in a pressurized chamber containing Na_2S and NaOH. This treatment condition is considered to be rather "moderate" as it still leaves 1 – 5% of lignin in the fiber wall. Kraft pulping is, therefore, usually paired with bleaching process to completely remove any residual lignin for an improved whiteness. Major advantages of kraft pulping is that: (1) it can be universally used for more or less any type of cellulose sources, (2) it produces stronger fibers compared to the ones that are prepared from the other pulping methods (i.e. sulfite pulping). Sulfite pulping is an acidic process which involves substantial amount of cellulose chain degradation. Pulp fibers produced from this method is

called dissolving pulp, which has a high cellulose content (> 90%). Due to the shortened chain length and high purity, dissolving pulp is widely used in the production of regenerated cellulose [4–6].

To compare the effect of the pulping process on the swelling behaviour, dissolving pulp fibers and chlorite delignified wood chips were carboxymethylated. Chlorite pulping was executed in a mixture of $NaClO_2$ and acetic acid at 70 ℃ for 7 hours [7]. Carboxymethylated chlorite pulp fibers are presented in **Figure A-3 (a, b)**; and carboxymethylated dissolving pulp fibers in **A-3 (c, d)**. Unlike chlorite pulp fibers which showed similar ballooning behaviour as kraft fibers, dissolving fibers do not seem to be able to maintain the fibers with balloon-like structures when it is highly swollen. **A-3d** shows that the balloons tend to break in the middle, and there is no "spherical gel" formation upon rupturing the balloons. This is likely due to the cellulose chain degradation which had occurred during the pulping process. Damaged cellulose chains no longer have the ability to rearrange themselves around the collars to form spherical gels as shown in Chapter 3.

Chlorite pulping is a mild chemical treatment which does not involve any pressure or high thermal treatments. When cellulose chain length and their microfibril arrangements within the fiber walls are preserved in their native state, fibers form balloon-like structures as presented throughout this thesis. In order to avoid ballooning, cellulose chains must be effectively damaged by chemical or mechanical means.

References

[1] Ilvessalo-Pfäffli M-S. Fiber atlas - Identification of papermaking fibers. Springer; 1995.

[2] Aloni R. Cellular Aspects of Wood Formation. vol. 20. 2013. doi:10.1007/978-3-642-36491-4.

[3] Van Luu P, Worry G, Marinack RJ, Ostrowski HS, Bhat DM. Prewettable high softness paper product having temporary wet strength 2000.

[4] Pokhrel D, Viraraghavan T. Treatment of pulp and paper mill wastewater--a review. Sci Total Environ 2004;333:37–58. doi:10.1016/j.scitotenv.2004.05.017.
[5] Gierer J. Chemical aspects of kraft pulping. Wood Sci Technol 1980;14:241–66.
[6] Chakar FS, Ragauskas AJ. Review of current and future softwood kraft lignin process chemistry. Ind Crops Prod 2004;20:131–41. doi:10.1016/j.indcrop.2004.04.016.
[7] Ahlgren P, Goring D. Removal of wood components during chlorite delignification of black spruce. Can J Chem 1971;11.